AD-A164 082 LIFE PREDICTION FOR A STRUCTURAL MATERIAL UNDER CYCLIC 1/2
LOADS WITH HOLD TI (U) GEORGE WASHINGTON UNIV
WASHINGTON DC SCHOOL OF ENGINEERING AN...
UNCLASSIFIED J EFTIS ET AL 31 DEC 84 AFOSR-TR-85-1237 F/G 20/11 NL

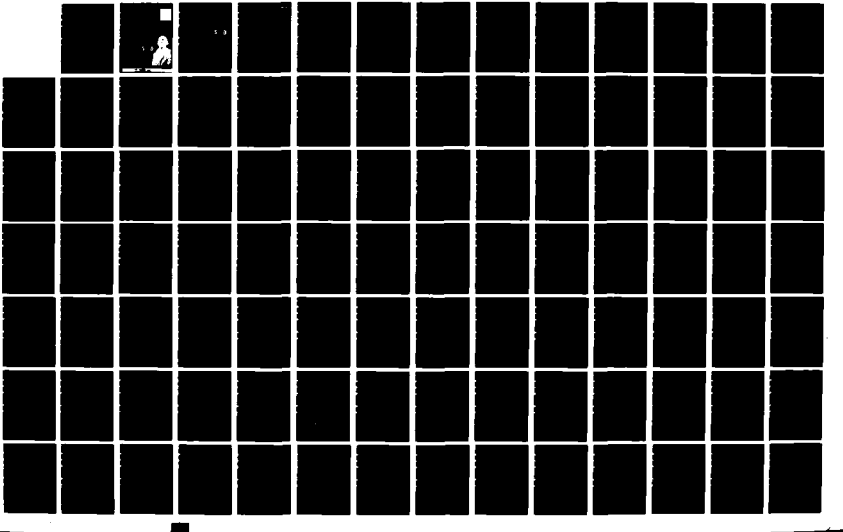

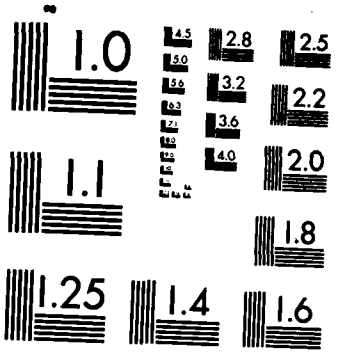

AFOSR-TR- 85-1237

(2)

E PREDICTION FOR A STRUCTURAL MATERIAL
UNDER CYCLIC LOADS WITH HOLD TIMES
ING A VISCOPLASTIC CONSTITUTIVE MODEL

THE
GEORGE
WASHINGTON
UNIVERSITY

Final Technical Report

AD-A164 082

STUDENTS FACULTY STUDY R
ESEARCH DEVELOPMENT FUT
URE CAREER CREATIVITY CC
MMUNITY LEADERSHIP TECH
NOLOGY FRONTIE ESIGN
ENGINEERING APP ENC
GEORGE WASHIN NIV

SCHOOL OF ENGINEERING
AND APPLIED SCIENCE

(2)

LIFE PREDICTION FOR A STRUCTURAL MATERIAL UNDER CYCLIC LOADS WITH HOLD TIMES USING A VISCOPLASTIC CONSTITUTIVE MODEL

Final Technical Report
AFOSR Grant 83-0066
February 1, 1983 - January 31, 1984

J. Eftis and D. L. Jones

Submitted to

Air Force Office of Scientific Research
Building 410
Bolling Air Force Base
Washington, DC 20332

School of Engineering and Applied Science
The George Washington University
Washington, DC 20052

UNCLASSIFIED

SECURITY CLASSIFICATION OF THIS PAGE

AD-A164082

REPORT DOCUMENTATION PAGE

1a. REPORT SECURITY CLASSIFICATION Unclassified	1b. RESTRICTIVE MARKINGS
2a. SECURITY CLASSIFICATION AUTHORITY	3. DISTRIBUTION/AVAILABILITY OF REPORT Approved for public release; distribution unlimited.
2b. DECLASSIFICATION/DOWNGRADING SCHEDULE	
4. PERFORMING ORGANIZATION REPORT NUMBER(S)	5. MONITORING ORGANIZATION REPORT NUMBER(S) AFOSR-TR- 85-1237
6a. NAME OF PERFORMING ORGANIZATION CMEE Department George Washington University 6b. OFFICE SYMBOL (If applicable)	7a. NAME OF MONITORING ORGANIZATION Air Force Office of Scientific Research
6c. ADDRESS (City, State and ZIP Code) Washington, D.C. 20052	7b. ADDRESS (City, State and ZIP Code) Bolling Air Force Base Washington, D.C. 20032
8a. NAME OF FUNDING/SPONSORING ORGANIZATION Air Force Office of Scientific Research 8b. OFFICE SYMBOL (If applicable) AFOSR	9. PROCUREMENT INSTRUMENT IDENTIFICATION NUMBER AFOSR 83-0066
8c. ADDRESS (City, State and ZIP Code) Bolling Air Force Base Washington, DC 20032	10. SOURCE OF FUNDING NOS. PROGRAM ELEMENT NO. 61102F; PROJECT NO. 2307; TASK NO. B1; WORK UNIT NO.
11. TITLE (Include Security Classification) Life Prediction for a Structual Material Under Cyclic Loads With Hold Times Using a Viscoplastic Constitutive Model	
12. PERSONAL AUTHOR(S) J. Eftis and D.L. Jones	
13a. TYPE OF REPORT Technical Report 13b. TIME COVERED FROM 2/1/83 TO 1/31/84	14. DATE OF REPORT (Yr., Mo., Day) 12/31/84 15. PAGE COUNT 121
16. SUPPLEMENTARY NOTATION	
17. COSATI CODES FIELD / GROUP / SUB. GR.	18. SUBJECT TERMS (Continue on reverse if necessary and identify by block number) Viscoplastic Constitutive Modeling, Low-cycle Fatigue Life.

19. ABSTRACT (Continue on reverse if necessary and identify by block number)

This investigation demonstrates the ability of the Chaboche viscoplastic constitutive theory to model the behavior of Ti-6Al-4V alloy at non-elevated temperature. The range of material behavior considered includes uniaxial monotonic stress-strain, primary creep, stress relaxation, kinematic and isotropic hardening (and softening) under cyclic loading with and without hold times. The six material parameters of the viscoplastic theory were evaluated from a series of strain-controlled stabilized cyclic loading tests, and room temperature primary creep tests. The viscoplastic strain calculations were integrated into a fatigue life prediction methodology for low cycle fatigue. Two sets of low cycle fatigue life predictions were carried out and compared with experimental data. One involved strain-controlled cyclic loading without hold times, and the other stress-controlled cyclic loading with hold times. Good agreement was found between predicted and actual results.

20. DISTRIBUTION/AVAILABILITY OF ABSTRACT UNCLASSIFIED/UNLIMITED ☒ SAME AS RPT. ☒ DTIC USERS ☐	21. ABSTRACT SECURITY CLASSIFICATION UNCLASSIFIED
22a. NAME OF RESPONSIBLE INDIVIDUAL ANTHONY K AMOS	22b TELEPHONE NUMBER (Include Area Code) (202) 767-4935 22c. OFFICE SYMBOL AFOSR/NA

DD FORM 1473, 83 APR EDITION OF 1 JAN 73 IS OBSOLETE.

SECURITY CLASSIFICATION OF THIS PAGE

NOMENCLATURE

$\underset{\sim}{\Sigma}'$ = elastic component of the total strain

$\underset{\sim}{\Sigma}''$ = inelastic component of the total strain

$\underset{\sim}{\Sigma}$ = infinitesimal strain tensor, where $\underset{\sim}{\Sigma} = \underset{\sim}{\Sigma}' + \underset{\sim}{\Sigma}''$

$\dot{\Sigma}$ = strain rate

$|\dot{\underset{\sim}{\Sigma}}|$ = norm or absolute value of, where $|\dot{\underset{\sim}{\Sigma}}| = \{tr(\dot{\underset{\sim}{\Sigma}} \cdot \dot{\underset{\sim}{\Sigma}})\}^{\frac{1}{2}}$

$\underset{\sim}{T}$ = stress tensor (Cauchy)

$\overset{\circ}{\underset{\sim}{T}}$ = stress deviator tensor, where $\overset{\circ}{\underset{\sim}{T}} = \underset{\sim}{T} - (\frac{1}{3} \text{ tr } \underset{\sim}{T})\underset{\sim}{1}$, $\text{tr } \underset{\sim}{T} = T^k_k$

$\underset{\sim}{1}$ = identity tensor

$\underset{\sim}{Y}$ = stress which determines the center of the yield surface

$\overset{\circ}{\underset{\sim}{Y}}$ = deviator of $\underset{\sim}{Y}$

$II'_{(\overset{\circ}{\underset{\sim}{T}}-\overset{\circ}{\underset{\sim}{Y}})}$ = second principal invariant of $(\overset{\circ}{\underset{\sim}{T}} - \overset{\circ}{\underset{\sim}{Y}})$, where $II'_{(\overset{\circ}{\underset{\sim}{T}}-\overset{\circ}{\underset{\sim}{Y}})} = tr\{(\overset{\circ}{\underset{\sim}{T}}-\overset{\circ}{\underset{\sim}{Y}}) \cdot (\overset{\circ}{\underset{\sim}{T}}-\overset{\circ}{\underset{\sim}{Y}})\}$

F = yield function, where F = 0 defines the yield surface in stress space

t = time

$\hat{R}$ = isotropic hardening parameter

p = cumulated inelastic strain

Σ' = uniaxial counterpart of $\underset{\sim}{\Sigma}'$

Σ'' = uniaxial counterpart of $\underset{\sim}{\Sigma}''$

Σ = uniaxial counterpart of $\underset{\sim}{\Sigma}$

$\dot{\Sigma}$ = uniaxial counterpart of $\dot{\underset{\sim}{\Sigma}}$

T = uniaxial counterpart of $\underset{\sim}{T}$

Y = uniaxial counterpart of $\underset{\sim}{Y}$

f = uniaxial counterpart of F

R = uniaxial counterpart of $\hat{R}$

Y_t = uniaxial yield stress in tension

E = elastic modulus

ΔT = stress range

$\Delta \Sigma$ = total strain range

$(\Delta T)_{fr}$ = equivalent fully reversed stress range

$(\Delta \Sigma)_{fr}$ = equivalent fully reversed strain range

$2N_f$ = number of load reversals to failure

D_i = fractional fatigue damage of the i-th load reversal

D_T = total accumulated fatigue damage

TABLE OF CONTENTS

FORWARD

This technical report, sponsored by the Air Force Office of Scientific Research under Grant 83-066, was prepared by Professors J. Eftis and D. L. Jones of the Department of Civil, Mechanical and Environmental Engineering, The George Washington University. Dr. Anthony K. Amos of AFOSR was the program manager.

I. INTRODUCTION

Methods originally developed by the ground vehicle and aerospace industries for predicting the life of a structural component under cyclic loading are now in routine use as design tools. There is need, however, to modify the current methodology to improve the capability for fatigue life prediction of structural members composed of materials that will be expected to exhibit time or rate dependent inelastic mechanical responses under the given operating conditions.

Design of high performance structures often requires the development of high strength, light weight materials, of which titanium and its alloys are examples. Titanium alloys have been produced with strengths comparable to many steels, but with approximately half the weight of the steels. However, pure titanium and Ti-6Al-4V alloy have been shown to display considerable time dependent strain response at room temperature under static torsional hold stress [1.1]*. Time dependent strains have also been observed for cyclic load tests (at room temperature) incorporating hold times, where the stress levels under consideration are less than the static yield strength of the material [1.2]. The observed time dependent behavior has some of the characteristics of primary creep, and provides a good opportunity to study time and cyclic deformation interaction in a structural metal without the necessity of conducting high temperature** testing with its associated difficulties of extensometry and environmental damage.

---

*Numbers in brackets refer to the list of References following the text.

**High temperature here meaning approximately one-half of the melting temperature of the material on an absolute scale.

The objective of this research program is to employ a particular viscoplastic constitutive theory to model the stress-strain behavior of Ti-6Al-4V alloy subject to uniaxial cyclic loads (interspersed with hold times), which is then used in conjunction with currently accepted fatigue life prediction methods to predict the fatigue life of smooth (unnotched) specimens. If successful, that is, should it be demonstrated that use of the viscoplastic constitutive theory enables the rate (or time) dependence of the material response to be successfully incorporated into the fatigue life prediction technique, then it would appear to be promising and justifiable to attempt to extend the work to notched specimen configurations as a second phase of the program.

II. CHABOCHE VISCOPLASTIC CONSTITUTIVE THEORY

Theories for time or rate dependent plastic deformation, i.e., viscoplasticity, have been proposed following two widely differing central assumptions: (i) Theories that assume a yield condition that separates time independent recoverable (elastic) deformation from time dependent nonrecoverable (viscoplastic) deformation, and (ii) theories that assume no yield condition, thereby allowing for the possibility of having both elastic and viscoplastic components of the total strain occuring in varying degrees at all stages of loading and unloading. The former category has followed a clearly visible line of evolution centered upon the notion of an overstress, originating with Bingham (1919), and thereafter successively generalized by Hohenemser-Prager (1932), Perzyna (1963), and most recently by Chaboche (1977). For this category of viscoplastic theory, a postulated normality condition of the inelastic strain rate to the initial and all subsequent rate dependent yield surfaces determines the general form of the constitutive equation. In its latest form, in addition to being able to account for strain rate effects, hardening rules appropriate for cyclic loading with stabilization, as well as for creep and stress relaxation effects are included. In the latter category of theories, the theoretical structure inherent with use of a yield surface is absent. A range of differing arguments which include appeals to microstructural models, empirical data correlations, modification of viscoelastic constitutive forms, and use of unspecified internal variables, are used instead as the basis for formulating the constitutive equations.

After critical examination of proposed viscoplastic theories from both categories [2.1], it was concluded that the theory of Chaboche, [2.2-2.5], appears to offer the greatest promise for successfully modeling a wide range of

inelastic material behavior and, also, for possible further development.

While it is recognized that most materials display, more or less, viscous behavior properties, for many of the structural materials, however, these properties become pronounced and significant only after the plastic state has been reached. In such cases, it may be assumed that the material displays viscous properties in the non-recoverable range of deformation only, and may therefore be characterized ideally by an elastic-viscoplastic theory. Accordingly, deformation is decomposed linearly into elastic and inelastic parts. The theory in its present form is limited to small isothermal deformations for which the inelastic (non-recoverable and time-dependent) part is taken to be incompressible, and which occurs only after a yield stress state is attained. Prior to yield and during unload portions of cyclic loading, the deformation is assumed to be elastic (recoverable and time-independent).

The complete set of elastic-viscoplastic constitutive equations of the Chaboche theory is summarized as follows:

$$\dot{\underset{\sim}{\Sigma}} = \dot{\underset{\sim}{\Sigma}}' + \dot{\underset{\sim}{\Sigma}}'' \ , \tag{2.1}$$

$$\dot{\underset{\sim}{\Sigma}}' = \frac{1}{2\mu} \frac{\partial \overset{\circ}{\underset{\sim}{T}}}{\partial t} + \frac{(1-2\nu)}{3E} \mathrm{tr}(\dot{\underset{\sim}{T}})\underset{\sim}{1} \ , \tag{2.2}$$

$$\dot{\underset{\sim}{\Sigma}}'' = \left\{ \frac{\sqrt{II'_{(\overset{\circ}{\underset{\sim}{T}}-\overset{\circ}{\underset{\sim}{Y}})}} - \hat{R}(p)}{K'} \right\}^n \frac{(\overset{\circ}{\underset{\sim}{T}} - \overset{\circ}{\underset{\sim}{Y}})}{\sqrt{II'_{(\overset{\circ}{\underset{\sim}{T}}-\overset{\circ}{\underset{\sim}{Y}})}}} \qquad \text{for } F > 0 \ , \tag{2.3}$$

and zero otherwise.

$$F = \sqrt{II'_{(\overset{\circ}{\underset{\sim}{T}}-\overset{\circ}{\underset{\sim}{Y}})}} - \hat{R}(p) \ , \tag{2.4}$$

$$\frac{d\hat{R}}{dt} = b(Q - \hat{R})\left|\dot{\underset{\sim}{\Sigma}}''\right| \ , \tag{2.5}$$

$$p = \int_0^t |\dot{\underset{\sim}{\Sigma}}''| d\tau = \int_0^{|\underset{\sim}{\Sigma}''|} |d\underset{\sim}{\Sigma}''| \ , \tag{2.6}$$

$$\frac{d\overset{\circ}{\underset{\sim}{Y}}}{dt} = C(A\dot{\underset{\sim}{\Sigma}}'' - \sqrt{2/3}\ \overset{\circ}{\underset{\sim}{Y}}|\dot{\underset{\sim}{\Sigma}}''|) - \Gamma\left(\sqrt{II'_{\overset{\circ}{\underset{\sim}{Y}}}}\right)^{m-1} \overset{\circ}{\underset{\sim}{Y}} \ . \tag{2.7}$$

The sets of elastic and viscoplastic material constants, $\{\mu,\nu,E\}$ and $\{n,K',b,Q,C,A,\Gamma,m\}$, respectively, are temperature dependent. Equation (2.5) describes the rate of isotropic hardening (or softening) appropriate for cyclic loading with cyclic stability, expressed as a function of the cumulated inelastic strain. Equation (2.7) models the rate of kinematic hardening as the sum of two contributions. The first is a nonlinear kinematic hardening rule which is appropriate for cyclic loading. The second term is added to account for high temperature effects such as secondary creep and long time stress relaxation.

For uniaxial (tension-compression) loading, Eqs. (2.1) thru (2.7) can be reduced to the following forms, where Σ, Σ', Σ'', $\dot{\Sigma}$, T, Y, R, f are the uniaxial counterparts of $\underset{\sim}{\Sigma}$, $\underset{\sim}{\Sigma}'$, $\underset{\sim}{\Sigma}''$, $\dot{\underset{\sim}{\Sigma}}$, $\underset{\sim}{T}$, $\underset{\sim}{Y}$, $\hat{R}$, F:

$$\dot{\Sigma} = \dot{\Sigma}' + \dot{\Sigma}'' \tag{2.8}$$

$$\dot{\Sigma}' = \frac{1}{E}\dot{T} \ , \tag{2.9}$$

$$\dot{\Sigma}'' = \left(\frac{|T-Y| - R(p)}{K}\right)^n Sg(T-Y) \qquad \text{for } f > 0 \ , \tag{2.10}$$

and zero otherwise.

$$Sg(T-Y) = \frac{(T-Y)}{|T-Y|} = \pm 1 \ , \tag{2.11}$$

$$f = (T-Y) - R(p) \ , \tag{2.12}$$

$$\frac{dR}{dt} = b(q - R)\left|\dot{\Sigma}''\right| \ , \tag{2.13}$$

$$p = \int_0^t \left|\dot{\Sigma}''\right| d\tau = \int_0^{|\Sigma''|} \left|d\Sigma''\right| \ , \tag{2.14}$$

$$\frac{dY}{dt} = c(a\dot{\Sigma}'' - Y\left|\dot{\Sigma}''\right|) - \gamma|Y|^m \, Sg(Y) \ , \tag{2.15}$$

and $\{n,K,b,q,c,a,\gamma,m\}$ are the set of temperature dependent viscoplastic material constants.

Since the room temperature behavior of Ti-6Al-4V β-annealed alloy under either monotonic or cyclic loads does not exhibit long term time dependent plastic deformation, the second contribution to the kinematic hardening rate, Eq. (2.15), can be assumed to be negligible, i.e., that $\gamma << 1$. Integration of the isotropic and kinematic hardening rate Eqs. (2.13) and (2.15) gives

$$R = q + (R_o - q)e^{-bp} \ , \tag{2.16}$$

where $R_o = Y_t$, q represents the value of R at cyclic stabilization, [cf. Fig. 2.1], and

$$Y = sa + (Y_o - sa)e^{-sc(\Sigma'' - \Sigma''_o)} \ , \quad s = \begin{cases} +1 \text{ for } d\Sigma'' > 0 \\ -1 \text{ for } d\Sigma'' < 0 \end{cases} \ , \tag{2.17}$$

where in Eq. (2.17) Σ''_o and Y_o represent the fixed values of Σ'' and Y at the beginning of the previous reversal of load direction of the load cycle as shown in Fig. 2.2.

Inversion of the viscoplastic strain rate Eq. (2.10) gives the stress-strain relation

$$T = Y + R + K(\dot{\Sigma}'')^{1/n} \quad , \tag{2.18}$$

which for monotonic tensile loading, with $Y_o = \Sigma''_o = 0$, $s = 1$ and $|d\Sigma''| = d\Sigma''$ in Eqs. (2.17) and (2.18) gives

$$T = a\left(1-e^{-c\Sigma''}\right) + \left\{ q + (Y_t - q)e^{-b\int_0^{\Sigma''} d\Sigma''} \right\} + K(\dot{\Sigma}'')^{1/n} \quad . \tag{2.19}$$

Figure 2.3 gives schematic illustration of Eqs. (2.18) and (2.19) with the elastic strain component added.

The curve represented by $Y + R$ represents the so-called 'static response' of the idealized rate independent model, and may be viewed as representing the material response when the strain rate approaches zero. $T - (Y + R) = K(\dot{\Sigma}'')^{1/n}$ is the 'viscous' strain-rate dependent 'overstress'.

In the following set of figures, Fig. 2.4-2.39, an optimized set of viscoplastic material parameter values for Ti-6Al-4V (cf. Section IV) were used to demonstrate the predictive capability of the Chaboche viscoplastic constitutive equation for several kinds of loading situations. The parameter values used in the computer runs are as follows: $a = 163.6$ MPa, $c = 250.0$, $n = 8.0$, $K = 300.0$ MPa, $q = 420.0$ MPa, $b = 4.1$, $R_0 = 630.0$ MPa. Note that the value of q is less than the value of R_0, the isotropic component of the material hardening is reverse hardening, i.e., softening.

Figures 2.4-2.12 show the variations of the strain components, the isotropic and kinematic hardening variables and the stress versus total strain for a load-time input that gives rise to primary creep. (Note that the vertical R scale of Figs. 2.9 and 2.10 are greatly exaggerated.) Although the material softens somewhat isotropically, it also hardens to a greater extent kinematically in monotonic loading. This is seen in Fig. 2.12 where the curved portion of the stress versus strain plot represents the relatively rapid (approximately time-independent) hardening part of the viscoplastic strain, and the straight line portion of the slower viscoplastic primary creep strain at fixed stress.

Figures 2.13-2.21 show the variations of the strain components, stress, the hardening variables and the stress versus total strain for a strain-time input that produces stress relaxation.

Figures 2.22-2.30 illustrate the effects of strain controlled cyclic loading. For cyclic loading the isotropic softening appears to outweight slightly the kinematic hardening. This can be seen in Fig. 2.30, the stress-total strain diagram, which indicates a small degree of cyclic softening behavior after two and one-half load cycles.

Figures 2.31-2.39 are for stress controlled cyclic loading with hold times, where the stress level at the hold times is above the yield stress. Viscoplastic primary creep strains are evident during the hold times as indicated by Figs. 2.34 and 2.39.

III. MECHANICAL PROPERTIES OF Ti-6Al-4V ELI FOR MONOTONIC AND CYCLIC LOADING

The material selected for this investigation, Titanium-6 Aluminum-4 Vanadium ELI (Extra Low Interstitial), hereinafter designated Ti-6Al-4V, was selected because of its availability and its tendency to creep at room temperature. This material requires a viscoplastic theory to accurately describe its room temperature response when hold times are included in the loading program. Since Ti-6Al-4V has been widely used by the aerospace and marine industries, a considerable data base is available [3.1-3.6], although most of the data were not taken from ELI grades. The chemical composition and heat treatment of the material used in this study is given in Table 3.1.

The test specimen selected for both the monotonic and fatigue tests was a slightly shortened version of a standard tensile test specimen as defined by ASTM Standard E8 [3.7]. The specimen was shortened in order to better sustain compressive loads without buckling. The geometry and surface finish requirements for this specimen are shown in Fig. 3.1. The specimens were machined from cross-rolled 25.4 mm (1.0 in.) thick plate, having the axial direction of the specimen aligned with the final rolling direction of the plate. No further heat treatment was performed after the specimens were machined. All tests were performed at the University of Illinois and additional information about the testing program is given in Ref. [3.1].

Static Tests

Tensile Properties

The results of tensile tests in the form of stress-strain curves, are used to establish many properties of a material. A summary of these properties obtained from a tensile test performed at a strain rate of 5.0×10^{-4} in/in/sec

is given in Table 3.2. The initial portions of the stress-strain curve shown for two different strain scales, are seen in Fig. 3.2. The early portion of the monotonic stress-strain curve can be represented by a power law in the form

$$\Sigma = \Sigma' + \Sigma'' = \frac{T}{E} + \left(\frac{T}{K''}\right)^{1/n''} \qquad (3.1)$$

where K = strength coefficient in MPa (or ksi), and n = strain hardening exponent.

Tensile and Compressive Creep Properties

Standard tensile and compressive creep tests were performed on this material at stress levels of +770 MPa (95 percent of Y_t) and $\pm$ 723 MPa (90 percent of Y_t). The results of these three tests are plotted as strain versus time curves in Fig. 3.3. These curves show that this material does creep significantly at room temperature when stressed between 90 and 100 percent of Y_t, and support the following conclusions.

- The shapes of all three curves indicate that the creep deformation is predominantly primary creep for the first 1500 minutes, although the compressive creep curve does exhibit some indications of secondary (steady state) creep.
- At 90 percent of the yield strength in tension ($\pm$ 723 MPa), tensile creep is considerably greater than compressive creep. This material behavior suggests that the yield criteria should probably be different for tension and compression.
- For applied stress levels between 90 and 100 percent of Y_t, the creep rates are very sensitive to the applied stress level. As seen in Fig. 3.3, a change of five percent of Y in the applied stress level causes the creep strains to increase by approximately 140 percent.

Efforts to model the primary creep behavior of structural materials have led to the development of many different expressions (creep laws) that are candidates for representing the creep response of any particular material or class of materials. In the analysis of the room temperature creep behavior of Ti-6Al-2Cb-1Ta-1Mo, Chu [3.8] has been able to obtain good agreement with the relation

$$\Sigma'' = \left(\frac{T_H}{\bar{T}} \right)^{m_1} t^{m_2} \tag{3.2}$$

where Σ'' = creep strain in percent,

t = time in hours, and

$\bar{T}, m_1, m_2$ = parameters determined from creep data.

Equation (3.2) is commonly known as the Bailey-Norton creep law [3.9].

In evaluating the parameters of this model, Chu reported that $\bar{T}$ is very close to the yield strength of the material. For this Ti-6Al-4V, a value of $\bar{T}$ was selected as $\bar{T}$ = 803 MPa (116 ksi), and, for the creep data at 770 MPa presented in Fig. 3.3, the following values for m_1 and m_2 were obtained

$$m_1 = 18.6 \quad , \quad m_2 = 0.37 \quad . \tag{3.3}$$

Substitution of the values for the constants gives

$$\Sigma'' = \left(\frac{T_H}{803} \right)^{18.6} t^{0.37} \quad . \tag{3.4}$$

The results of Eq. (3.4) are compared with the experimental data plotted on a log-log scale in Fig. 3.4. At the higher hold stress, agreement between Eq. (3.4) and the experimental data is quite good. However, at the lower hold stress, Eq. (3.4) significantly underpredicts the amount of creep strain for the first part of the curve.

An expression for the primary creep rate can be obtained by taking the time derivative of Eq. (3.4), which yields

$$\dot{\Sigma}'' = \frac{\partial \Sigma''}{\partial t} = 0.37\left(\frac{T_H}{803}\right)^{18.6} t^{-0.63} \tag{3.5}$$

Since the creep strain rate is a function of stress and time, Eq. (3.5) is considered to represent a time-hardening formulation. If, Eq. (3.4) is solved for t and then substituted into Eq. (3.5), the creep rate becomes a function of applied stress and creep strain, or

$$\dot{\Sigma}'' = 0.37\left(\frac{T_H}{803}\right)^{50.4} \Sigma''^{-1.70} \tag{3.6}$$

In general, the strain-hardening formulation as represented by Eq. (3.6), leads to more accurate solutions than time-hardening formulations.

Cyclic Tests

Although many types of cyclic or fatigue tests have been developed to examine different cyclic properties of materials, the most valuable fatigue characterization for constitutive theory development purposes appears to be the cyclically stabilized stress-strain curve. A number of methods have been proposed for determining such curves, including incremental step tests, cyclic tests with continuously increasing amplitudes, cyclic tests with constant amplitudes, and others. In all of these types of tests, either stress or strain may be the controlled variable. In this experimental program, both strain-controlled incremental step tests and constant amplitude cyclic tests have been employed to establish the cyclically stabilized stress-strain curve, which is considered to represent a basic property of the material.

Incremental Step Tests

Incremental step tests are performed by applying a fixed pattern of cyclic stresses or strains and then repeating this pattern, called a block, until the specimen fails or some other test objective is attained. As an example of the type of block loading employed in this test program, Specimen #14 was subjected to a completely reversed cyclic strain function that increased from zero to a maximum of 1.2 percent in ten cycles and then decreased to zero in ten additional cycles. Seven blocks were applied to the specimen in an attempt to cyclically stabilize it. The locus of the tips of each cycle in Block No. 8, which was nearly the midpoint of the cyclic life, was used to construct the cyclically stabilized stress-strain curve.

The hysteresis loops for Blocks 1, 8, and 20 are shown in Fig. 3.5, and the associated stabilized stress-strain curves are given in Fig. 3.6. The maximum tensile and compressive stresses for each block are plotted in Fig. 3.7, where it is seen that the compressive stresses were always greater than the tensile stresses, and both stresses decreased during the cyclic life. This decrease in maximum cyclic stress is interpreted to be a manifestation of the cyclically softening behavior of this material. The material appeared to be cyclically stable during the middle portion of the cyclic life (Blocks 7 to 17). Since inelastic strain is being accumulated during each block of cyclic loading, it is reasonable to assume that the cyclic softening exhibited by this alloy is related to the accumulated inelastic strain. The uniformity of the reductions in tensile and compressive stress amplitudes versus block number also suggests that the cyclic softening is isotropic. Other tests that were part of this testing program confirmed the behavior of Specimen No. 14.

Figure 3.8 shows the relationship between the tensile stress peaks and the plastic strain amplitudes for Block 8 of Specimen 14. The straight line

in the figure is the best least-squares fit to the data, using a power function to relate the stable cyclic stress amplitude $\Delta T/2$ to the cyclic plastic strain amplitude, $\Delta\Sigma''/2$, as

$$\frac{\Delta T}{2} = K''\left(\frac{\Delta\Sigma''}{2}\right)^{n''} \tag{3.8}$$

where K'' = cyclic strength coefficient (MPa) and n'' = cyclic strain-hardening exponent. The best fit line in Fig. 3.8 provides the following values for the constants in Eq. (3.8),

$$K'' = 1433 \text{ MPa} \qquad \text{and} \qquad n'' = 0.104 \ . \tag{3.9}$$

An equation which describes the stable cyclic stress-strain curve can be obtained by solving Eq. (3.8) for the plastic strain amplitude and adding it to the elastic strain amplitude, resulting in

$$\frac{\Delta\Sigma}{2} = \frac{\Delta T}{2E} + \left(\frac{\Delta T}{2K''}\right)^{1/n''} \ . \tag{3.10}$$

Equation (3.10) provides an expression for the determination of total cyclic strain amplitude when the cyclic stress amplitude is known and is particularly useful when fatigue tests are performed under load control.

The constant strain amplitude fatigue testing portion of the experimental program to be described later provides information for such a determination. The cyclically stable stress-strain curve obtained from such tests is compared with an actual monotonic stress-strain curve in Fig. 3.10. The data points plotted are the stress versus strain amplitudes at half-life and it is seen that there is considerable scatter in the results.

Cyclic Tests With Stress or Strain Hold Times

In order to better understand the time-dependent behavior of this alloy, a number of tests were performed in which cyclic loads were interspersed with constant stress or strain hold times. A total of ten specimens were tested in this portion of the experimental program, with eight specimens subjected to single-level stress hold times, one specimen subjected to multiple-level stress hold times, and one specimen subjected to multiple-level strain hold times. The results of the hold times on the material response were evidenced by the size and shape of the hysteresis loops, and were not otherwise used in the constitutive theory development. In all cases the specimens were cyclically stabilized before any cycles incorporating hold times were applied.

One unusual aspect of the behavior of this material is that prior hold times of opposite sign above a particular level serve to enhance the amount of creep deformation at that level. This behavior is apparent in Fig. 3.9a, in which the amount of creep at + 600 MPa is considerably less than at - 600 MPa and is apparently facilitated by the additional creep that occurred at + 712 MPa. The hysteresis loop of the subsequent cycle, which was subjected to the identical loading sequence and is shown in Fig. 3.9b, exhibited a symmetric behavior nearly identical to the compressive portion of the curve shown in Fig. 3.9a. Such an interpretation of the creep deformation is supported by the results of the single level stress hold-time tests; in which it was observed that, once a specimen exhausted its time-dependent deformation at one level, unloading and reloading to the same stress level does not cause significant time-dependent deformation.

Fatigue Life Tests

Two additional fatigue test series were performed to verify the fatigue life predictions and to determine whether hold times influence the cyclic life.

One series of tests was performed under constant strain amplitude cycling while the other employed constant stress amplitude cycling with hold times.

Constant Strain Amplitude Fatigue

This test series was comprised of thirteen specimens subjected to fatigue cycling under different levels of constant strain amplitudes, with $\Delta\Sigma/2$ ranging from 0.003 to 0.015. The tests were performed at a strain rate of $\dot{\Sigma}$ = 0.005 in/in/sec and the results are summarized in Table 3.3a. The notations $2N_{10\%}$ and $2N_{75\%}$ identify the number of cycles necessary to achieve a stress drop of 10 percent and 75 percent respectively from the average peak tensile stress attained during cycles 17-26. No special physical significance is placed on either the 10 percent or 75 percent stress drops, although at 75 percent stress drop a crack encompassing more than half of the cross-sectional area was observed. The life at 75 percent stress drop was arbitrarily defined as the fatigue life.

The half-life tensile stress peaks, T_t, compressive stress peaks, T_c, and stress amplitudes are also included in Table 3.3a. For the low strain tests, i.e., $\Sigma_a < 0.005$, the tensile peaks were observed to be consistently higher than the compressive peaks. Thus a tensile mean stress developed in these tests, although the reasons for this behavior are not certain. For the higher strain amplitudes, the tensile peaks were slightly less than the compressive peaks. The surfaces of three of the specimens, 2R, 7R and 6R, were replicated at periodic intervals by the use of an acetate tape. The tape was pressed against the specimen surface and the resulting replicas were examined under a microscope to determine the number and size of the surface cracks. Multiple cracks of length $\ell \simeq 0.1$ mm (0.004 in) were observed within the first 10 percent of the fatigue life of the specimens tested at higher strain levels, $\Delta\Sigma/2$ = 0.0075 and 0.01. Some of these cracks tended to link up to form a

dominant crack as cycling continued. These cracks probably caused the half-life tensile stress peaks to be less than the compressive peaks. For the smallest strain amplitude replicated ($\Delta\Sigma/2 = 0.005$), the hysteresis loops displayed essentially elastic response during most of the fatigue life. The first fatigue crack was observed at approximately half of the fatigue life. Therefore, it was concluded that metallurgical processes were responsible for the differences between tension and compression half-life peaks at the low strain levels, whereas microcrack formation and linking was considered to be responsible for the differences at the higher strain levels.

The results of this test series can be used to calculate the constants K" and n" by two independent procedures. These constants may be obtained from stable cyclic stress-strain curves obtained by connecting the tips of several stable hysteresis loops obtained from tests performed at different strain ranges. The cyclically stable stress-strain curve obtained from such data is compared with an actual monotonic stress-strain curve in Fig. 3.10. The data points represent the stress versus strain amplitudes at half-life and it is noted that there is significant scatter in the data.

A log-log linear regression was performed on the half-life true stress amplitude versus plastic strain amplitude data obtained from the constant fatigue tests. This regression analysis resulted in the following values for the cyclic constants

$$K'' = 1{,}105 \text{ MPa} \qquad \text{and} \qquad n'' = 0.0655 \ , \tag{3.11}$$

which was not in very good agreement with the corresponding values obtained from the incremental step tests.

As discussed previously, the strain-cyclic life data can be described by an equation of the form

$$\frac{\Delta\Sigma}{2} = \frac{\Delta\Sigma'}{2} + \frac{\Delta\Sigma''}{2} = \frac{T_f^*}{E}(2N_f)^{b'} + \Sigma_f^*(2N_f)^{c'} \quad . \tag{3.12}$$

This equation can also be used to describe the short-life portion of the strain-cyclic life curve whenever the plastic strain range exceeds 10^{-4}. For the long life portion of the curve, where $\Delta\Sigma''/2$ is minimal, Basquin's equation

$$\frac{\Delta\Sigma}{2} = \frac{T_f^{**}}{E}(2N_f)^{b''} \tag{3.13}$$

may be used.

The material constants for Eqs. (3.12) and (3.13) are summarized in Table 3.3b. The experimental data and the curves represented by Eqs. (3.12) and (3.13) are given in Fig. 3.11. This figure shows that Eq. (3.12) fits the short life data quite well, whereas Eq. (3.13) fits the data much better for $2N_f > 10^4$.

Values of the constants K'' and n'' can be obtained in terms of the constants b', c', T_f^* and Σ_f^* as

$$K'' = T_f^*/(\Sigma_f^*)^{n''} \tag{3.14}$$

and

$$n'' = b'/c' \quad . \tag{3.15}$$

For the values of the constants b', c', T_f^* and Σ_f^* given in Table 3.4, the values for K'' and n'' are obtained as

$$K'' = 1{,}165 \text{ MPa} \qquad \text{and} \qquad n'' = 0.0745 \quad . \tag{3.16}$$

Table 3.4 compares the different K'' and n'' obtained from the three different procedures discussed in this chapter. The agreement between the two sets of values obtained from the constant amplitude tests is quite good, although these values differed significantly from the results obtained from the incremental step tests.

Constant Amplitude Stress Cycling With Hold Times

This test series was comprised of eight specimens subjected to constant amplitude cyclic stress control with hold times. A stress rate of 6.00 MPa/sec was employed for all tests, which were fully reversed, i.e., $T_{min}/T_{max} = -1.0$. The test results are summarized in Table 3.5. The hold times were applied at peak load for 30 minutes, with the exception of Specimens 39 and 59, which were held for 15 minutes. Specimens 51 and 52 were cycled under engineering stress control which resulted in a net positive cyclic creep strain. This behavior was manifested by a shift in the hysteresis loops toward increasing tensile strain and is often called ratcheting. The ratcheting phenomenon was more pronounced for Specimen 52, which was stressed at $\pm$ 800 MPa, than for Specimen 51, which was stressed at $\pm$ 725 MPa. Subsequently, control of the hold time tests was altered such that the same true stress was achieved at the beginning of each hold period. This modification of the testing procedure minimized the ratcheting problem.

The cyclic life of these eight specimens is plotted as a function of the half-life total strain amplitude in Fig. 3.12. These results are in good agreement with the baseline low cycle fatigue curve obtained under constant strain amplitude cycling. All of the results except one (Specimen 52) show slightly greater lives than indicated by the solid line obtained from Fig. 11. The lives of Specimens 51 and 52 appear to have been shortened by cycling under engineering stress control, which is not surprising since it results in the application of a higher cyclic load for a given stress quantity.

Another objective of this test series was to determine whether the application of hold times had any influence on the fatigue life. Since the test data from this series was in good agreement with the strain controlled results, it was tentatively concluded that the hold times did not significantly influence

the fatigue life. Another indication of this is provided by comparing the results of the two tests subjected to 15 minute hold times to 30 minute hold time tests at the same applied stress level. These comparisons reveal very little differences in life, with the lives of the 15 minute hold time tests longer in one case and shorter in the other. However, both results are within the normal scatter range of other tests having identical hold times and stress levels. These results thus lead to the conclusion that the hold times employed in this testing program do not exert a significant influence on the fatigue life.

Table 3.1 Chemical Composition and Heat Treatment for Ti-6Al-4V ELI.

Chemical Composition

Al	V	C	N	Fe	O	H (PPM)	Y (PPM)	Ti
6.0	3.7	0.02	0.012	0.08	0.082	54	<50	balance

Heat Treatment (β annealed)

1. Soak at 1057°C (1835°F) for 1/2 hour.
2. Air cool to room temperature.
3. Soak at 732°C (1350°F) for 2 hours.
4. Air cool to room temperature.

β transus temperature = 974 ± 8°C (1785 ± 15°F)

Table 3.2 Mechanical Properties of Ti-6Al-4V ELI.

Modulus of elasticity, E = 121 GPa (17.6×10^3 ksi)
Yield strength (0.2% offset), Y_t = 803 MPa (116 ksi)
Ultimate strength, U_t = 884 MPa (122 ksi)
True fracture ductility, Σ_f = 0.252
Reduction in area at fracture (percent), RA = 22.3
Strength coefficient, K' = 982 MPa (142 ksi)
Strain hardening exponent, n' = 0.032

Table 3.3 Summary of Constant Strain Amplitude Fatigue Results.

(a) Constant Amplitude Strain Control Fatigue Data

Specimen No.	$\Delta\Sigma/2$	$\overline{T}^t$ (MPa)	$\overline{T}^c$ (MPa)	$\Delta\overline{T}/2$ (MPa)	$2N_{10\%}$	$2N_{75\%}$
23	.003	432	288	363	1,190,000	1,200,000
22	.0035	453	379	416	288,000	234,000
4	.004	-	-	471	87,600	89,800
27	.004	521	435	478	51,700	52,100
2R	.005	618	566	592	15,500	16,600
25	.005	580	610	590	19,900	21,800
18	.0072	-	-	677	2,000	2,200
7R	.0075	738	782	760	1,740	2,010
13	.0075	713	735	724	1,780	2,420
6R	.01	763	810	787	-	602
26	.01	712	713	721	238	616
32	.015	800	830	815	148	158
33	.015	800	850	825	88	102

Note: $\overline{T}/2$ represents the half-life values typically reported.

(b) Summary of Constant Amplitude Constants

c', Bilinear Fatigue Ductility Exponent	-.615
Σ_f^*, Bilinear Fatigue Ductility Coefficent	.168
b', Bilinear Fatigue Strength Exponent	-.0458
T_f^*, Bilinear Fatigue Strength Coefficient	1,020 MPa (148 ksi)
b", Bilinear Fatigue Strength Exponent	-.122
T_f^{**}, Bilinear Fatigue Strength Coefficient	1,960 MPa (284 ksi)
2N*, Bilinear Transition	5,300

Table 3.4 Cyclic Stress-Strain Properties Obtained by Three Methods.

Test Method	K"	n"
Obtained from incremental step test	1433 MPa (208 ksi)	0.104
Obtained from stable cyclic stress-strain curve	1105 MPa (160 ksi)	0.0655
Obtained from Eqs. (3.13) and (3.14)	1165 MPa (191 ksi)	0.0745

Table 3.5 Stress Control Hold-Time Test Results.

Specimen No.	T_{hold} (MPa)	$\Delta\bar{\Sigma}/2^+$	$\Delta\bar{\Sigma}\ /2^+$	$(\Sigma_c^T + \Sigma_c^C)/2^+$	$2N_f$ (Reversals)
54	±700	.0078	.0024	.0022	1,190
59*	±700	.0073	.0017	.0015	1,242
51	±725	.0093	.0035	.0032	660
55	±725	.0086	.0027	.0026	820
53	±750	.0100	.0040	.0038	566
39*	±750	.0110	.0049	.0038	338
52	±800	.0152	.0086	.0081	56
61	±800	.0146	.0080	.0051	116

$^+$Reported strains are half-life values.

*15 minute hold time, all other hold times are 30 minutes.

IV. DETERMINATION OF MATERIAL PARAMETERS FOR THE CONSTITUTIVE EQUATIONS

In the absence of high temperatures, six material constants {n,K,b, q,c,a} are needed to completely specify the viscoplastic constitutive equations for the material, Ti-6Al-4V Super ELI. The material characterization tests discussed and summarized in Section III were designed and performed at the University of Illinois (Urbana), and were not specifically tailored for determination of these material parameters. Nevertheless, it was possible to determine the values for each of the constants from the test data that were available. It should be noted however, that the methods described herein to evaluate the six constants should not be considered to be unique.

Determination of Constants a and c.

From a series of strain-controlled cyclic loading tests at constant strain rate for which cyclic stabilization has taken place, a cyclic stress-strain curve can be drawn through the peaks of the stabilized hysteresis loops [4.1]. During the stabilized phase of the load cycling, the isotropic hardening variable approaches a fixed value $R(\Sigma'') = q$, [cf. Fig. 2.1]*, so that use of Eqs. (2.18) and (2.19) allows the viscoplastic stress-strain relation to be written in the form

$$T = a(1 - e^{-c\Sigma''}) + q + K(\dot{\Sigma}'')^{1/n} \quad , \tag{4.1}$$

for which

$$\frac{dT}{d\Sigma''} = a\,c\,e^{-c\Sigma''} \quad , \tag{4.2}$$

*That this is actually so is shown subsequently.

along the curved portion (inelastic strain range) of the cyclic stress-strain curve. The logarithm of this equation gives

$$\ell n\left(\frac{dT}{d\Sigma''}\right) = A - c\Sigma'' \qquad A = \ell n(ac) \quad , \tag{4.3}$$

which represents a straight line on a semi-log plot, where c represents the value of the slope and A the vertical (log) axis intercept. This expression allows determination of the values of the constants a and c from stabilized cyclic stress-strain experimental data.

From constant strain amplitude fatigue test data, the cyclic stress-strain curve for Ti-6Al-4V was determined [cf. Fig.3.10], and modeled by the Ramberg-Osgood formula

$$\Sigma = \Sigma' + \Sigma'' = \frac{T}{E} + \left(\frac{T}{K''}\right)^{1/n''} \tag{4.4}$$

The elastic modulus E = 121,400 MPa, and the cyclic strength and hardening exponent have the values K" = 1,105 MPa and n" = 0.0655. For the inelastic portion of the cyclic stress-strain curve, that is, for the strain range $0.004 \leq \Sigma'' \leq 0.017$, where the lower bound is the strain at the proportional limit, and the upper bound is the strain at the ultimate strength of Ti-6Al-4V for monotonic loading, it follows that

$$T = 1{,}105(\Sigma'')^{0.0655} \tag{4.5}$$

and

$$\frac{dT}{d\Sigma''} = 72.4(\Sigma'')^{-0.9345} \quad . \tag{4.6}$$

The above empirical representation of the slope of the cyclic stress-strain curve (corresponding to stabilized cyclic test data) can be used to calculate values of $\ell n(dT/d\Sigma'')$ versus Σ''. The tabulated values shown below are plotted

in Fig. 4.1, from which the values of a and c can be determined to be a = 163.6, c = 134.6.

Σ''	$dT/d\Sigma''$ = Eq. (4.6)	$\ell n(dT/d\Sigma'')$
0.0033	1.509×10^4	9.62
0.0049	1.042×10^4	9.25
0.0072	7.260×10^3	8.89
0.0105	5.104×10^3	8.54
0.0152	3.619×10^3	8.19

Substitution of the values of a and c into the viscoplastic expression (4.2) gives

$$\frac{dT}{d\Sigma''} = 2.202 \times 10^4 \, e^{-(134.6)\Sigma''} \tag{4.7}$$

A comparison of the plots of Eqs. (4.6) and (4.7) over the appropriate inelastic strain range is shown in Fig. 4.2.

Determination of Constants n and K.

Referring to Eqs. (2.18) or (2.19) and Fig. 2.3, it is apparent that the material constants n and K characterize the rate dependency of the material behavior. Room temperature primary creep data may be used to evaluate these parameters. In Section III it was shown by means of the Bailey-Norton creep law that the creep rate associated with primary creep for Ti-6Al-4V at room temperature can be empirically expressed in strain-hardening form by the relation [cf. Eq. (3.6)]

$$\dot{\Sigma}'' = 0.37\left(\frac{T_H}{803}\right)^{50.4} (\Sigma'')^{-1.70} , \tag{4.8}$$

where T_H = 771.7 MPa is the hold stress at which the test was run. The strain rate in Eq. (4.8) is expressed in percent per hour. Taking the logarithm of both sides of this expression leads to the relation

$$\ell n(\dot{\Sigma}'') = -2.98 - 1.70\ell n(\Sigma'') . \tag{4.9}$$

For a tensile creep test run at a hold stress of T_H, the viscoplastic description of the creep strain rate is given by

$$\dot{\Sigma}'' = \left(\frac{T_H - Y - R}{K}\right)^n , \tag{4.10}$$

with

$$Y = a(1 - e^{-c\Sigma''}) = 163.6(1 - e^{-134.6\Sigma''}) . \tag{4.11}$$

As the monotonic creep deformation takes place at the fixed stress T_H, any hardening that occurs will be assumed to be essentially kinematic, in other words, that isotropic hardening can, in a first approximation, be assumed to be negligible. The results of the cyclic load tests with hold stress indicate that primary creep deformation does not occur when the hold stress level is less than about 80% of the tensile proportional limit (which for Ti-6Al-4V is approximately 630 MPa). The assumed fixed value for R to be used in Eq. (4.10) can therefore be taken to equal R = (0.80)(630) = 504 MPa. With T_H = 771.7 MPa, the viscoplastic creep strain rate, Eq. (4.10) becomes

$$\dot{\Sigma}'' = \left\{\frac{104.1 + 163.6\ e^{-134.6\Sigma''}}{K}\right\}^n . \tag{4.12}$$

This equation can be expressed in logarithmic form as

$$\ell n(\dot{\Sigma}'') = n\,\ell n\,(104.1 + 163.6\ e^{-134.6\Sigma''}) - n\,\ell n\,K . \tag{4.13}$$

The empirical and theoretical logarithmic expressions for the creep strain rate, Eqs. (4.9) and (4.13), respectively, can now be used to evaluate the constants n and K. Figure 3.3 of Section III, (monotonic creep test data), shows that for a hold stress at 770 MPa, an upper bound for the primary creep strain can be taken at approximately 2%.

For creep strains of 0.01% and 2.0% the corresponding empirical creep strain rates calculated by means of Eq. (4.9) are

$$\Sigma'' = 0.0001 \quad , \quad \dot{\Sigma}'' = 127.91 \text{ percent/hr.} = 3.6\text{x}10^{-4} \text{ in/in/sec.}$$

$$\Sigma'' = 0.0200 \quad , \quad \dot{\Sigma}'' = 0.0157 \text{ percent/hr.} = 4.4\text{x}10^{-8} \text{ in/in/sec.}$$

Substitution of each of these sets of creep strain and strain rate values into Eq. (4.13) yields two equations for the unknowns n and K, from which, when solved, give

$$n = 8.5 \quad , \quad K = 581 \text{ MPa} .$$

Determination of Constants q and b.

The constants b and q appearing in the expression for the isotropic hardening variable R, here written in the log form

$$\ell n(R - q) = \ell n(R_o - q) - bp \tag{4.14}$$

where $R_o = Y_t$ is the uniaxial tensile yield stress, can be evaluated from cyclic loading tests which demonstrate the cyclic hardening or softening characteristics of the material. Table 4.1 shows cyclic hysteresis loop test data for several different load cycles. These data were obtained from constant strain amplitude cyclic tests where the strain range $\Delta\Sigma/2 = 0.01$ and the strain rate $\dot{\Sigma}'' = 0.005 \text{ sec}^{-1}$. The test data from Table 4.1 enable construction of Table 4.2, which shows the stress and corresponding inelastic strain of the positive stress-strain quadrant of the hysteresis loop for the associated load cycle, as well as the accumulated inelastic strain p [cf. Eq. (2.14)]. To calculate p it was necessary to make the assumption that the tensile part of the inelastic strain enclosed by a hysteresis loop is approximately equal to the compressive part. (Examination of Table 4.1 shows that over the first thirty or so load cycles this assumption involves

Table 4.1 Constant Strain Amplitude Cyclic Hysteresis Loop Test Data for Specimen TI-6Al-4V, No. 26*.

Cycle #1		
MAX STRAIN, MIN STRAIN	9.93649E-03	-8.83243E-03
MAX STRESS, MIN STRESS	839.619	-906.06
ZERO STRAIN STRESSES	0	0
ZERO STRESS STRAINS	0	0
Cycle #2		
MAX STRESS, MIN STRAIN	9.96580E-03	-0.0100147
MAX STRESS, MIN STRESS	857.301	-851.407
ZERO STRAIN STRESSES	517.06	-271.657
ZERO STRESS STRAINS	-5.39326E-03	2.60381E-03
Cycle #4		
MAX STRAIN, MIN STRAIN	9.95603E-03	-9.97557E-03
MAX STRESS, MIN STRESS	847.656	-845.513
ZERO STRAIN STRESSES	334.347	-278.355
ZERO STRESS STRAINS	-2.85295E-03	2.60381E-03
Cycle #8		
MAX STRAIN, MIN STRAIN	9.95603E-03	-9.95603E-03
MAX STRESS, MIN STRESS	823.545	-826.224
ZERO STRAIN STRESSES	344.528	-293.893
ZERO STRESS STRAINS	-3.02882E-03	2.79922E-03
Cycle #16		
MAX STRAIN, MIN STRAIN	9.95603E-03	-9.97557E-03
MAX STRESS, MIN STRESS	790.86	-805.863
ZERO STRAIN STRESSES	352.565	-316.13
ZERO STRESS STRAINS	-3.22423E-03	2.98974E-03
Cycle #32		
MAX STRAIN, MIN STRAIN	9.92672E-03	-0.0100537
MAX STRESS, MIN STRESS	759.783	-780.68
ZERO STRAIN STRESSES	354.708	-339.438
ZERO STRESS STRAINS	-3.37078E-03	3.32193E-03
Cycle #64		
MAX STRAIN, MIN STRAIN	9.94626E-03	-0.0100537
MAX STRESS, MIN STRESS	729.777	-747.459
ZERO STRAIN STRESSES	361.942	-348.278
ZERO STRESS STRAINS	-3.57108E-03	3.53200E-03
Cycle #128		
MAX STRAIN, MIN STRAIN	9.95603E-03	-9.96580E-03
MAX STRESS, MIN STRESS	712.631	-731.921
ZERO STRAIN STRESSES	375.605	-347.207
ZERO STRESS STRAINS	-3.80068E-03	3.56131E-03
Cycle #256		
MAX STRAIN, MIN STRAIN	9.96580E-03	-0.0100342
MAX STRESS, MIN STRESS	695.485	-716.382
ZERO STRAIN STRESSES	352.297	-342.652
ZERO STRESS STRAINS	-3.78603E-03	3.56619E-03

*Amplitude of Test: .01 10% Load Shed 119.5 Failure 308.5

some small error, which becomes very small thereafter.) The accumulated inelastic strain for each hysteresis loop is equal to twice the inelastic strain within the loop.

Table 4.2 Cycle Number, Maximum Tensile Stress Amplitude and Accumulated Inelastic Strain.

Cycle No.	Max. Tensile Stress Amplitude MPa	Max. Total Tensile Strain Amplitude $x10^{-3}$	Tensile Inelastic Strain $x10^{-3}$	Accumulated Inelastic Strain p
1	839.619	9.93649		
2	857.301	9.96580	2.60381	0.0209
4	847.656	9.95603	2.60381	0.0423
8	823.545	9.95603	2.79922	0.0865
16	790.860	9.95603	2.98974	0.1797
32	759.783	9.92672	3.32193	0.3835
64	729.777	9.94626	3.53200	0.8258
128	712.631	9.95603	3.56131	
256	695.485	9.96580	3.56619	

A plot of the maximum tensile stress amplitude versus the accumulated inelastic strain, Fig. 4.3, indicates cyclic softening of the Ti-6Al-4V alloy with inelastic strain accumulation.

Determination of, in this case, the lower cyclic softening limit value of R = q, [cf. Fig. 2.1], requires an experimental construction of the R vs. p curve from the cyclic stress-strain data. To illustrate the procedure involved the calculation for load cycle No. 4 will be used. Fig. 4.4 shows the hysteresis loop for this cycle. From Eq. (2.18)

$$R = T - Y - K(\dot{\Sigma}'')^{1/n} \tag{4.15}$$

Referring to Fig. 4.4, for the load segment OA with load reversal at point A, $Y_o = \Sigma''_o = 0$ and s = 1 in Eq. (2.17), so that with $\Sigma''_A = 2.60x10^{-3}$ [cf. Table 4.2], a = 163.6, c = 134.6,

$$Y = a(1 - e^{-c\Sigma''}) = 163.6\left[1 - e^{-134.6(2.60\times10^{-3})}\right] = 48.32 \qquad (4.16)$$

Since for these cyclic tests the constant strain amplitude $\Delta\Sigma/2 = 0.01$ and the strain rate $\dot{\Sigma}'' = 0.005\ \text{sec}^{-1}$, the time for completion of the load reversal AD in Fig. 4.4 is 0.02/0.005 = 4 sec., and the time taken to load from points O to A is thus approximately 2 sec. The inelastic strain rate in loading from point O to point A is $\dot{\Sigma}''_A = 2.60\times10^{-3}/2 = 1.30\times10^{-3}\ \text{sec}^{-1}$. At point A $T_A = 847.7$ MPa. With K = 581 MPa and n = 8.5 the value of R at point A for load cycle No. 4 is

$$R = 847.7 - 48.32 - 581(1.30\times10^{-3})^{1/8.5} = 533.5\ \text{MPa} .$$

The associated value of the accumulated inelastic strain p, gotten from Table 4.2, is p = 0.0423.

Similar calculations determining the values of R and p for load cycles 8, 16, 32 and 64 allow for construction of Fig. 4.5, which determines the isotropic cyclic softening stabilization value at $q \cong 400$ MPa. With $R_o = Y_t = 630$ MPa, the logarithmic Eq. (4.14) becomes

$$\ell n(R - 400) = \ell n(630 - 400) - bp = 5.44 - bp . \qquad (4.17)$$

Using the values of R and p from Fig. 4.5, a semi-log plot of Eq. (4.17) gives Fig. 4.6, from which the value of the constant b can be determined to be b = 4.8.

Modification of the Initial Set of Parameter Values

The full range of inelastic behavior characteristics of Ti-6Al-4V alloy that the Chaboche viscoplastic constitutive equations attempt to model include isotropic and kinematic hardening under monotonic and cyclic loading, strain rate effects, creep, and stress relaxation. The set of material

parameters needed to complete the viscoplastic characterization of the titanium alloy were determined to have the following initial set of values:

$a = 163.6$ MPa (23.7 ksi)

$c = 134.6$ MPa (19.5 ksi)

$n = 8.5$

$K = 581$ MPa (84.4 ksi)

$q = 400$ MPa (59.0 ksi)

$b = 4.8$

These values were calculated in pairs from the data provided by strain controlled cyclic load tests, and from room temperature primary creep tests. The parameters (a,c) characterize kinematic hardening and the Bauschinger effect, the parameters (n,K) characterize the rate dependency of the material response, and the parameters (b,q) are associated with isotropic hardening.

In determining the values of the parameter pairs, the test situations were such that one or several of the other parameters remained fixed, or did not enter into the calculation. However, several approximations and assumptions had to be introduced since all six parameters cannot possibly be measured simultaneously from the data of a single test, or from a series of tests of the same type. In determining the parameter pair (a,c), it was necessary to assume that cyclic stabilization had occurred and that the isotropic hardening variable R was therefore fixed at its saturation value. In determining the parameters (n,K) from creep tests, it was assumed that during primary creep all hardening was essentially kinematic, i.e., isotropic hardening was negligible, with the isotropic variable fixed at a stress level below which no creep had been observed to occur. In evaluating the parameters (b,q), it was concluded on the basis of cyclic hysteresis loop test data that it was reasonable to assume that the tensile part of the inelastic

strain was approximately equal to the compressive part. Furthermore, because of the interrelatedness of several of the physical processes involved, the parameters are not completely independent of one another. With these considerations in mind, the initial set of values shown above should be considered as a first approximation.

Figures 4.7 through 4.10 show predicted versus experimental curves for monotonic stress-strain, primary creep and stress relaxation, using the original set of material parameter values for the predicted calculations. The primary creep and stress relaxation responses are underpredicted, while the initial yield is overpredicted. A parameter value optimization procedure was next carried through by trial and error.

Several series of model parameter variations were carried out for the purpose of optimizing each parameter or pair of parameters in the model. Analytical predictions were compared with appropriate experimental results and each parameter or pair of parameters was then selected to optimize that particular material response. Since the parameters K and n play major roles in predicting the time-dependent deformation, these parameters were adjusted to provide an optimum fit to all of the creep and stress relaxation data. As a result of this procedure the value of K was decreased from 581 to 300 and the value of n was decreased from 8.5 to 8.0.

While the values of K = 300 and n = 8.0 fit the stress relaxation and creep data quite well, they tend to overpredict the creep rate. Thus the parameter c, which is a measure of the strain-hardening rate, was increased from 134.6 to 250. This change did not eliminate the overprediction of the initial creep rate, however it resulted in much better agreement with the subsequent creep behavior.

Two additional parameters b and q in Chaboche's theory model the cyclic hardening or softening behavior of the material. Thus data from hysteresis

loops and cyclically-stable stress-strain curves were used to modify the values for these parameters. The parameter q represents the size of the cyclically-stable yield surface. It was increased from 400 to 420 MPa, while the parameter b was decreased from 4.8 to 4.1. These two changes resulted in considerably better agreement between the theoretical and experimental results.

Thus an "optimal" set of values, that is a set which gives good predictions in an overall sense, was determined to be

a = 164 MPa (23.7 ksi)	c = 250 MPa (36.3 ksi)
K = 300 MPa (43.5 ksi)	n = 8.0
b = 4.1	q = 420 MPa (61.0 ksi)

With these values the ability of the Chaboche viscoplastic constitutive equations to describe the general inelastic mechanical behavior of Ti-6Al-4V at non-elevated temperatures is quite good, as demonstrated by Figures 4.11 through 4.16. Figure 4.16 shows the cyclic softening behavior of this alloy. Predictions of monotonic stress-strain curves over a range of strain rates were not made, because the University of Illinois test program did not provide test data that could be used for comparison purposes.

It was mentioned at the outset of this section that the manner by which the material parameter values were determined is not unique. The procedures adopted here were largely dictated by the types of test data that were made available to this research project after having been generated elsewhere for other purposes. It seems more desirable to be able to evaluate the material parameters from a "standard" set of test results, and work is presently underway to specify the necessary tests in such a standard data set.

V. LOW CYCLE FATIGUE LIFE PREDICTION

Equivalent Fully Reversed Cycles.

In order to assess fatigue damage from unsymmetric stress-strain cycles by means of baseline fatigue life data that is obtained from symmetric cycles, it is necessary to transform the unsymmetric stress-strain cyclic data into so-called 'equivalent fully reversed cycles' that are symmetric. Asymmetry of a stress-strain cycle can be caused by mean stress and/or by unequal tensile and compressive creep strains.

Previous studies have indicated the possibility of defining certain normalizing stress or strain parameters that reduce data from tests that are conducted at stress ratios other than unity, to a single relationship in which the effect of mean stress has been normalized. The common objective being the establishment of an equivalent fully reversed cyclic stress-strain that will result in the same fatigue life as that caused by the applied stress or strain coupled with mean stress. Several parameters have been proposed for this purpose [5.1-5.3], with the one developed by Smith, Watson and Topper having the distinct advantage of not having to depend upon any experimentally determined empirical constants. In all of these studies asymmetry of cyclic stress-strain induced by unequal creep deformations were not considered.

For time dependent material behavior in which cyclic loading with stress hold times appear, some creep deformation can be expected to appear in the stress-strain cycles during the hold time. It was found necessary, therefore, to use a modified form of the Smith-Watson-Topper equivalent fully reversed cycle relation. The modified relation that is used here states that for any i-th stress-strain cycle

$$\{T_{max}\left(\frac{\Delta\Sigma}{2}\right)E\}^{1/2} = \{(T)_{fr}\left(\frac{\Delta\Sigma}{2}\right)_{fr}E\}^{1/2} , \qquad (5.1)$$

that is, the quantity $\{T_{max}(\Delta\Sigma/2)\}$ from the i th test cycle having asymmetry of the stress-strain is equal to $\{(\Delta T)_{fr}(\Delta\Sigma/2)_{fr})\}$ for an equivalent fully reversed cycle (cf. Fig. 5.1). The left side of Eq. (5.1) is known (from the computed nominal stress-strain-time history). The right side consists of two unknowns that determine the equivalent fully reversed cycle. An additional equation is needed to allow for calculation of the two unknowns, and is provided by the viscoplastic constitutive relations (2.10)-(2.15). The viscoplastic constitutive equations however are expressed in terms of rates, consequently the rate form of Eq. (5.1) is needed, and can be shown to have the form

$$(\dot{\Delta T})_{fr} = \frac{T_{max}[\dot{\Delta T} + E\dot{\Delta\Sigma}''] - E(\Delta T)_{fr}(\dot{\Delta\Sigma}'')_{fr}}{2(\Delta T)_{fr} + E(\Delta\Sigma'')_{fr}} \qquad (5.2)$$

Referring to Figures 5.1, Figure (5.1a) shows the i th nominal stress-strain cycle ABCDA having a mean stress and tensile creep caused by a load hold time at T_{max}. Figure 5.1b shows the corresponding symmetric equivalent fully reversed cycle A'B'C'D'A', constructed such that Eq. (5.1) is satisfied at each point. Actually it is Eq. (5.2) and the viscoplastic constitutive equations that are solved simultaneously by time integration.

Cyclic Load Damage and Fatigue Life.

The baseline fatigue life test data for smooth Ti-6Al-4V specimens, shown in Figure 3.11, which were obtained from room temperature constant strain amplitude fully reversed tests with zero mean stress and no load hold times, is shown redrawn in Figure 5.2 in terms of total strain amplitude versus the number of observed load reversals to failure. Here failure is defined as

a 75% decrease in the cyclic load. An empirical two-parameter correlation of the data is given by the expression

$$\frac{\Delta\Sigma}{2} = C_1(2N_f)^{C_2} = 0.0474(2N_f)^{-0.240} \quad , \tag{5.3}$$

in which $\Delta\Sigma/2$ is the total strain amplitude and $2N_f$ is the number of load reversals to observable crack initiation.

The fractional fatigue damage caused by the i th load reversal is defined as the ratio

$$D_i = \frac{1}{(2N_f)_i} \quad , \tag{5.4}$$

where $(2N_f)_i$ is the number of load reversals to failure corresponding to the total strain amplitude $(\Delta\Sigma/2)_i$ at the i th load reversal. The baseline constant strain amplitude fatigue life test data correlation, Eq. (5.3), can be used to express the fractional fatigue damage in terms of the total strain amplitude at each load reversal, that is,

$$D_i = \left\{\frac{1}{C_1}(\Delta\Sigma/2)_i\right\}^{-1/C_2} \quad . \tag{5.5}$$

The total damage D_T is assumed to be a linear sum of the individual damage increments for each load reversal (Palmgren-Miner linear damage accumulation hypothesis).

$$D_T = \sum_{i=2} D_i = \sum_{i=2}\left\{\frac{1}{C_1}(\Delta\Sigma/2)_i\right\}^{-1/C_2} = 1 \quad , \tag{5.6}$$

that is, fatigue failure (as defined above) is supposed to occur when the sum D_T reaches the value of unity. There are several difficulties associated with this damage accumulation rule. One is the deviation from linear summation observed in some materials. Another is the fact that usually $D_T \neq 1$ at

the definition of failure. Despite these limitations, the rule is simple to apply and when used to predict crack initiation gives as good agreement with data as another cumulative damage rule for Ti-6Al-4V [5.4].

In actuality it is highly impractical, computationally speaking, to perform fatigue life predictions using Eq. (5.6), even for low cycle fatigue life. A linear extrapolation based upon a calculated fractional fatigue damage accumulation D_N involving 2N load reversals is used instead. The number of load cycles N must be sufficient, however, for cyclic stabilization to have taken place. The predicted number of load reversals $2N_f$ to failure is thus calculated by the ratio

$$\frac{2N_f}{D_T=1.0} = 2N_f = \frac{2N}{\sum_{i=2}^{N} D_i} \quad . \tag{5.7}$$

Low Cycle Fatigue Life Prediction For Constant Strain Amplitude Cyclic Loading Without Hold Time.

The objective here is to see how well the FATIQ computer program, which couples the viscoplastic constitutitve equations and the fatigue life prediction methodology, can, under the same loading conditions, predict several of the eleven baseline fatigue life data points. These constant strain amplitude, strain controlled fully reversed fatigue tests, without mean stress or hold times, were run on smooth test specimens that were load cycled with strain amplitudes ranging from 0.003 in/in to 0.015 in/in. Since the tests do not involve load hold times or mean stress, cumulative fatigue damage may be calculated directly, right after the net section stress-strain history for each load reversal has been determined. However, the fatigue data also provides an

opportunity to gain some measure of the capability of Eq. (5.2), since fatigue life computed from equivalent fully reversed symmetric cycles ought to be close to the fatigue life computed from symmetric nominal stress-strain cycles. Consequently, life predictions using both methods were performed.

Another important point that requires discussion indicates along what portion of a stress-strain cycle fatigue damage is presumed to occur. Figure 5.3a shows a typical strain control loading spectrum. Figure 5.3b shows the corresponding cyclic stress-strain for the first three load reversals (OA, ABC, CDE). No fatigue damage is assumed by the first load reversal OA. For the subsequent load reversals, an increment of fatigue damage D_i is assumed to take place in either tension or compression only for the portion of the stress-strain cycle where the stress rate, the stress and the total strain all have the same sign. (This is shown by the heavily drawn segments DE and BC of Figure 5.3b). Thus fatigue damage is computed and accumulated concurrently with the calculation of the hysteresis loop segments DE and BC, where equal damage is assumed for the tensile and compressive reversals of each closed hysteresis loop. Since the loop is symmetric the damage in the entire hysteresis loop is twice the damage of either loop segment DE or BC.

For the equivalent fully reversed cycle calculation, the nominal stress-strain history such as CDE of Fig. 5.3b is first calculated and stored in the computer program. Equation (5.2) is then used, along with the stored net section information, to obtain a fully reversed equivalent cycle such as CDEC of Fig. 5.3c. The fatigue damage increment is computed for a segment of the equivalent cycle which corresponds to the same 'damaged' portion of the net section stress-strain cycle, e.g., segment DE in Figure 5.3c corresponds to segment DE in Fig. 5.3b. The fatigue damage in segment DE is computed incrementally. Table 5.1 and Figure 5.4 shows the comparison between the measured and the predicted number of load reversals to crack initiation.

Table 5.1 Measured Versus Predicted Fatigue Life.

Strain Amplitude	Number of Load Reversals To Failure		
	Measured	Predicted Using Nominal Stress-Strain Cycles	Predicted Using Equivalent Cycles
0.0150	102 ; 158	120	150
0.0100	602 ; 616	654	893
0.0075	2,010 ; 2,420	2,169	3,406
0.0050	16,600 ; 21,800	11,749	37,415

The predicted life obtained using the nominal cycles in the low cycle range of large strain amplitudes are good. They underpredict the fatigue life at the smaller strain amplitudes. This is explained by Figure 5.2 which shows that the empirical correlation Eq. (5.3), which is incorporated into the fractional damage expression (5.5), underpredicts the fatigue life data as the strain amplitudes approach 0.005 in/in. An improvement in the predictive accruacy could be achieved by use of a bi-linear empirical correlation curve to cover the very small amplitude strain high cycle range. Predictions based on the equivalent cycle concept compare reasonably well with the experimental data at the larger strain amplitudes, and over predict fatigue life as the strain amplitudes assume smaller values.

Figure 5.4 shows that the predictive methodology here employed is more appropriate for application to the low cycle fatigue life region (less than 10^4 cycles) where the larger strain amplitudes include significant inelastic deformation.

Low Cycle Fatigue Life Prediction For Cyclic Loading With Mean Stress And Load Hold Time.

Eight stress-controlled fatigue tests which incorporated 15 minute and 30 minute stress hold times in tension and compression were performed. The

stress amplitudes ranged from ± 700 MPa (± 102 ksi) to ± 800 MPa (± 116 ksi). During the stress hold time periods primary creep deformation took place. All specimens were cycled to failure, which was defined as a 75% load drop-off (concurrent with the appearance of large cracks). Figure 5.5 shows the total strain amplitude versus the number of observed load reversals to failure for the eight tests. For purposes of comparison Eq. (5.3) which correlates the fatigue life data for tests without stress hold times, is also drawn on this figure. It shows that the creep deformation associated with the stress hold time periods appear to reduce the fatigue life somewhat, but not significantly.

Two approaches were used to predict the fatigue life of specimens subject to stress hold times. The first uses the equivalent cycle method to convert non-symmetric stress-strain cycles, caused possibly by means stress and/or unequal tensile and compressive creep strains, into equivalent fully reversed symmetric stress-strain cycles in the manner described earlier. The baseline relation, Eq. (5.3), for fatigue life tests having symmetric stress-strain cycles was used in the damage expression (5.5) and (5.7) to compute the predicted fatigue life.

The second method uses the Smith-Watson-Topper parameter $\{T_{max}(\Delta\Sigma/2)\}^{1/2}$, where T_{max} is the maximum tensile hold stress. It was evaluated for all stress hold time fatigue data points. A plot of the log of this expression versus the log of the number of load reversals to failure fall along a straight line, allowing the two-parameter correlation expression

$$\{T_{max}(\Delta\Sigma/2)\}^{1/2} = 7.362(2N_f)^{-0.162} \qquad (5.8)$$

as shown by Figure 5.6. This equation is then used to assess the fractional fatigue damage, Eq. (5.5), concurrently with the calculation of the nominal stress strain cycles.

Table 5.2 and Figure 5.7 illustrate the comparison between the observed and the predicted number of load reversals to failure against the stress amplitudes used for the tensile and compressive stress hold times.

Table 5.2 Measured Versus Predicted Fatigue Life With Stress Hold Times.

		Number Of Load Reversals To Failure		
Stress Amplitude MPa	Hold Period Minutes	Measured	Predicted Using Nominal Cycles With the SWT Parameter	Predicted Using Equivalent Cycles With Eq. (5.3)
± 800	30	56 ; 116	122	130
± 750	30	556	554	711
± 750	15	388	597	801
± 725	30	660 ; 820	980	1,434
± 700	30	1,190	1,609	2,800
± 700	15	1,242	1,679	3,079

The predicted fatigue lives calculated by the two techniques compare quite favorably with the measured fatigue lives and with each other in the higher stress amplitudes, and tend to overpredict fatigue life at the lower stress amplitudes. The predicted life results for 30 and 15 minute hold times at the ± 750 MPa and ± 700 MPa hold stress levels, are what one would expect, that is, with the longer hold times at a given hold stress level there should be more creep deformation per load cycle and thus more damage, leading to a shorter predicted life. The experimental data, however, shows the opposite, with longer life when the hold time is longer. No explanation for this seemingly anamolous data is currently available.

VI. CONCLUSIONS AND RECOMMENDATIONS

1. The Chaboche viscoplastic constitutive theory has been shown to be capable of describing a broad range of inelastic material behavior characteristics for uniaxial states of stress. These include monotonic stress-strain in the inelastic range of deformation, isotropic and kinematic hardening, variation of hardening (or softening) under cyclic loading, strain rate effects, creep with stress hold times and stress relaxation.

2. Initial values of the set of six material parameters were obtained from a test program that was performed elsewhere and not designed specifically for this purpose. These initial values were then modified to obtain an "optimum" fit to all of the experimental data that were available for comparison with predicted results.

3. With an optimum set of the viscoplastic material parameter values appropriate for Ti-6Al-4V determined, the Chaboche theory can adequately predict the monotonic and cyclic behavior of this alloy, including primary creep and stress relaxation.

4. The Chaboche viscoplastic constitutive relations when integrated into the current fatigue life prediction methodology (FATIQ computer program) appears to be successful, and provides an improved technique for low cycle fatigue life prediction of rate-dependent materials subject to cyclic loading with and without load hold times.

5. The effect of load hold times of thirty minute duration, or less, during the load cycling of Ti-6Al-4V alloy did not appear to have a

significant effect on the low cycle fatigue life, even though creep deformation during the load hold times was observed (and predicted). However the available test data was not considered to be sufficient to warrant any strong conclusions in this regard.

6. The choice of the tests to determine the viscoplastic material parameter values is not unique. It would be desirable therefore to be able to evaluate them from as small a number of simple test procedures as possible, even pointing toward a 'standard' set of tests. Some initial work has been done in this regard and appears to be promising. It would also be desirable, if possible, to develop a computerized material parameter value optimization scheme, since some of the parameter values are interdependent, to greater or lesser degree, and cannot be evaluated simultaneously from a single test, or from a series of one type of test.

7. Since cracks initiate most readily at notches, it seems appropriate now to apply the methodology developed here for fatigue life prediction of smooth rate-dependent material specimens to notched specimens. It should now be possible, for a given material, to predict reasonably well the stress-strain-time history of the material near the root of a notch under cyclic loading, either initially using the Neuber notch simulation technique, or by integration of the viscoplastic constitutive equations into a suitable finite element program for the notch geometry. This would represent the first part of the problem. Having this information, the FATIQ computer program could then be used to predict the low cycle fatigue life of time-dependent notched structural components.

8. The set of viscoplastic material constants of the Chaboche theory have also been determined for Inconel 100 at elevated temperatures from test data supplied by the Materials Laboratory, Wright-Patterson AFB. Since the viscoplastic material constants for this material described by the Bodner-Partum theory are also known, it should now be possible to make quantitative comparisons (against experimental data) of the uniaxial predictive capabilities of both theories over the range of inelastic material behavior characteristics.

9. For applications to high strain rate types of problems such as impact and penetration, it would be useful to explore the capability of the Chaboche viscoplasticity theory to predict inelastic material response at very high ranges of strain rates.

VII. REFERENCES

1.1 Wood, W.A., Instability of Titanium and Ti-6Al-4V alloy at Room Temperature, Tech. Report No. 45, Institute for the Study of Fatigue and Reliability, Dept. of Civil Engr. and Engr. Mech., Columbia University, New York, 1967.

1.2 Imam, M.A., and C.M. Gilmore, Fatigue and Microstructural Properties of Quenched Ti-6Al-4V, Metallurgical Trans., A, V. 14A, 233, (1983).

2.1 Eftis, J., and D.L. Jones, Evaluation and Development of Constitutive Relations for Inelastic Behavior, Final Technical Report, AFOSR, Washington, D.C. 1983.

2.2 Chaboche, J.L., Viscoplastic Constitutive Equations for the Description of Cyclic and Anisotropic Behavior of Metals, Bulletin De L'Academie Polanaise des Sciences, V. XXV, 33, (1977).

2.3 Chaboche, J.L., Description Thermodynamic et Phénomenologique de la Viscoplasticitie Cyclique avec Endomanagement, These de Doctorat, Paris, VI, 1978.

2.4 Chaboche, J.L., and G. Rousselier, On the Plastic and Viscoplastic Constitutive Equations - Part 1: Rules Developed With Internal Variable Concept, J. Pressure Vessel Technology, ASME, V. 105, 153, (1983).

3.1 Kurath, P., Extension of the Local Strain Fatigue Analysis Concepts to Incorporated Time Dependent Deformation in Ti-6Al-4V at Room Temperature, T.&A.M. Report No. 464, University of Illinois, February 1984.

3.2 Gelas, B., M. Arman, and R. Tricot, Low-Cycle Fatigue Behavior of Titanium Alloys, Revue Materiaux et Techniqes, Nr. 5, Special Aeronautique, pp. 3-15, 1975, translated by U.S.A.F., Report No. FTD-ID(RS)T-1478-79, 1979.

3.3 Evans, W.J., and C.R. Gostelow, The Effect of Hold Time on the Fatigue Properties of a β-Processed Titanium Alloy, Metallurgical Transactions A, Vol. 10A, pp. 1837-1846, 1979.

3.4 Hatch, A.J., J.M. Partridge, and R.G. Groadwell, Room Temperature Creep and Fatigue Properties of Titanium Alloys, Journal of Materials, Vol. 2, pp. 111-119, 1967.

3.5 Imam, M.A., and C.M. Gilmore, Room Temperature Creep of Ti-6Al-4V, Metallurgical Transactions A, Vol. 10A, pp. 419-425, 1979.

3.6 Katcher, M., Creep of Titanium Alloys, Metals Engineering Quarterly, American Society for Metals, pp. 19-27, 1968.

3.7 ASTM Standard E8-79. Standard Methods of Tension Testing of Metallic Materials, ASTM Book of Standards, Part 10, 1980.

3.8 Chu, H.P., Effect of Yield Strength on Room-Temperature Creep of Ti-6Al-2Cb-1Ta-1Mo Alloy, DTNSRDC Materials Department Report 4188, Feb. 1974.

3.9 Chu, H.P., A Comparison of Tensile and Compressive Creep of Ti-6Al-2Cb-1Ta-0.8Mo Alloy at Room Temperature, DTNSRDC Materials Department Report MAT-75-68, January 1976.

4.1 Landgraf, R.W., J. Morrow and T. Endo, Determination of the Cyclic Stress-Strain Curve, Journal of Materials, Vol. 4, pp. 176, 1969.

5.1 Morrow, J., Fatigue Properties of Metals, in Fatigue Design Handbook, Soc. Auto. Engrs, 1968.

5.2 Topper, T.H., and B. I. Sandor, Effects of Mean Stress and Prestrain on Fatigue Damage Summation, ASTM, STP 462, 1970.

5.3 Smith, C., P. Watson and T. H. Topper, A Stress Function for the Fatigue of Metals, Journ. Materials, Vol. 5, No. 4, 767, 1970.

5.4 Manson, S.S., Fatigue: A Complex Subject - Some Simple Approximations, Exper. Mech., Vol. 5, No. 7, 1965.

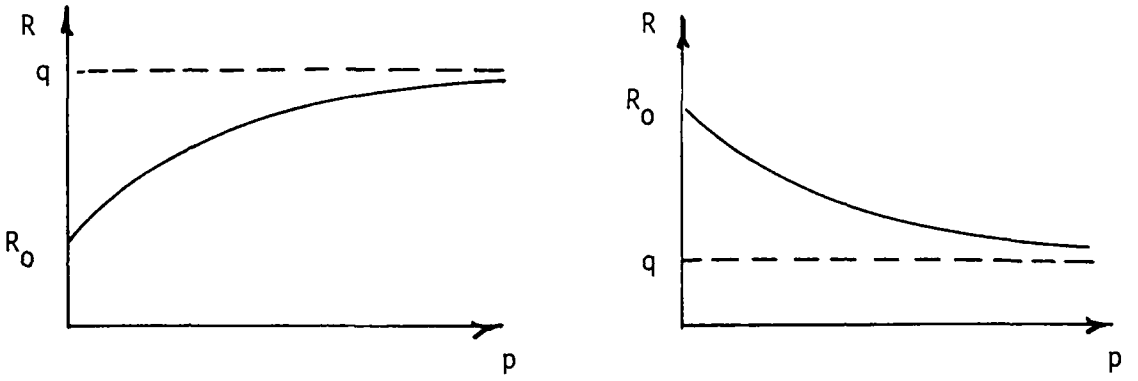

Fig. 2.1. Isotropic hardening and softening with cumulated plastic strain.

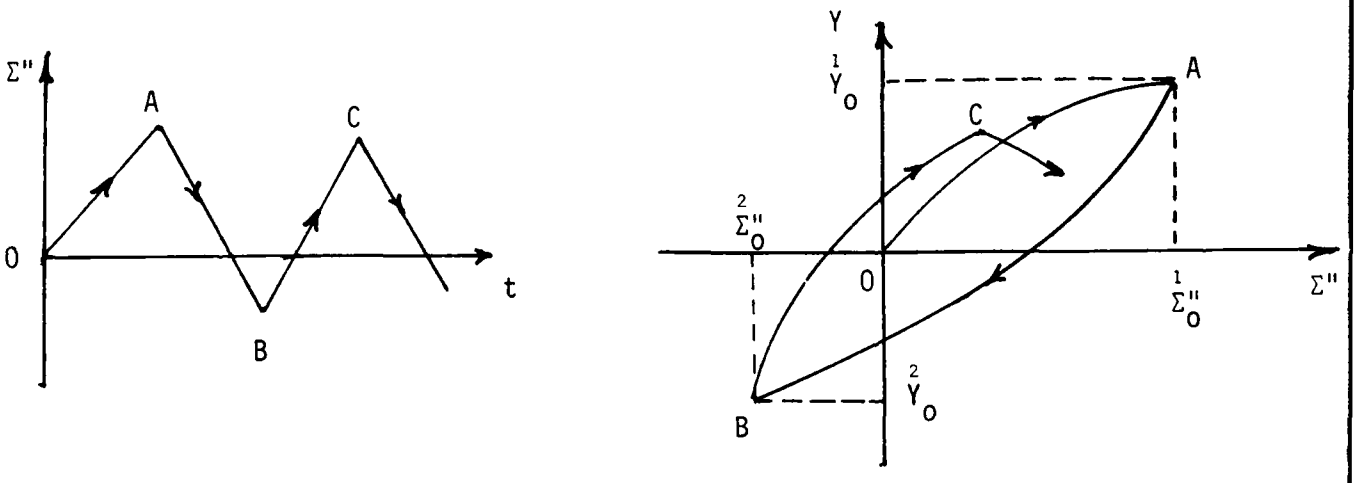

Fig. 2.2. Inelastic strain-time history and corresponding variation of the kinematic hardening variable.

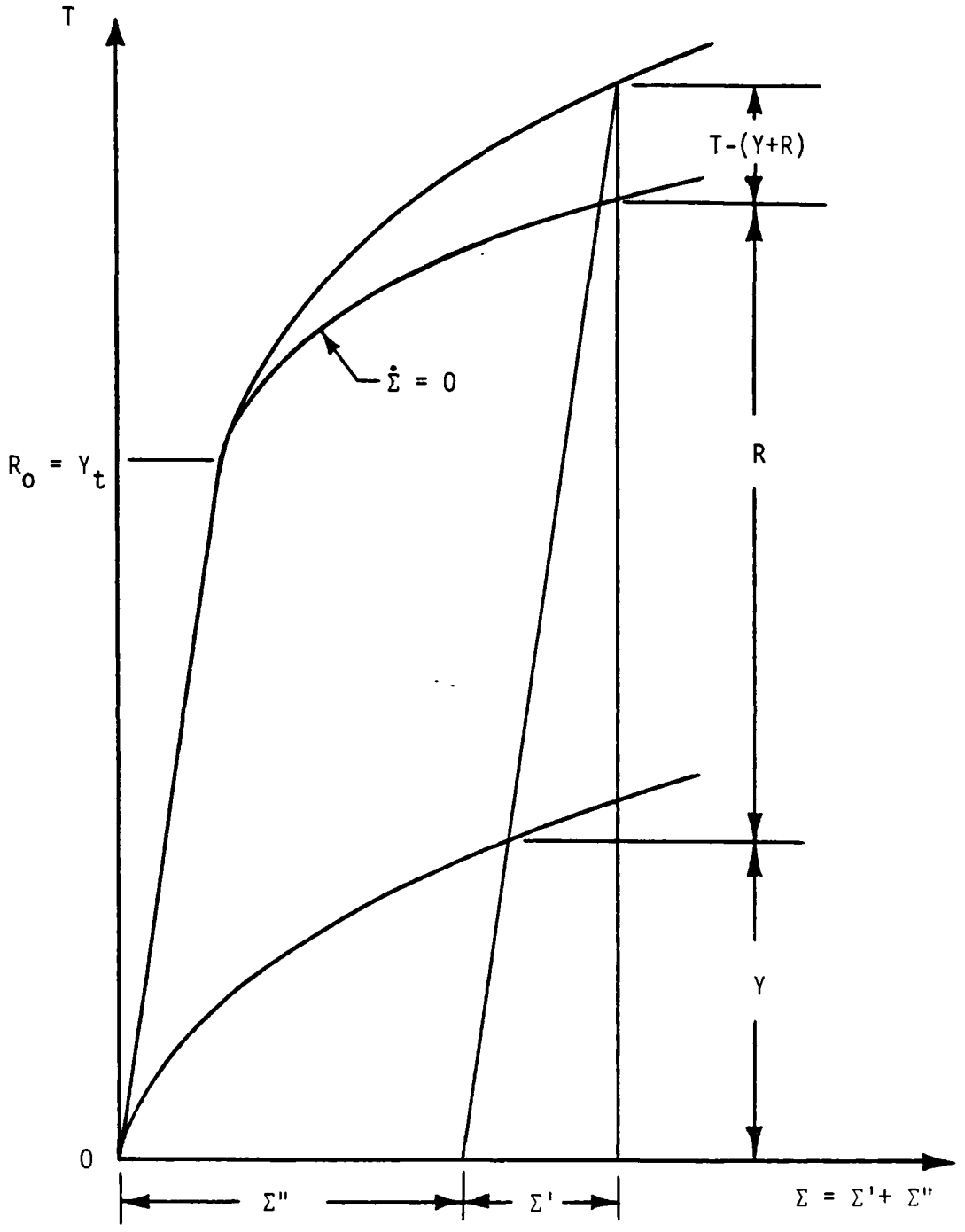

Fig. 2.3. Schematic decomposition of stress in tensile loading.

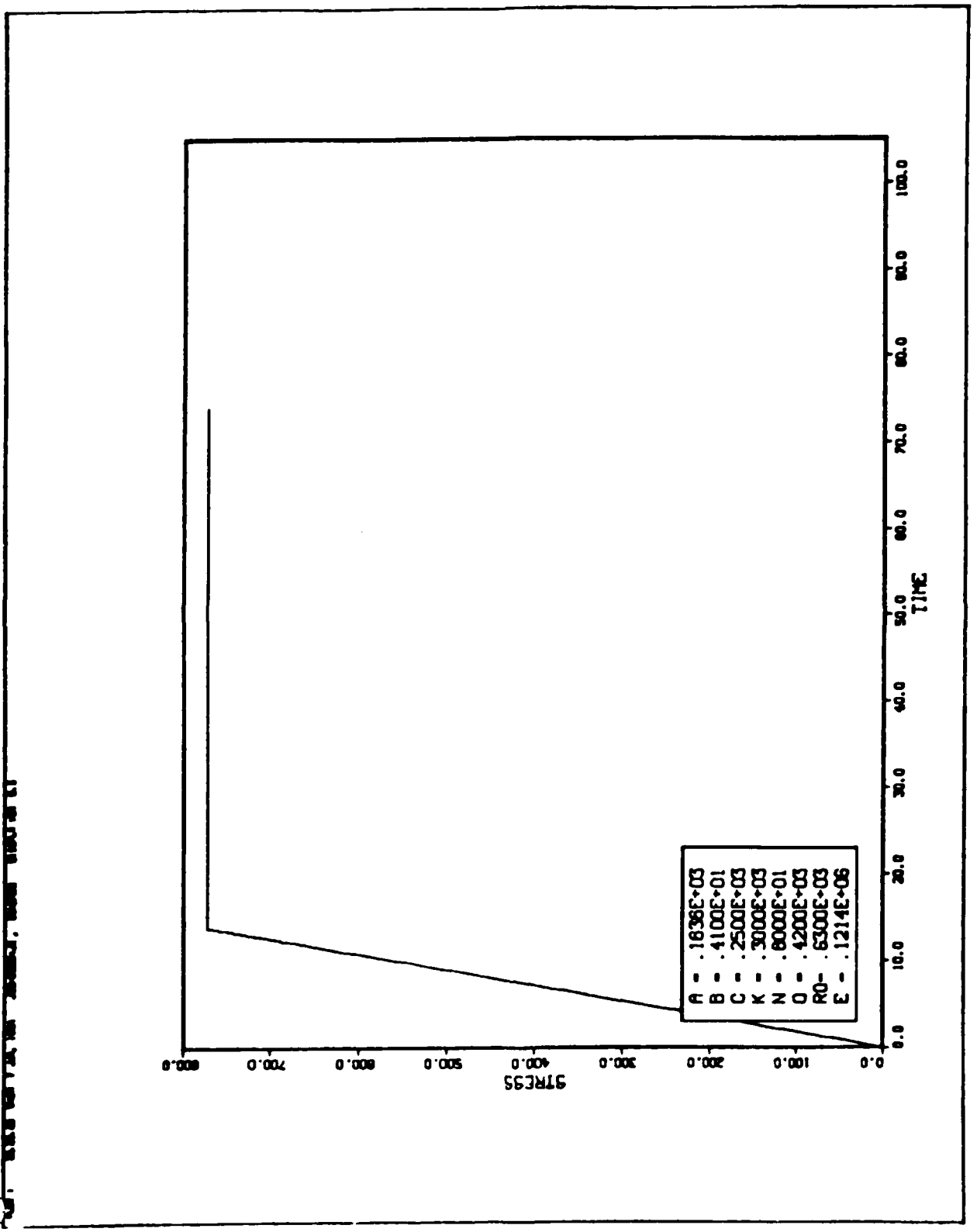

Fig. 2.4. Applied stress versus time for primary creep.

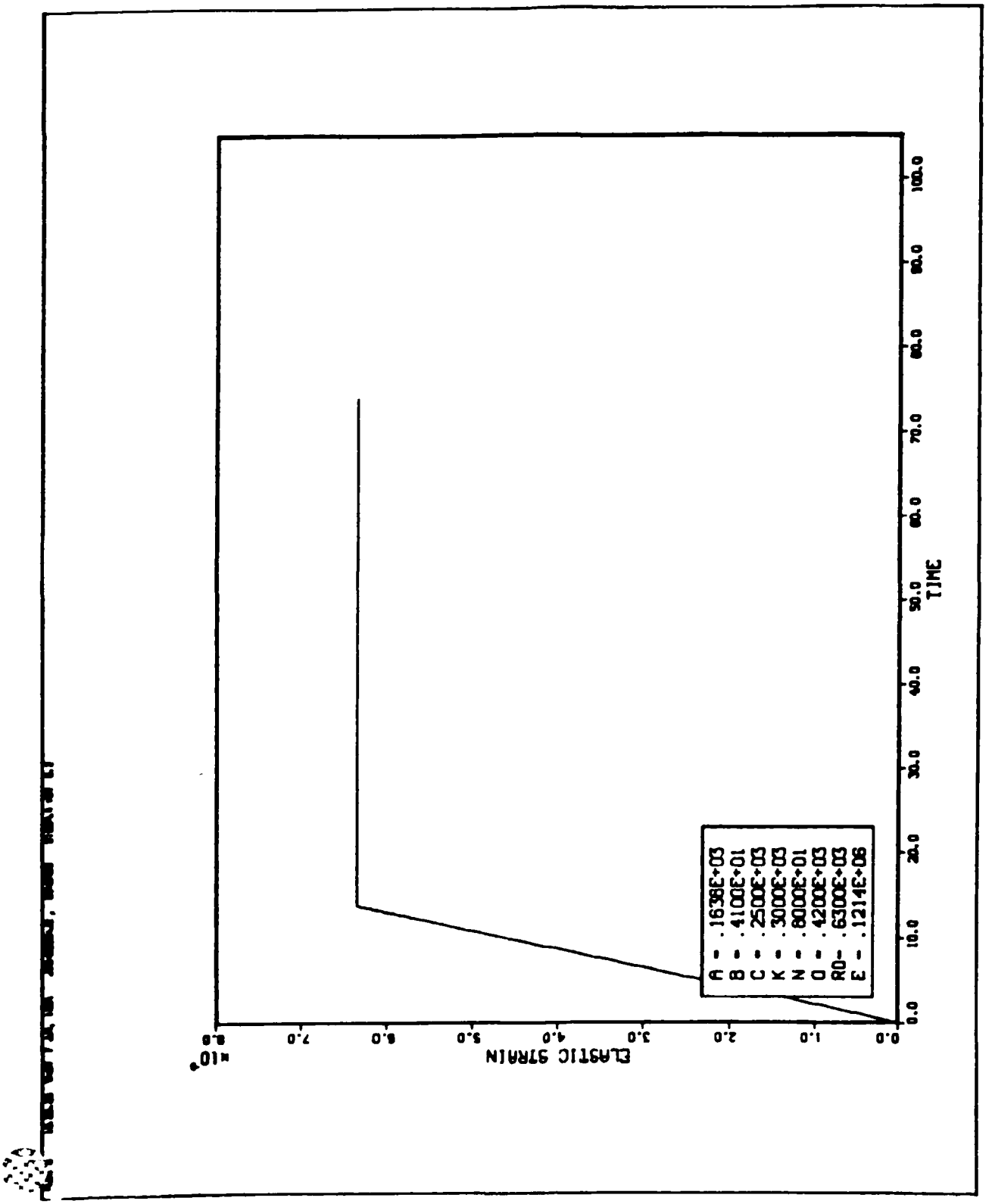

Fig. 2.5. Elastic strain versus time for primary creep.

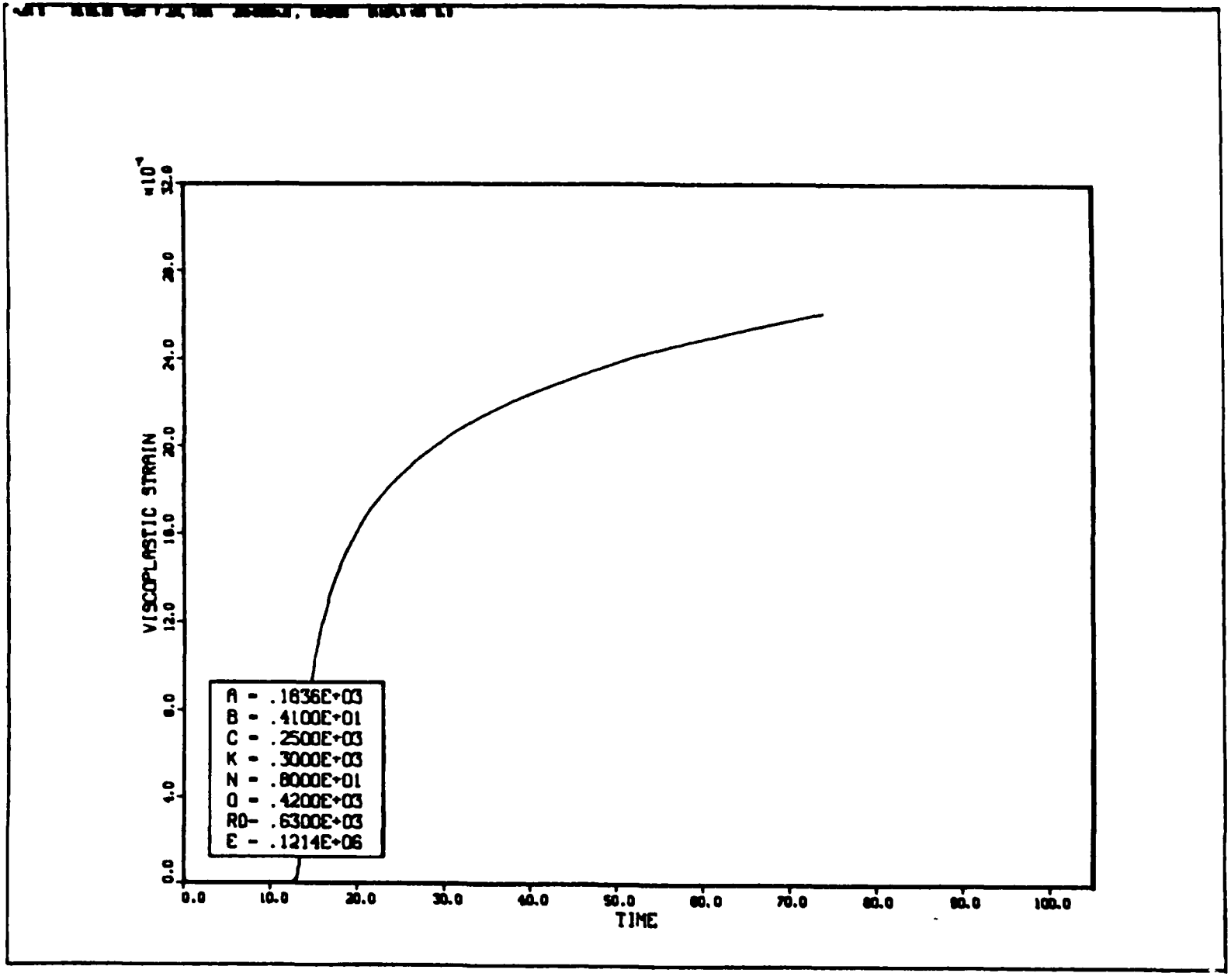

Fig. 2.6. Viscoplastic strain versus time for primary creep.

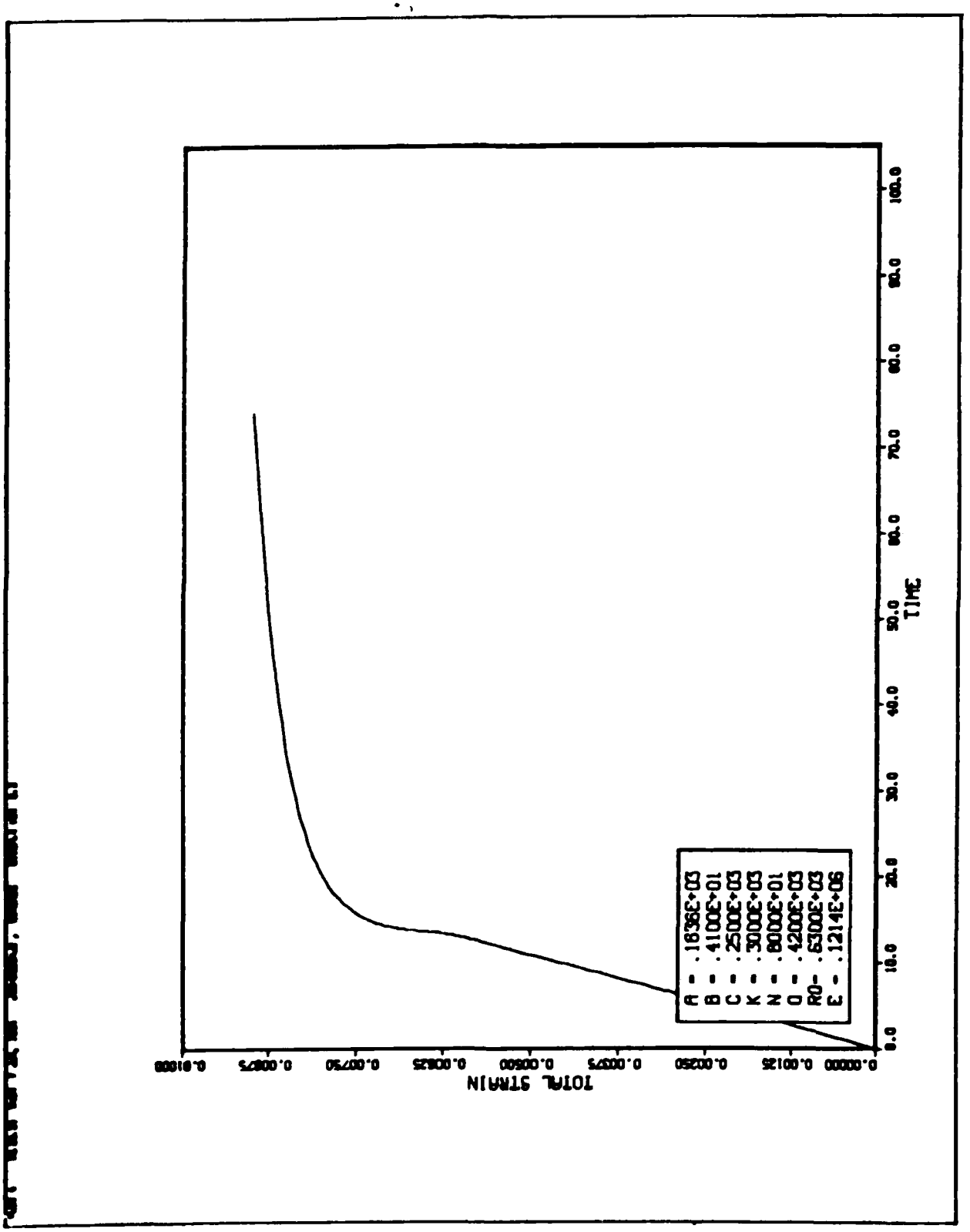

Fig. 2.7. Total strain versus time for primary creep.

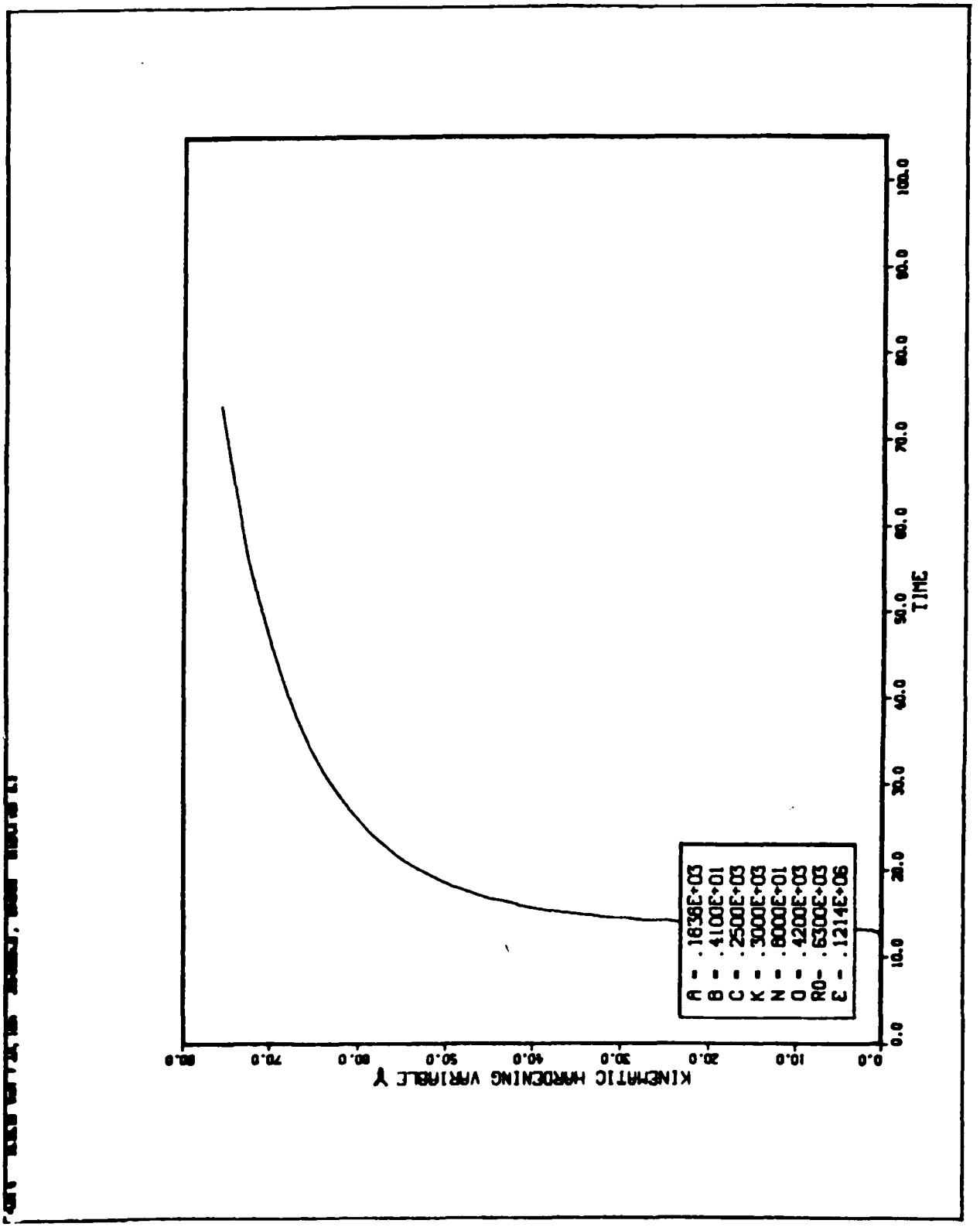

Fig. 2.8. Kinematic hardening variable versus time for primary creep.

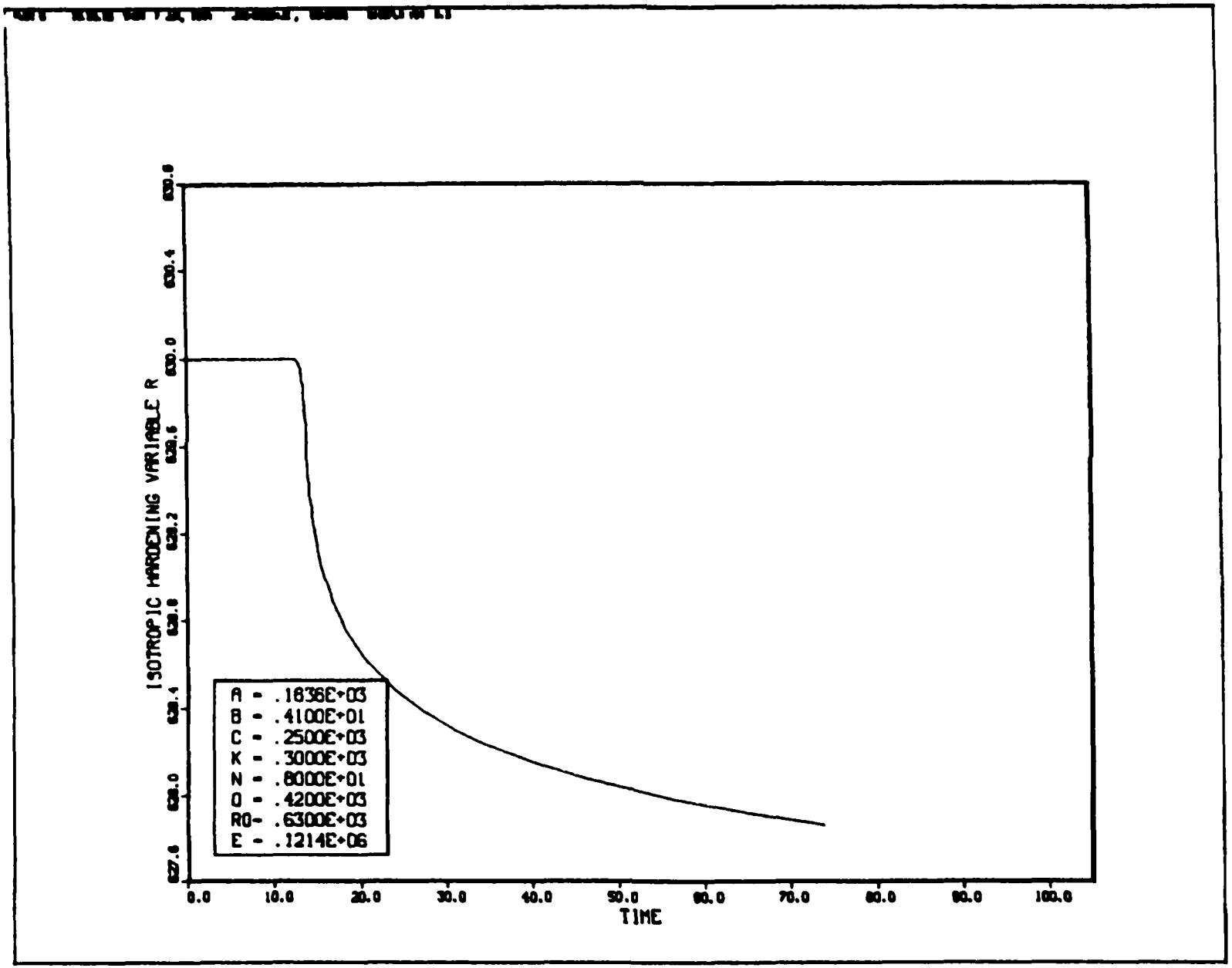

Fig. 2.9. Isotropic hardening variable versus time for primary creep.

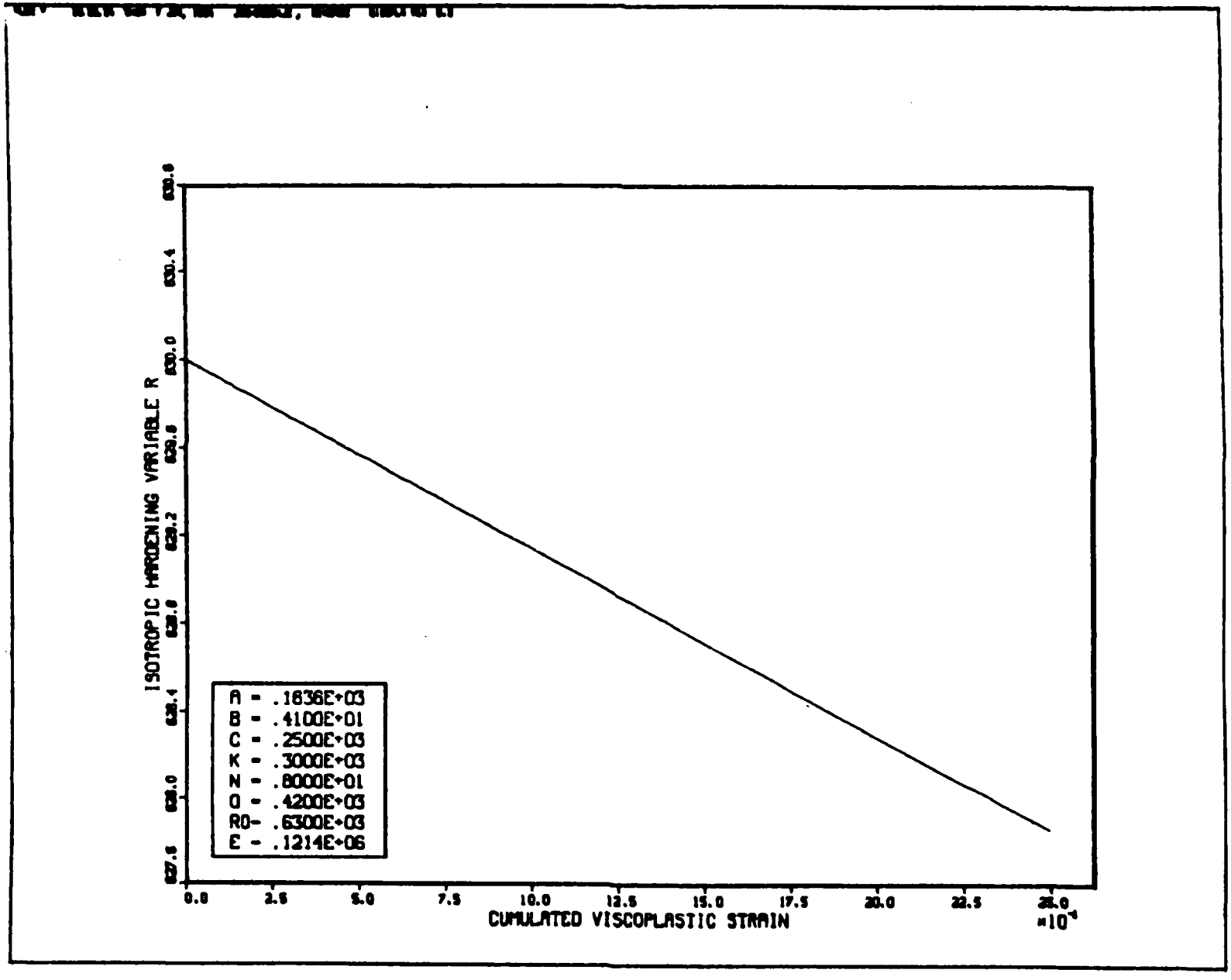

Fig. 2.10. Isotropic hardening variable versus accumulated viscoplastic strain for primary creep.

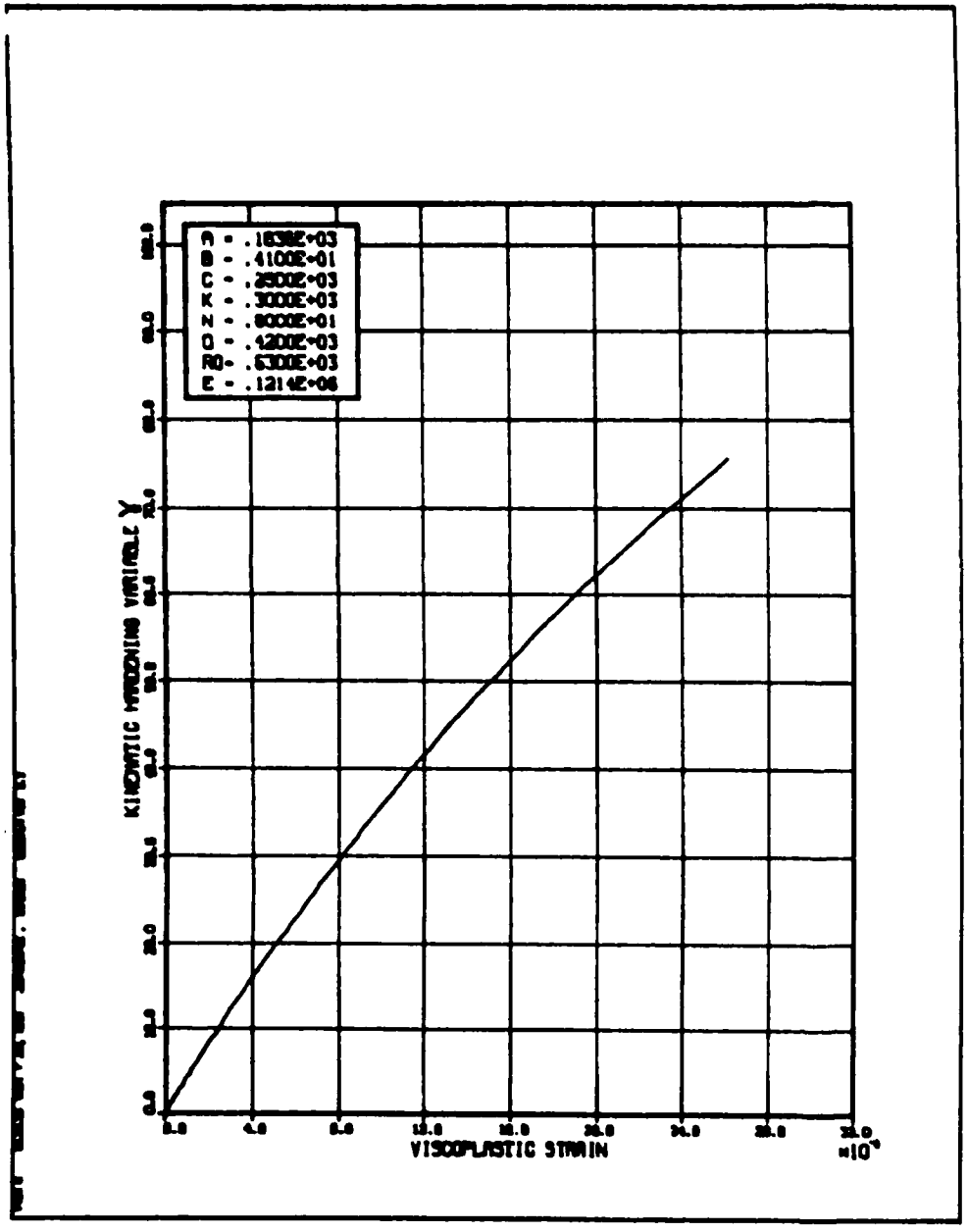

Fig. 2.11. Kinematic hardening variable versus viscoplastic strain for primary creep.

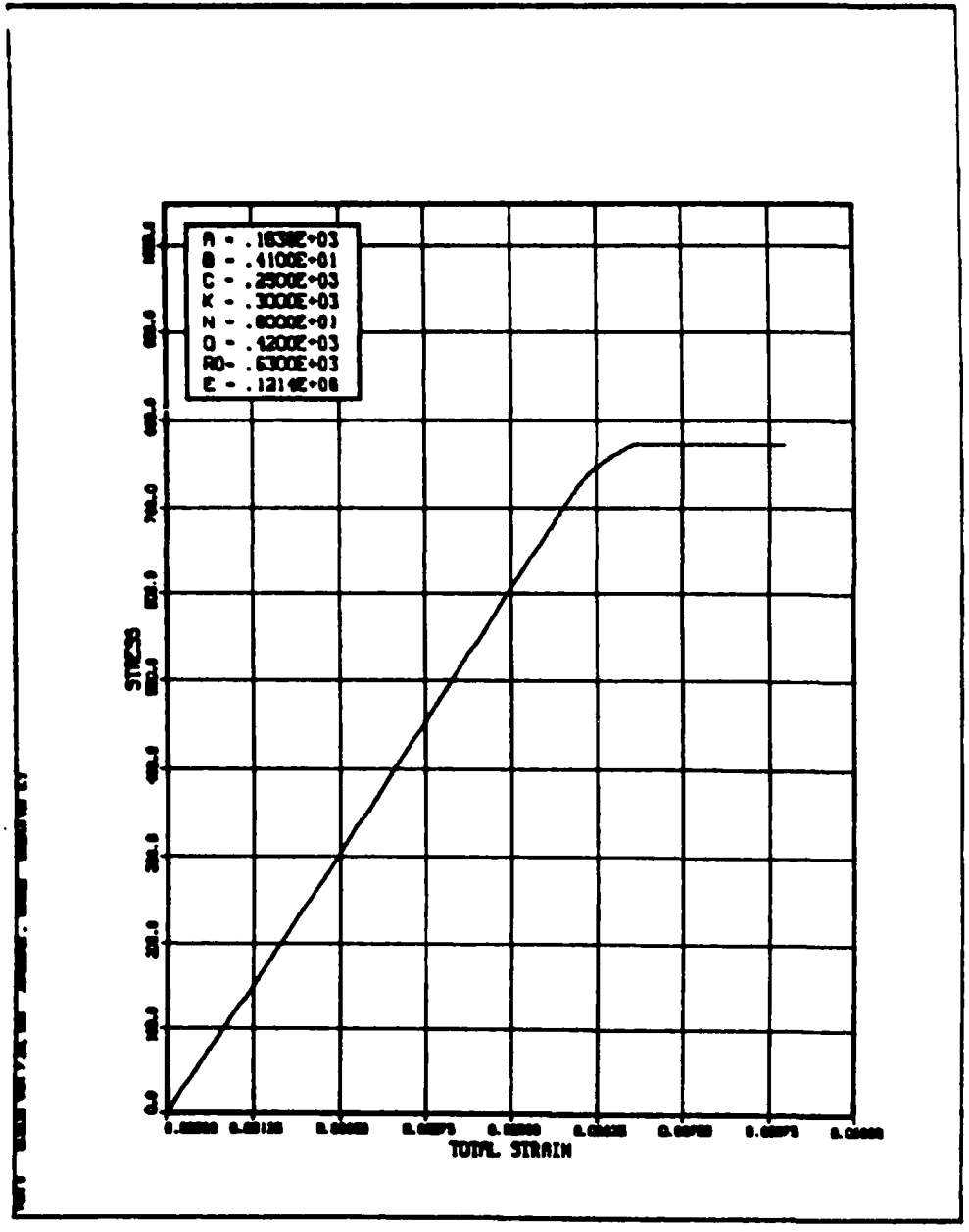

Fig. 2.12. Stress versus total strain for primary creep.

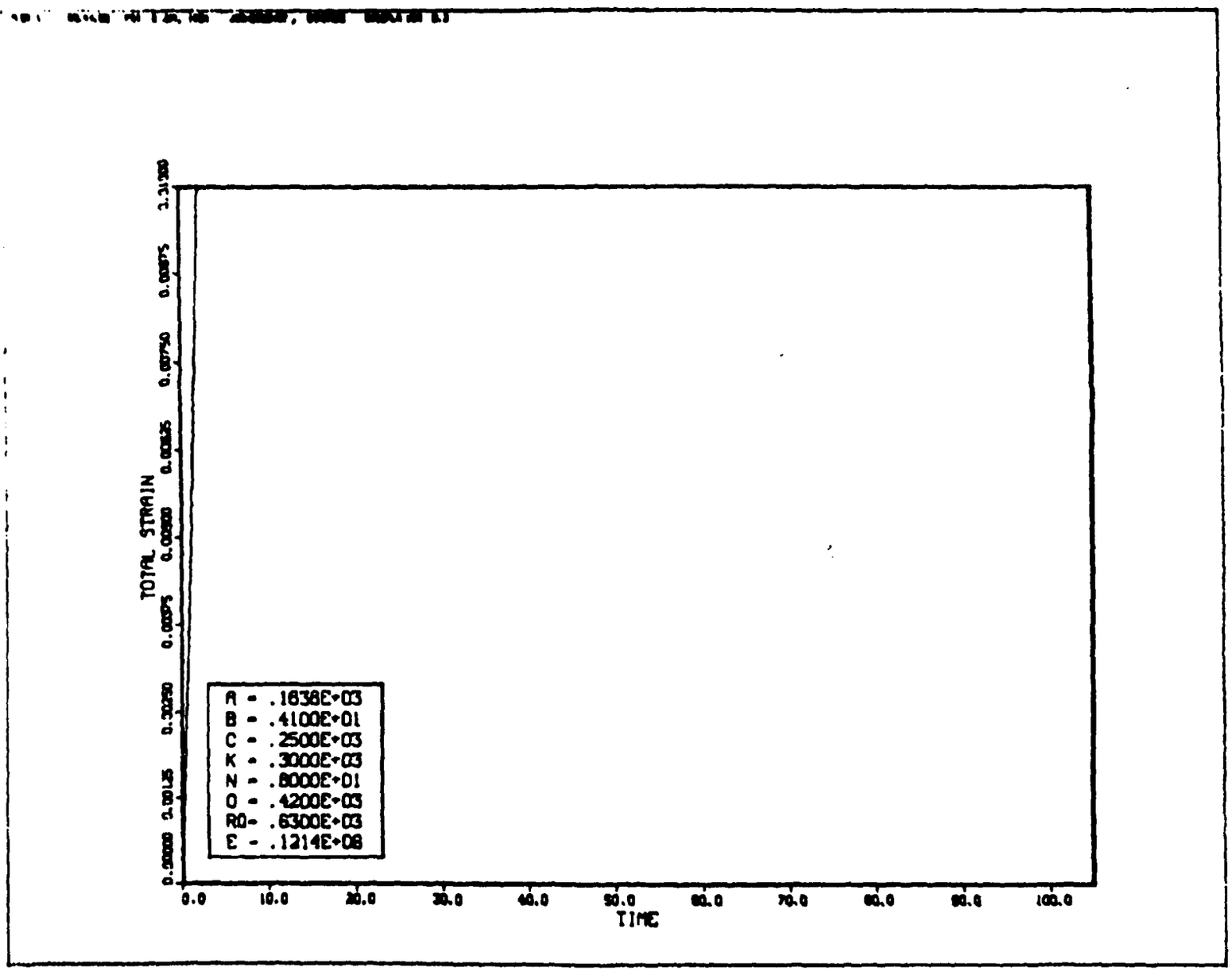

Fig. 2.13. Total strain versus time for stress relaxation.

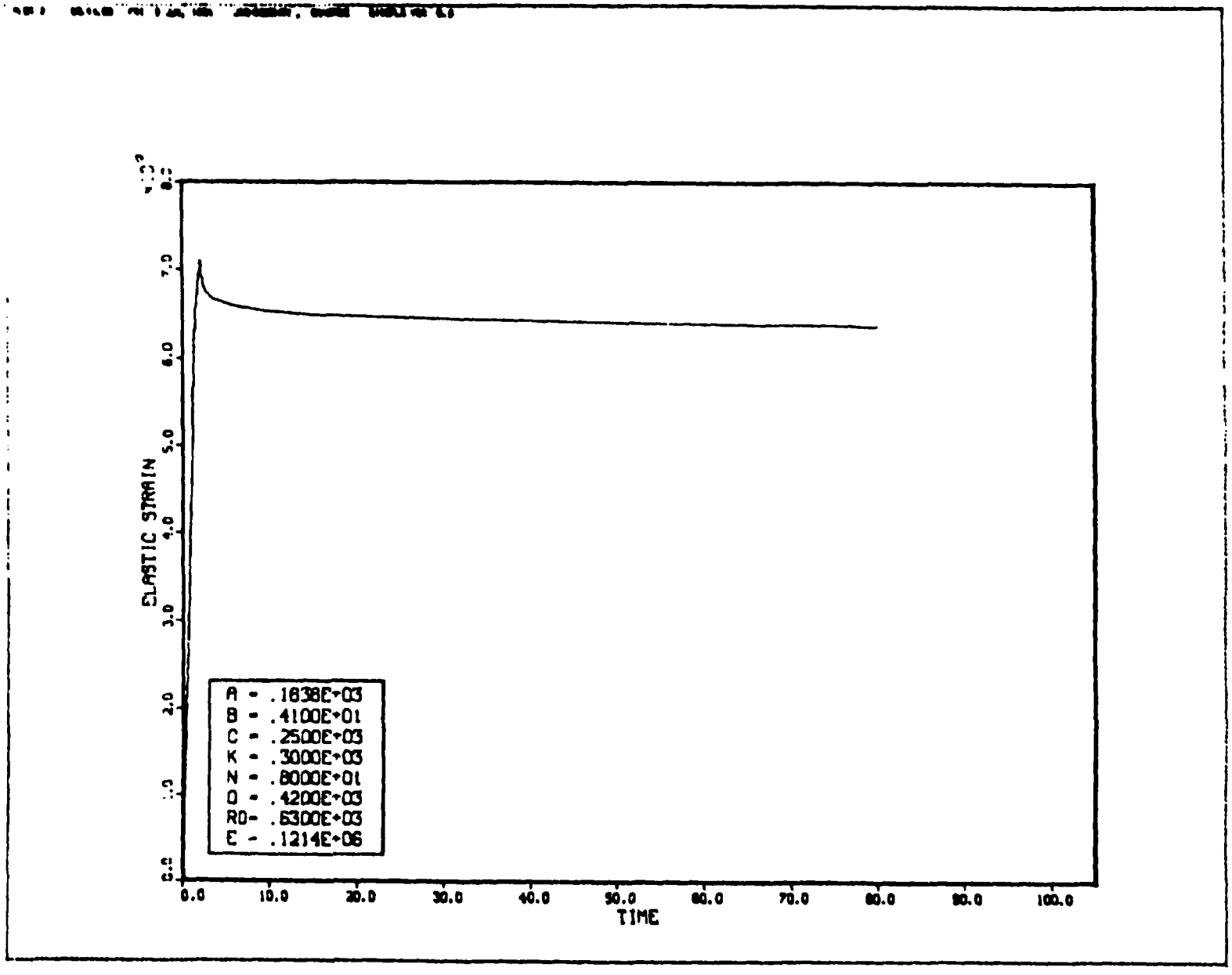

Fig. 2.14. Elastic strain versus time for stress relaxation.

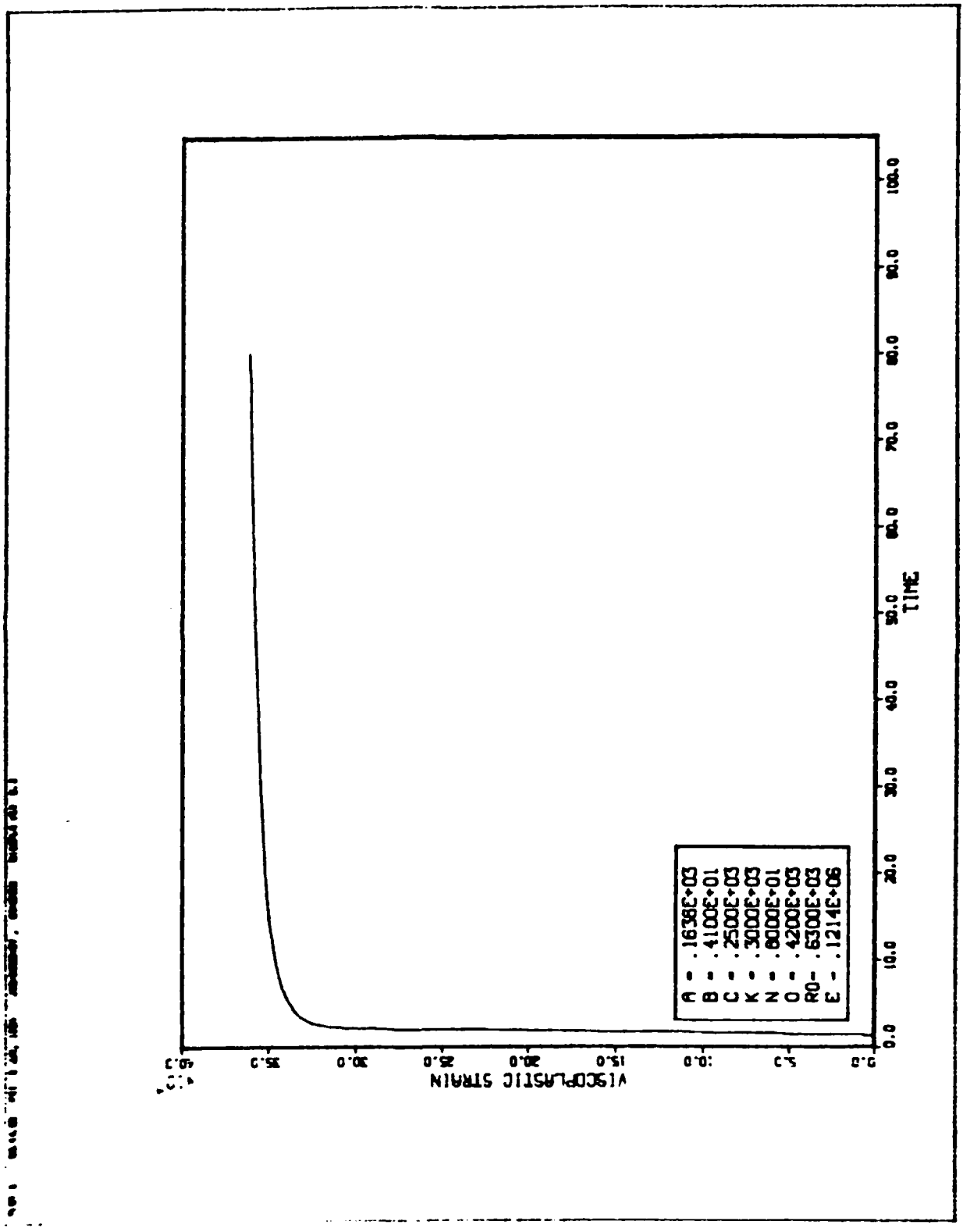

Fig. 2.15. Viscoplastic strain versus time for stress relaxation.

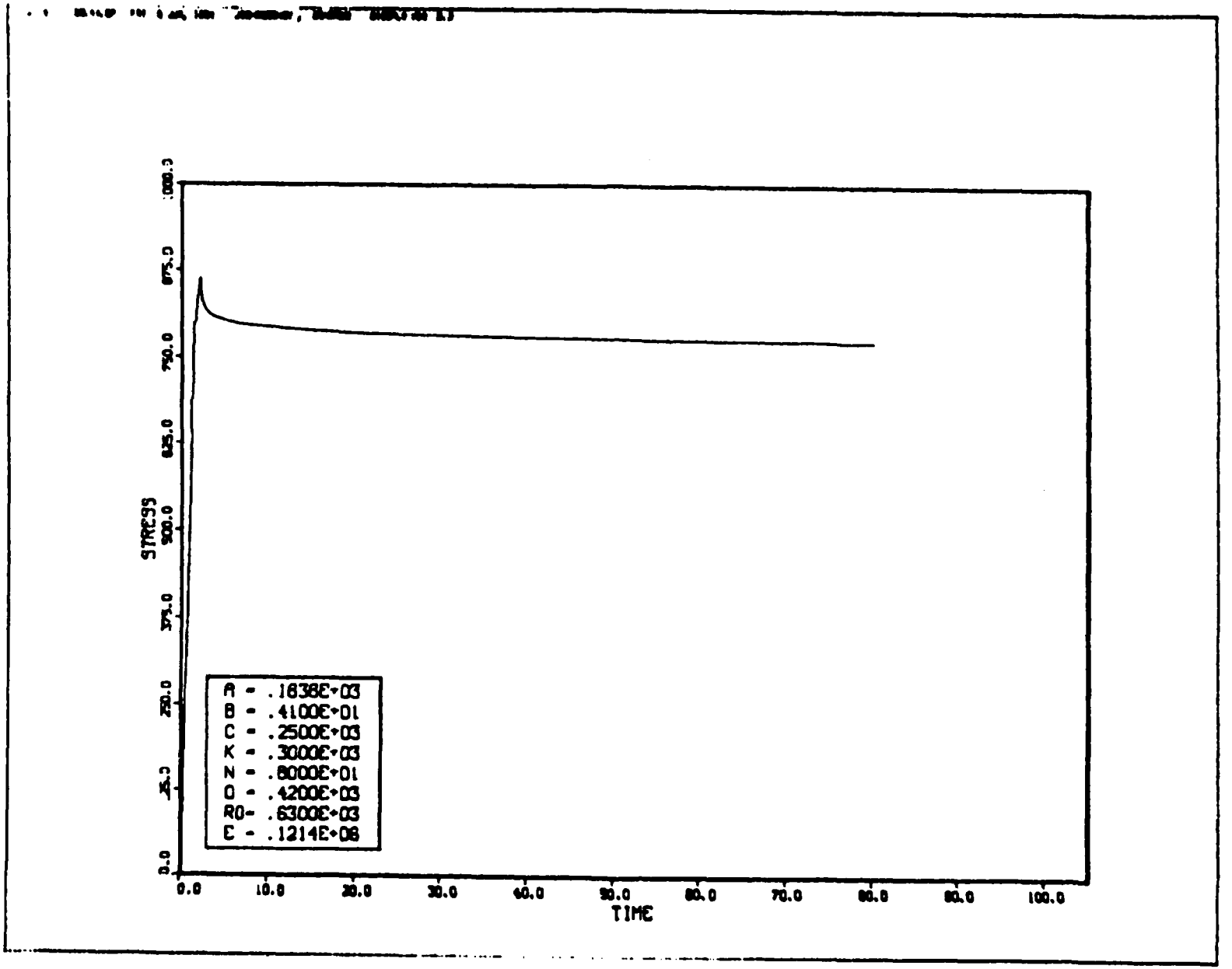

Fig. 2.16. Stress versus time for stress relaxation.

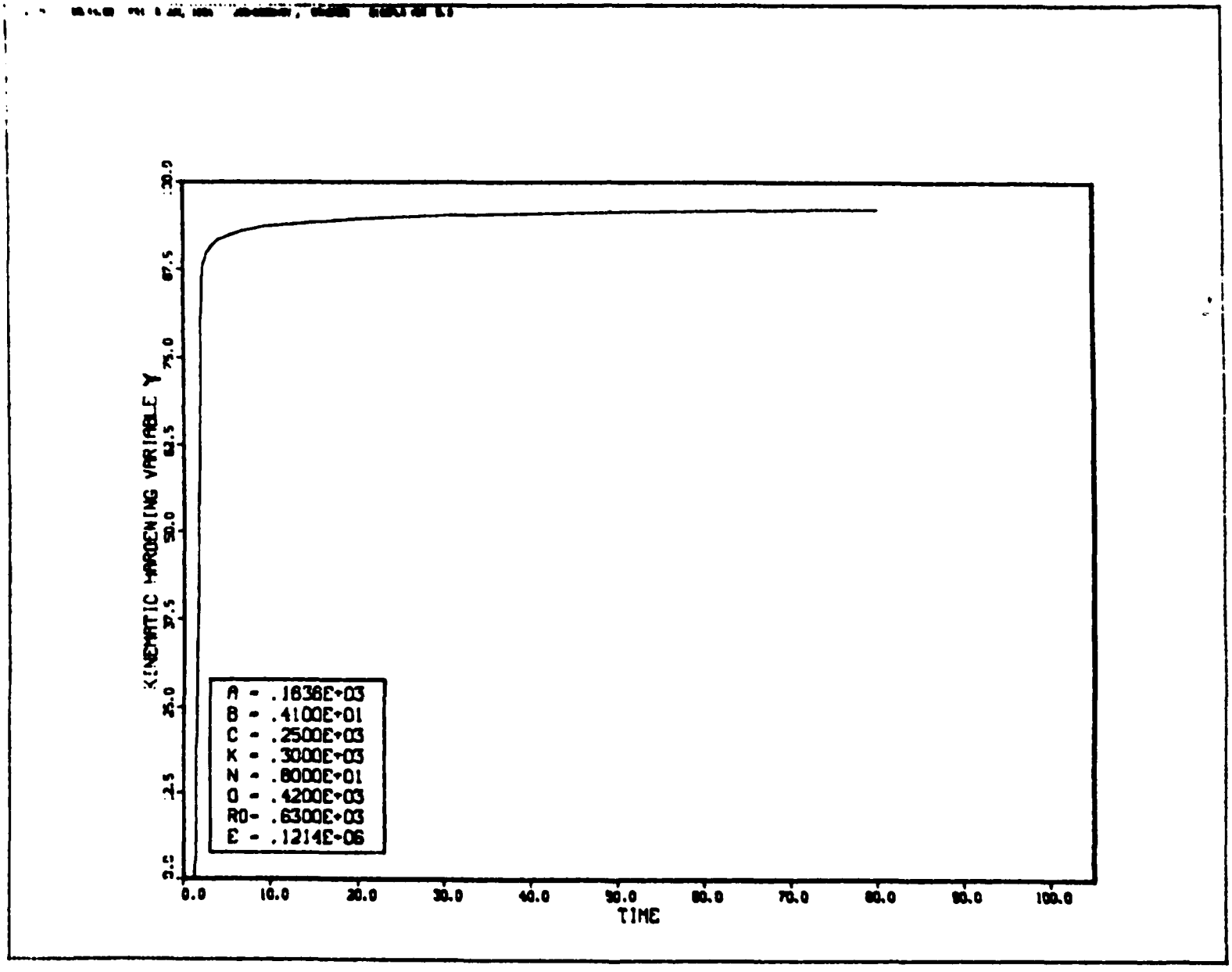

Fig. 2.17. Kinematic hardening variable versus time for stress relaxation.

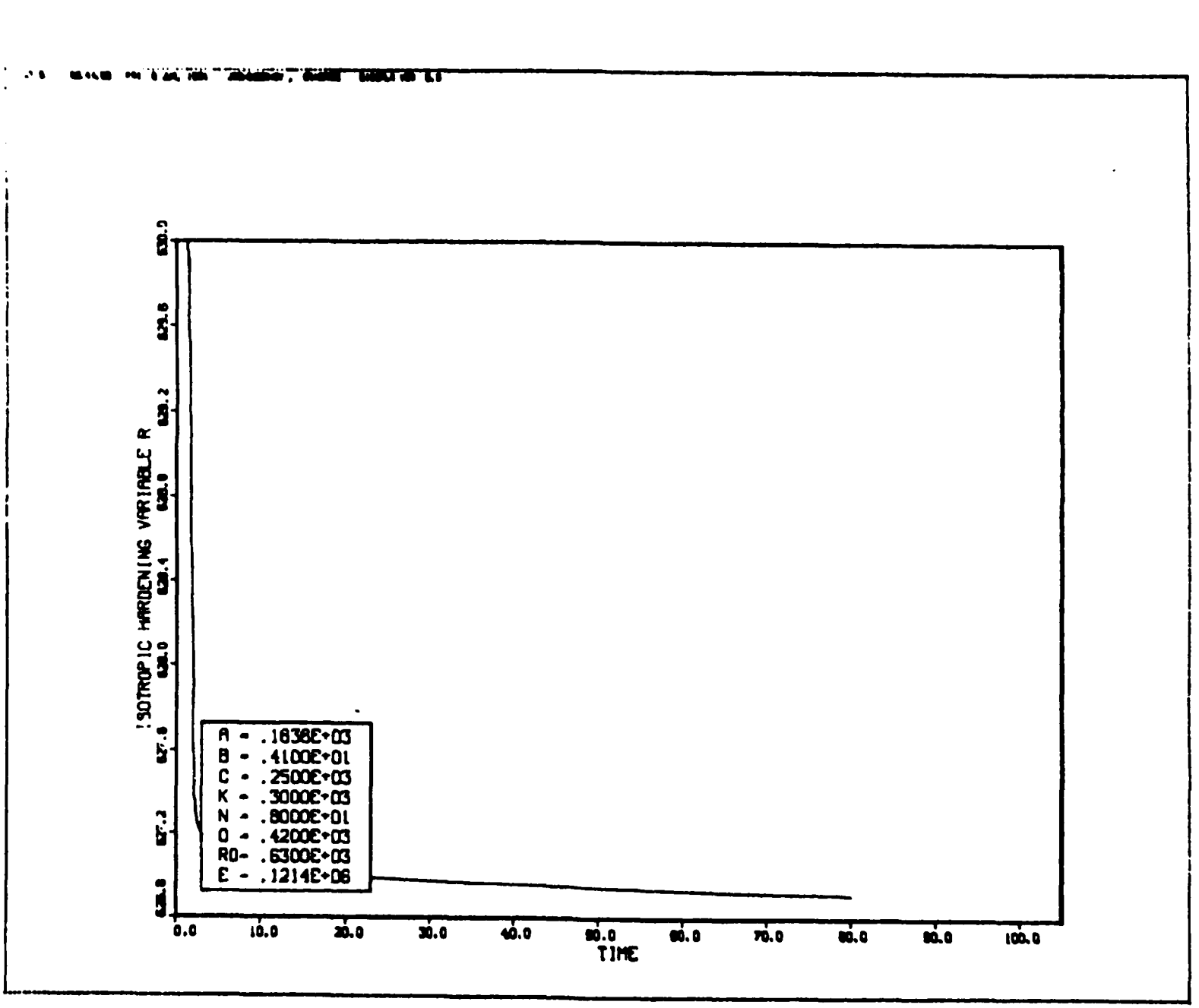

Fig. 2.18. Isotropic hardening variable versus time for stress relaxation.

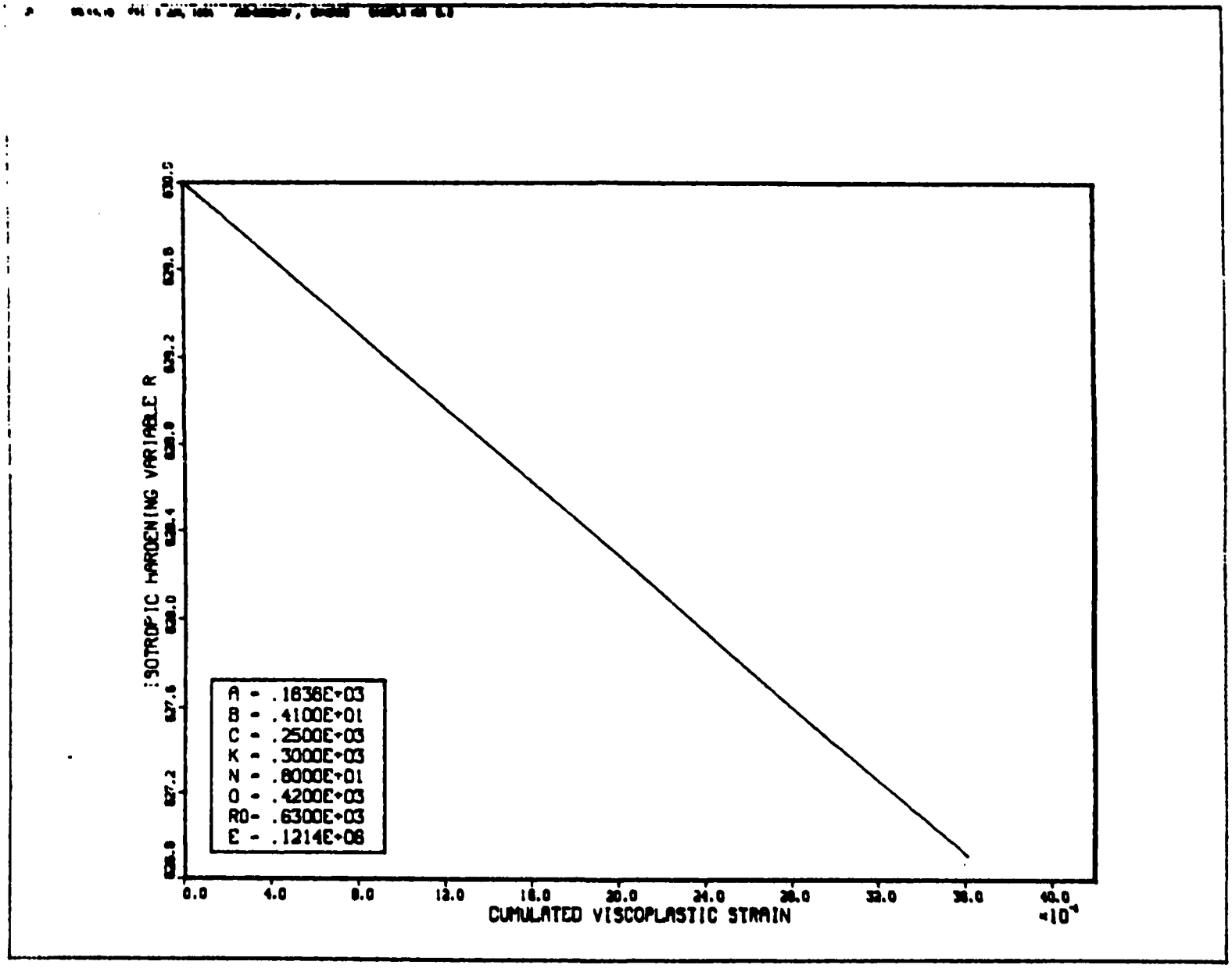

Fig. 2.19. Isotropic hardening variable versus accumulated viscoplastic strain for stress relaxation.

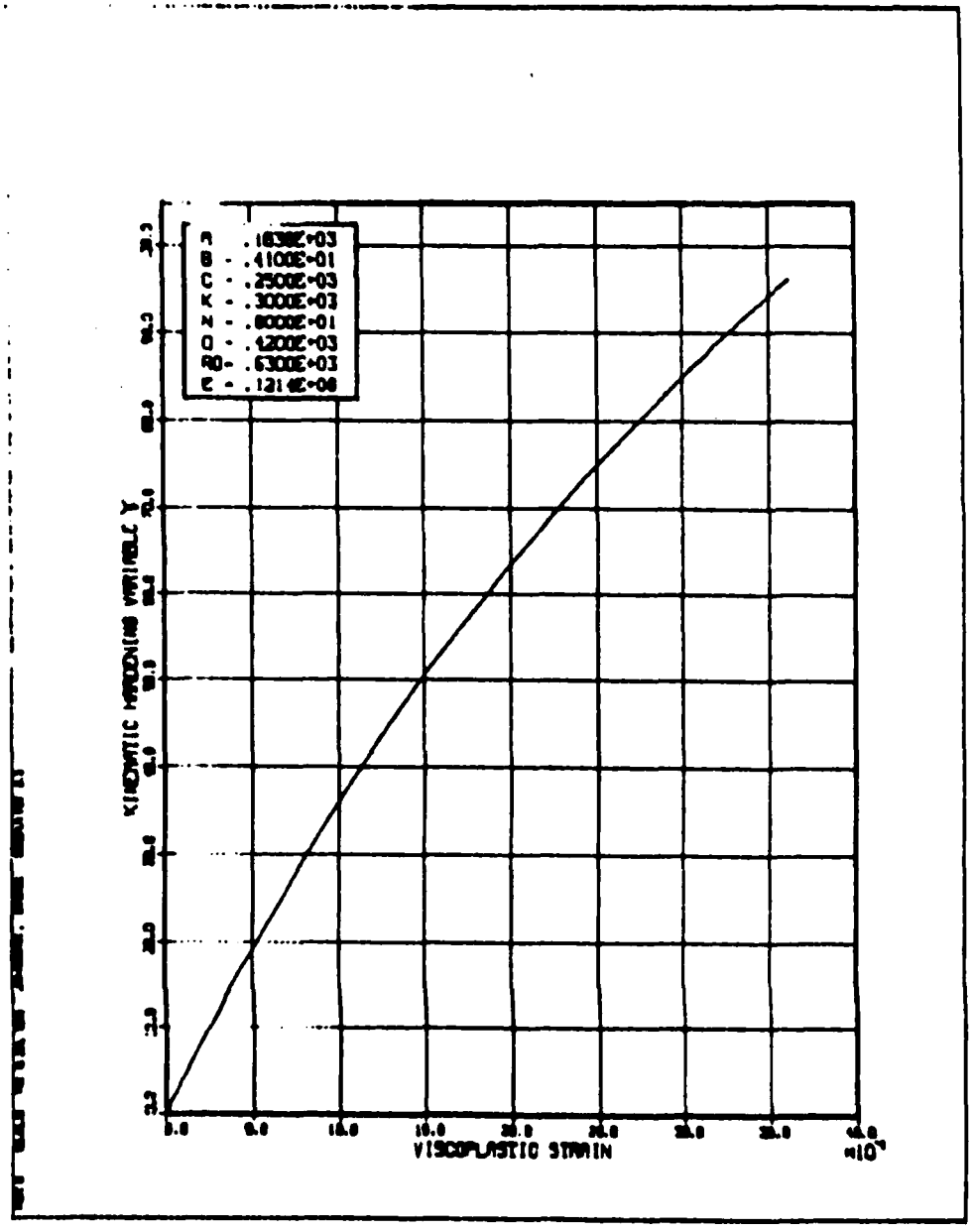

Fig. 2.20. Kinematic hardening variable versus viscoplastic strain for stress relaxation.

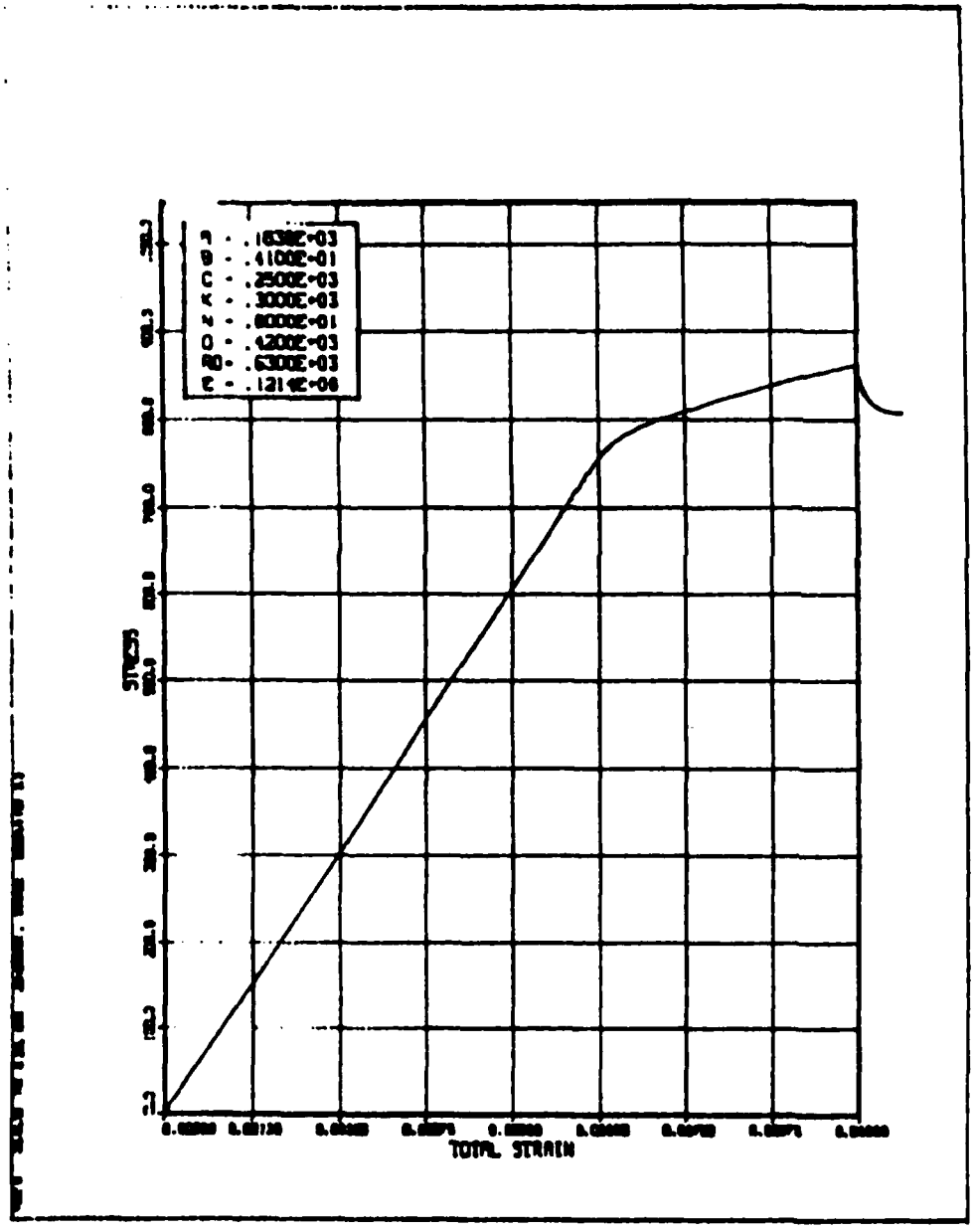

Fig. 2.21. Stress versus total strain for stress relaxation.

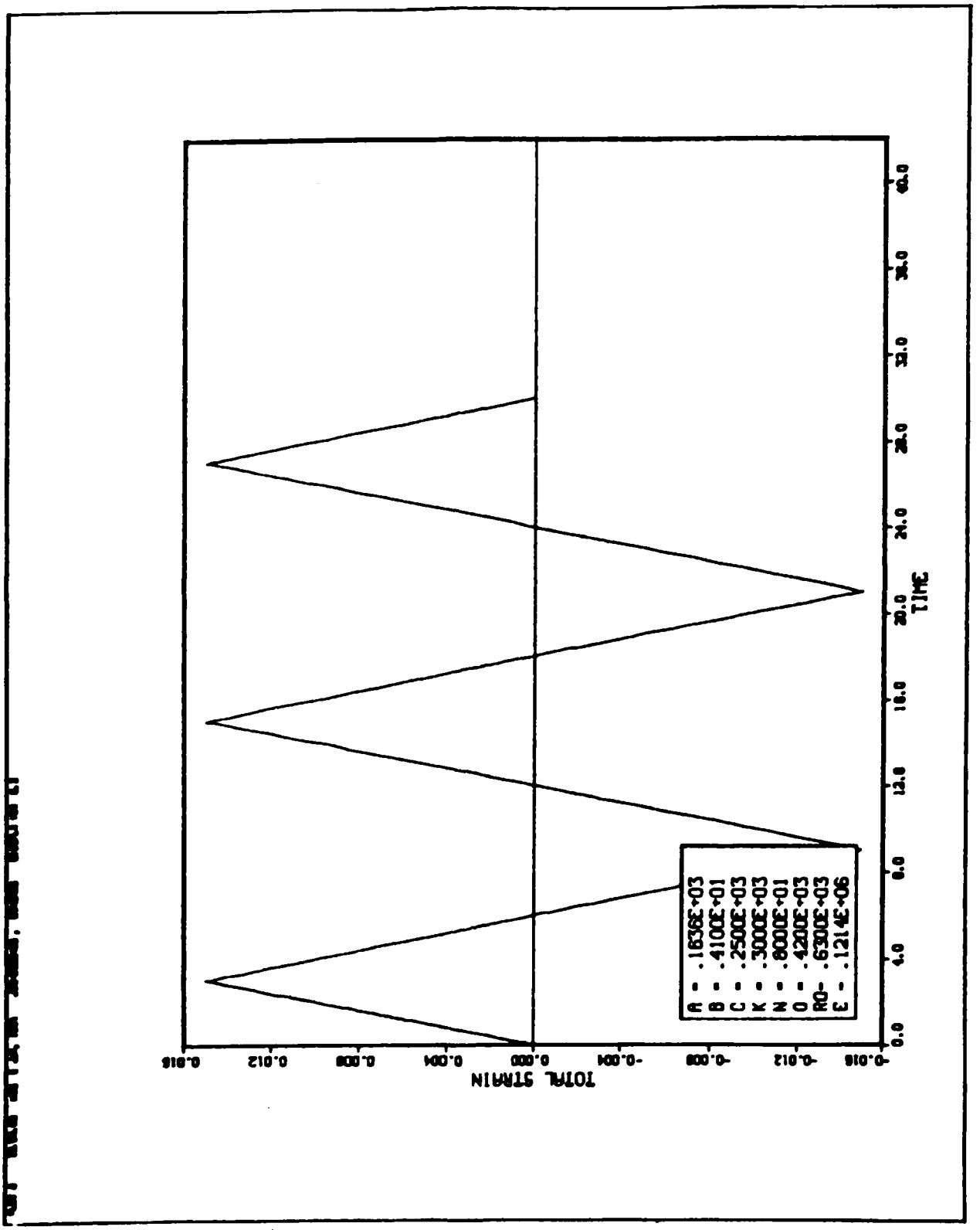

Fig. 2.22. Total strain versus time for strain-controlled cyclic loading.

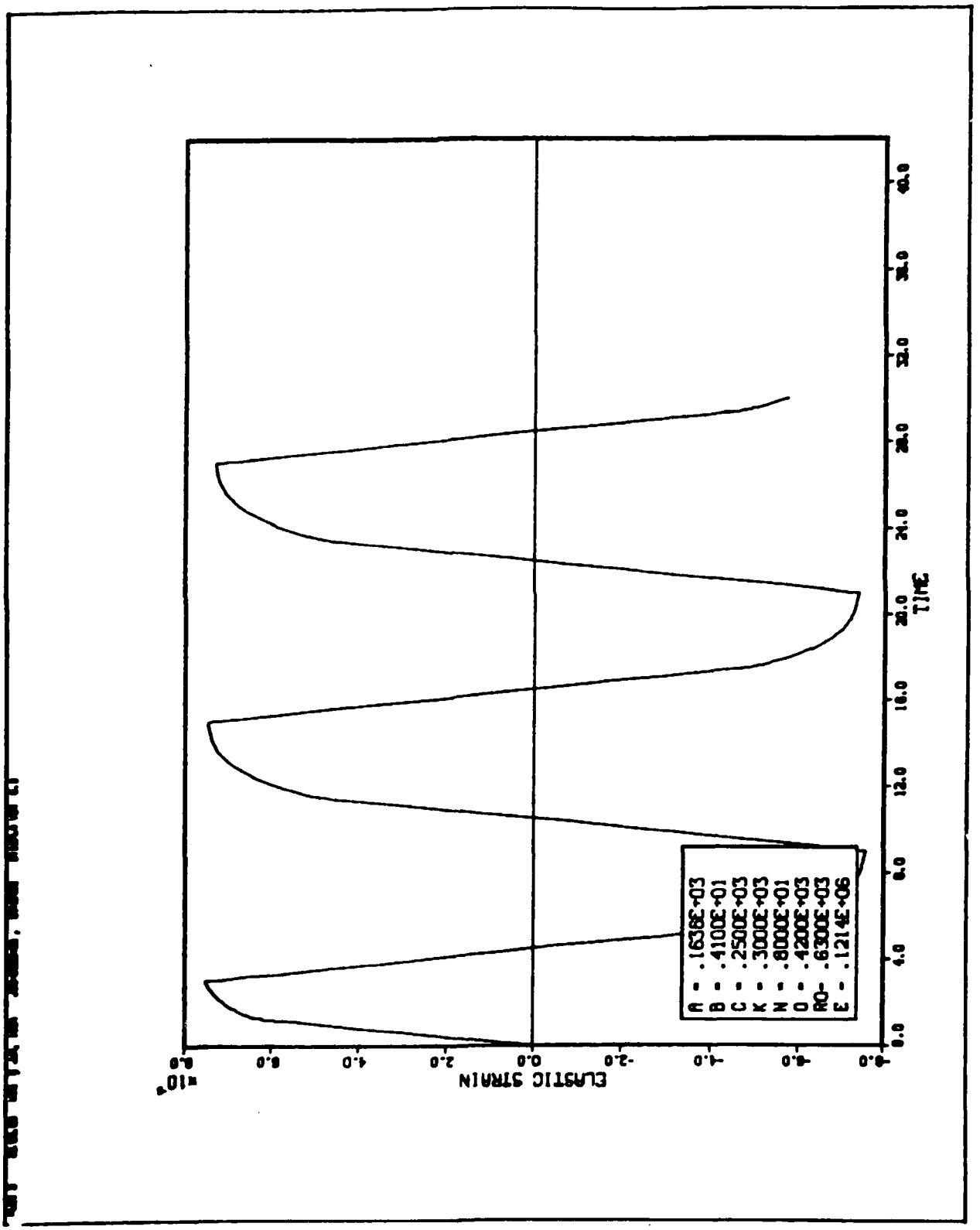

Fig. 2.23. Elastic strain versus time for strain-controlled cyclic loading.

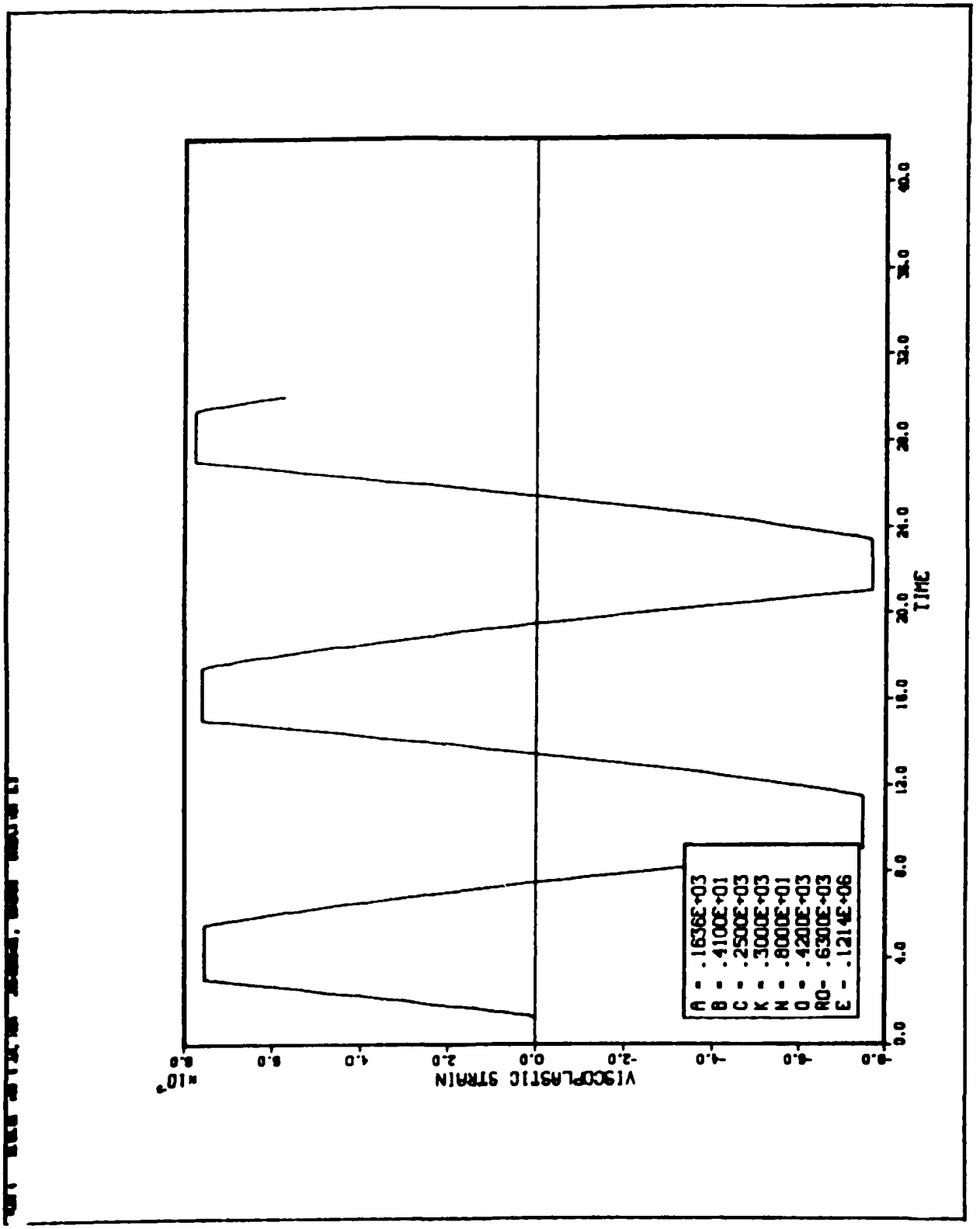

Fig. 2.24. Viscoplastic strain versus time for strain-controlled cyclic loading.

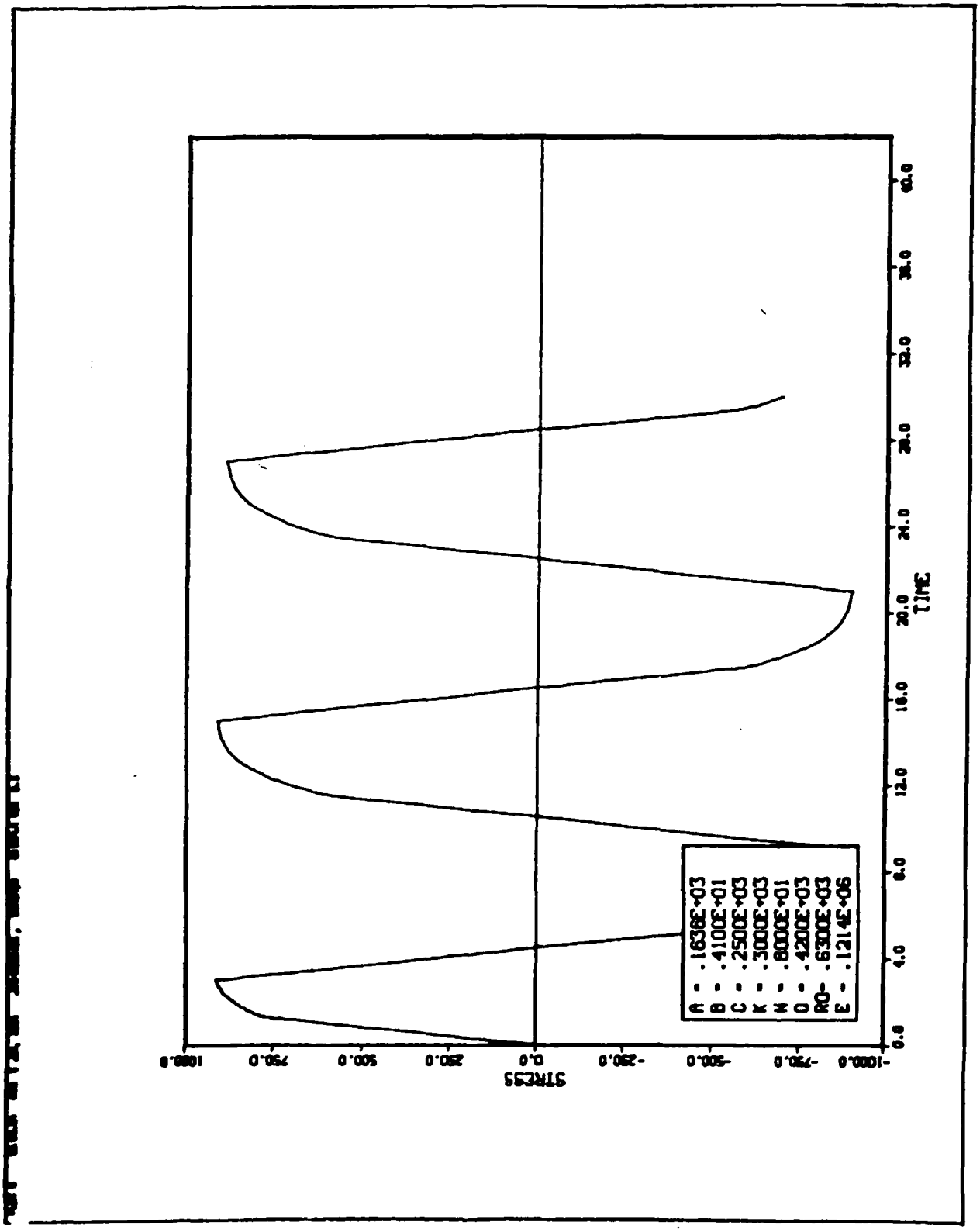

Fig. 2.25. Stress versus time for strain-controlled cyclic loading.

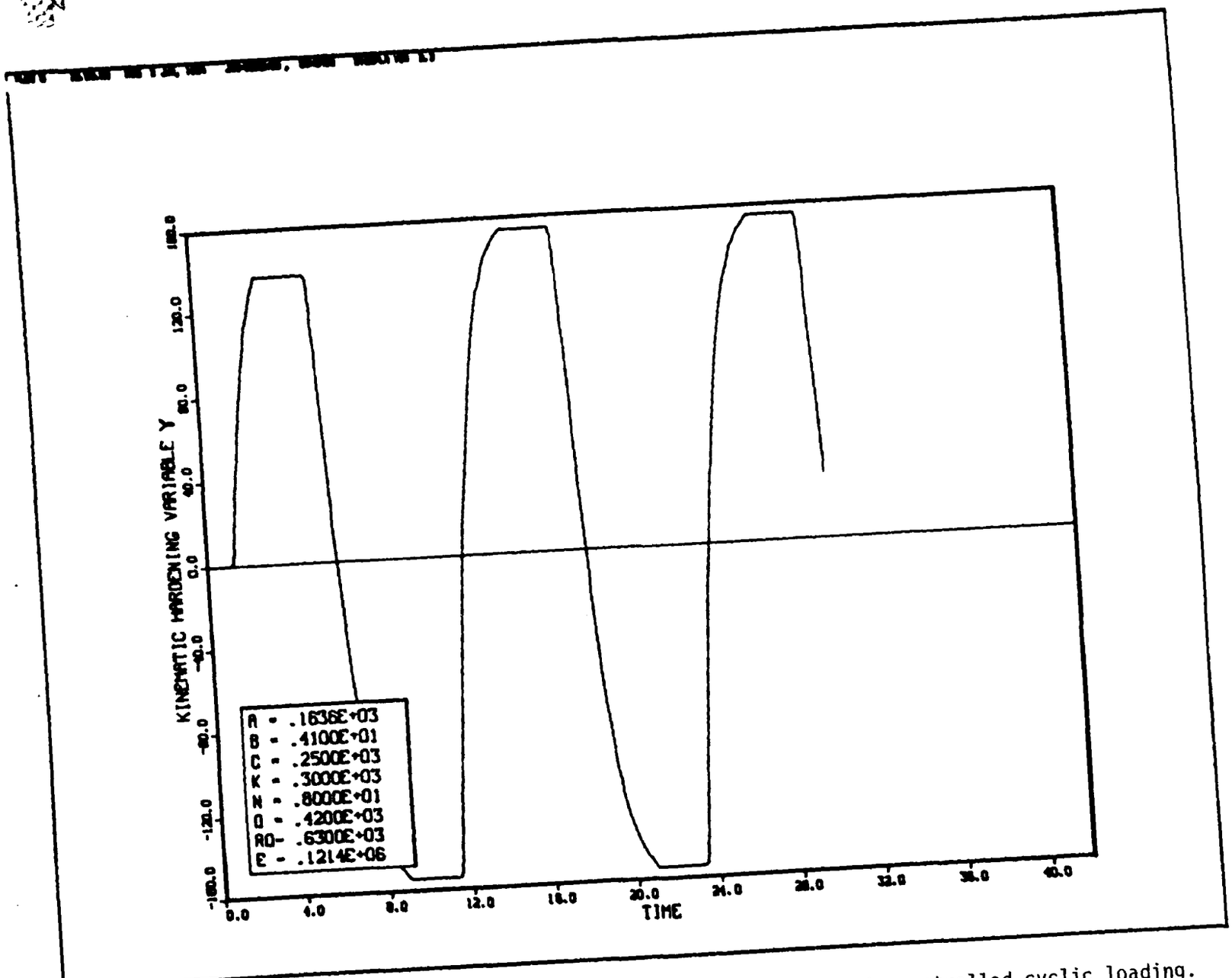

Fig. 2.26. Kinematic hardening variable versus time for strain-controlled cyclic loading.

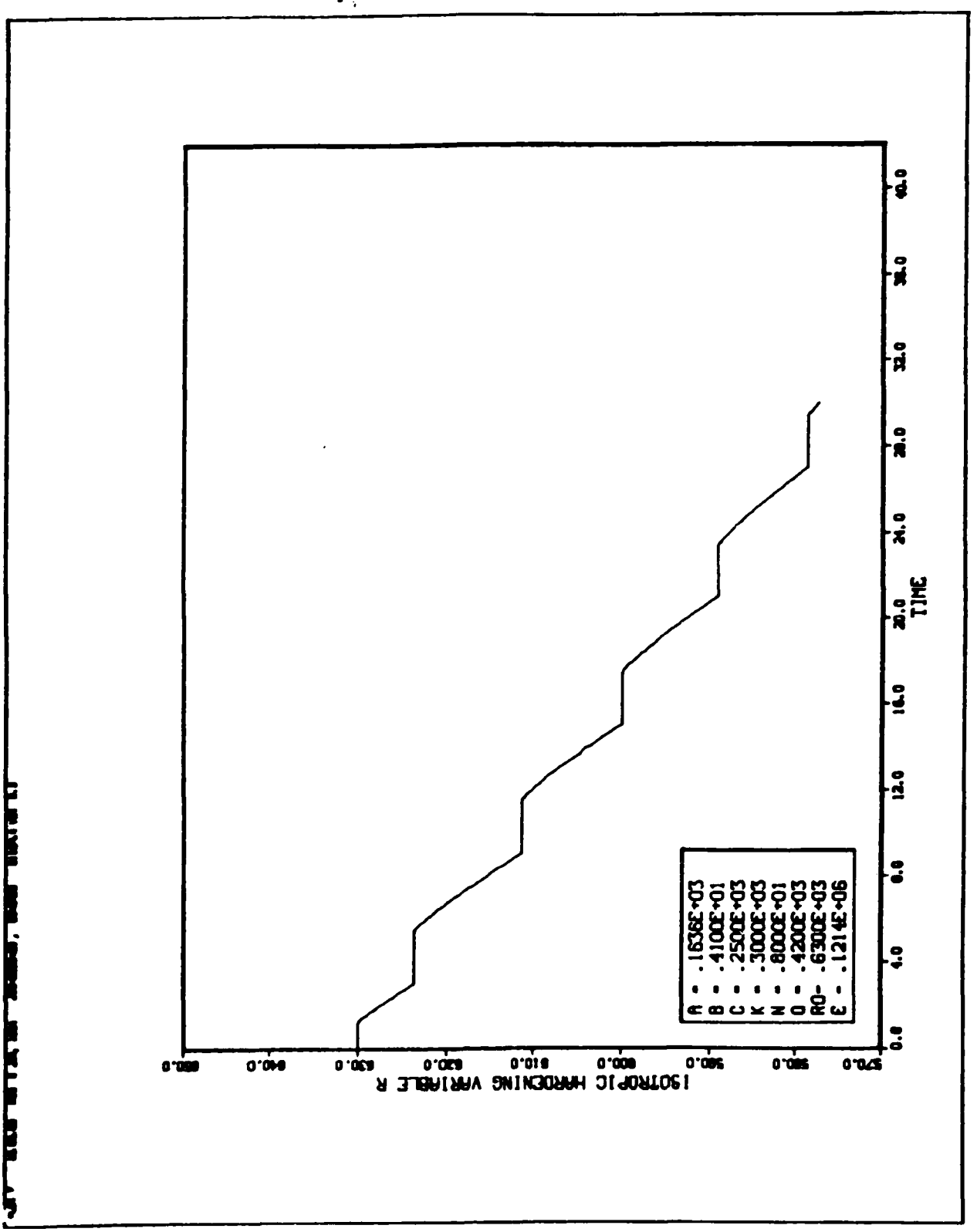

Fig. 2.27. Isotropic hardening variable versus time for strain-controlled cyclic loading.

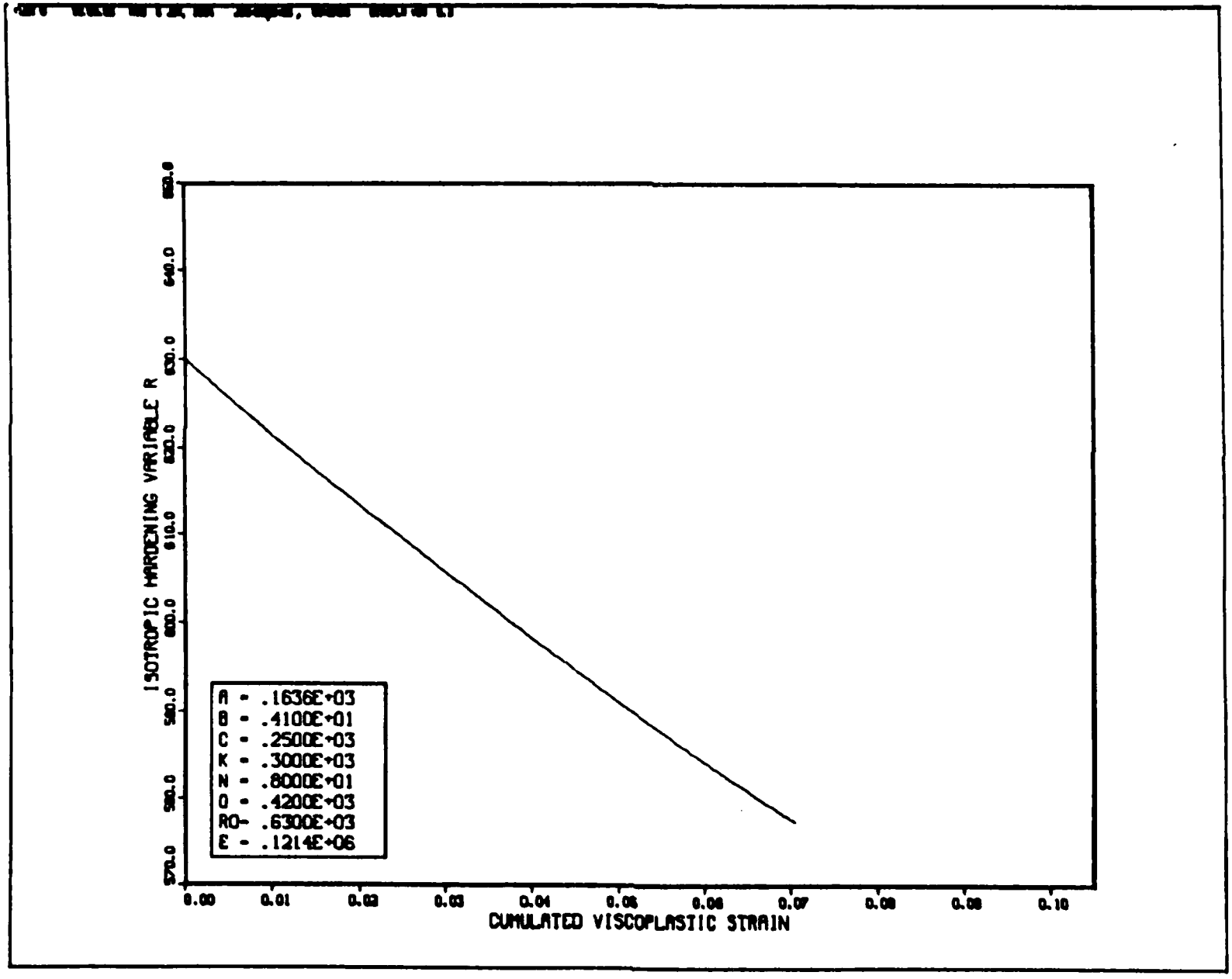

Fig. 2.28. Isotropic hardening variable versus accumulated viscoplastic strain for strain-controlled cyclic loading.

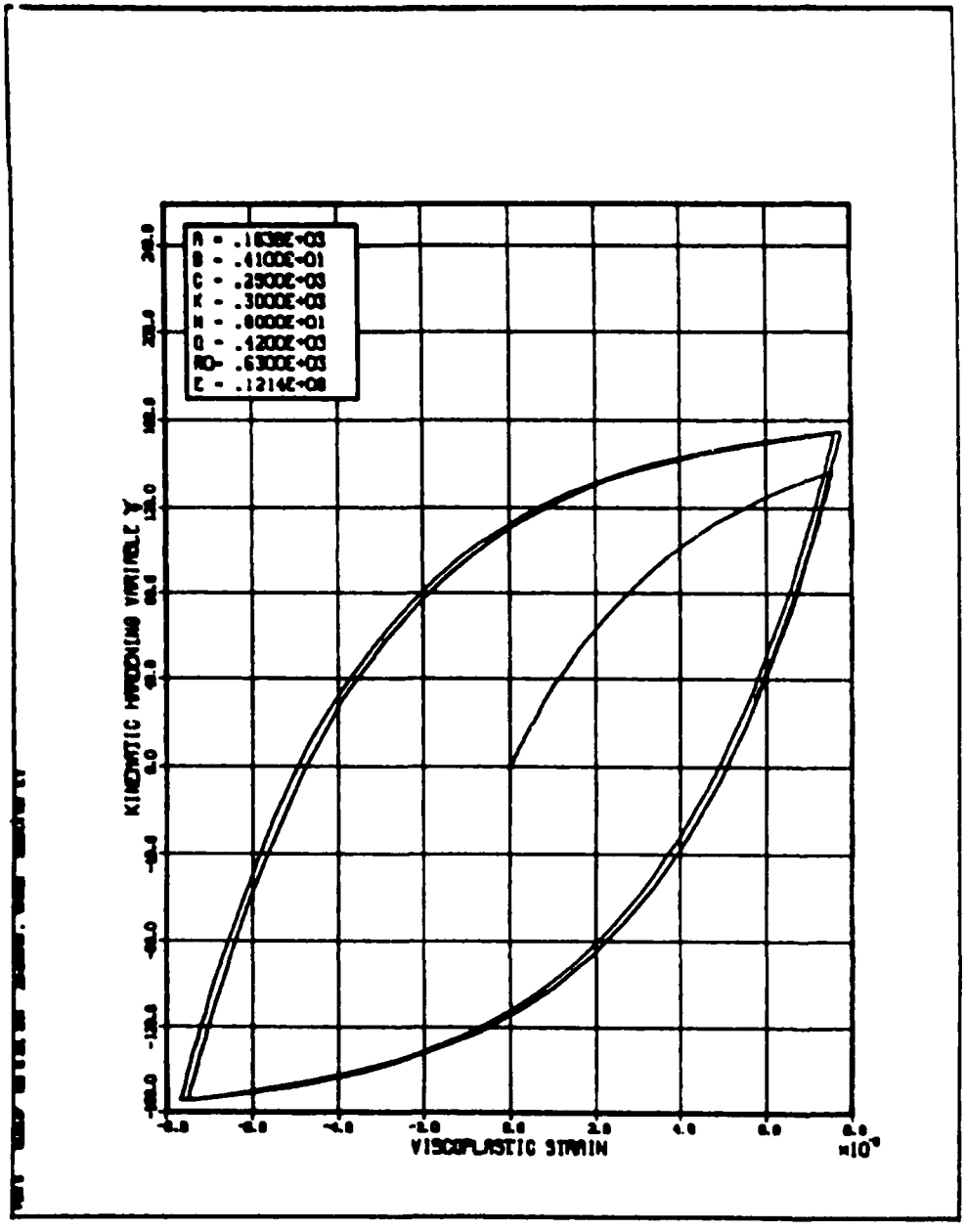

Fig. 2.29. Kinematic hardening variable versus viscoplastic strain for strain-controlled cyclic loading.

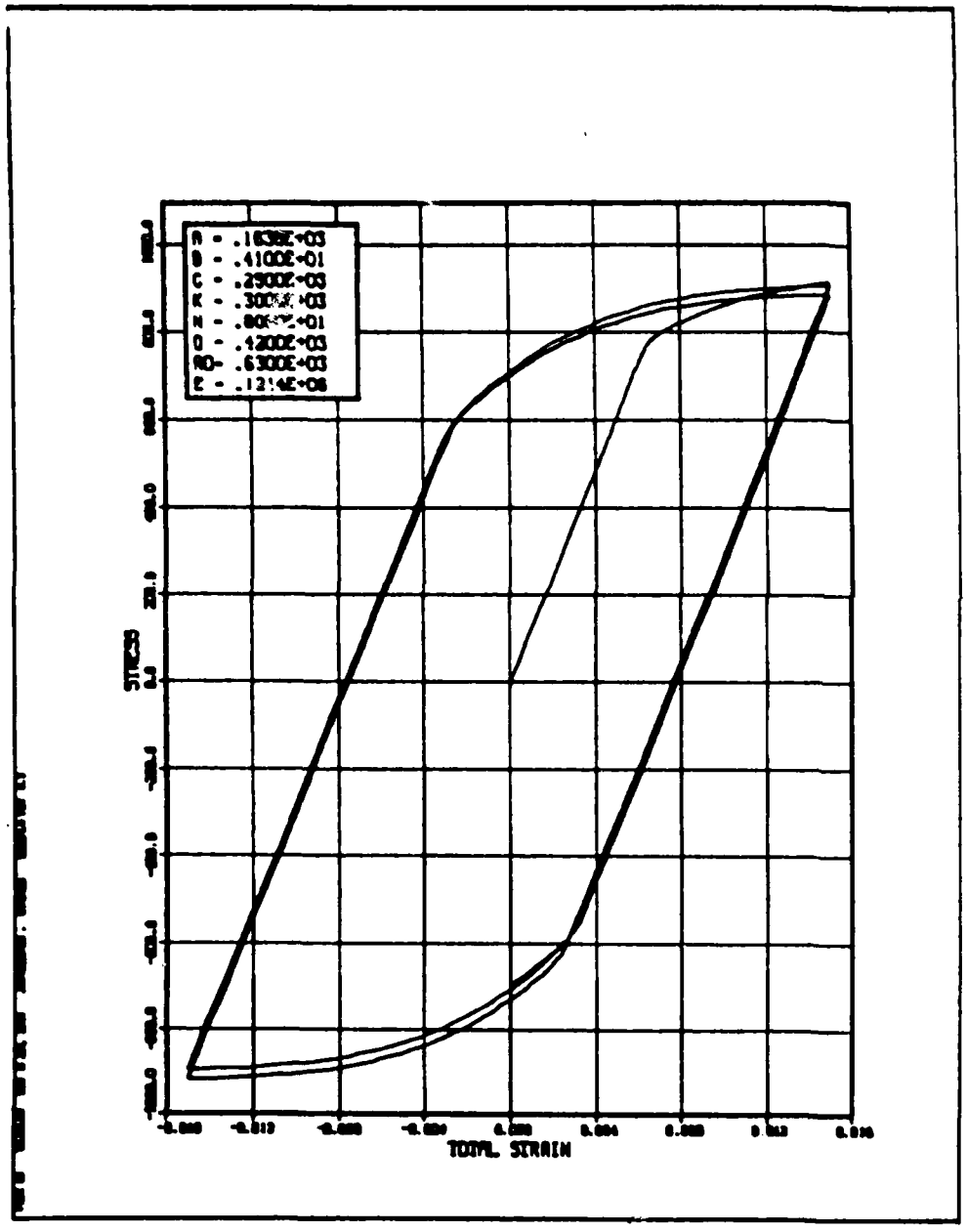

Fig. 2.30. Stress versus total strain for strain-controlled cyclic loading.

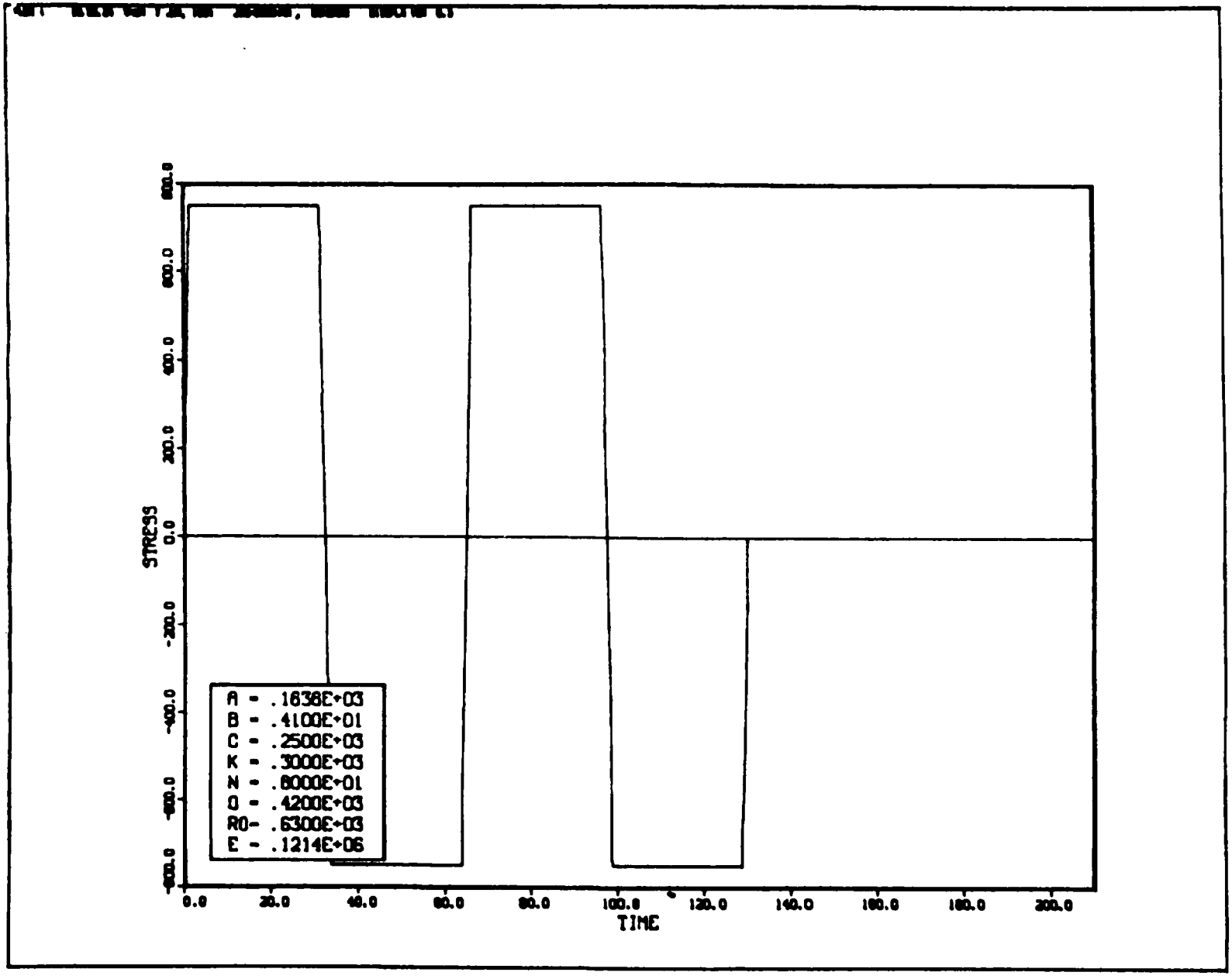

Fig. 2.31. Stress versus time for stress-controlled cyclic loading with hold times.

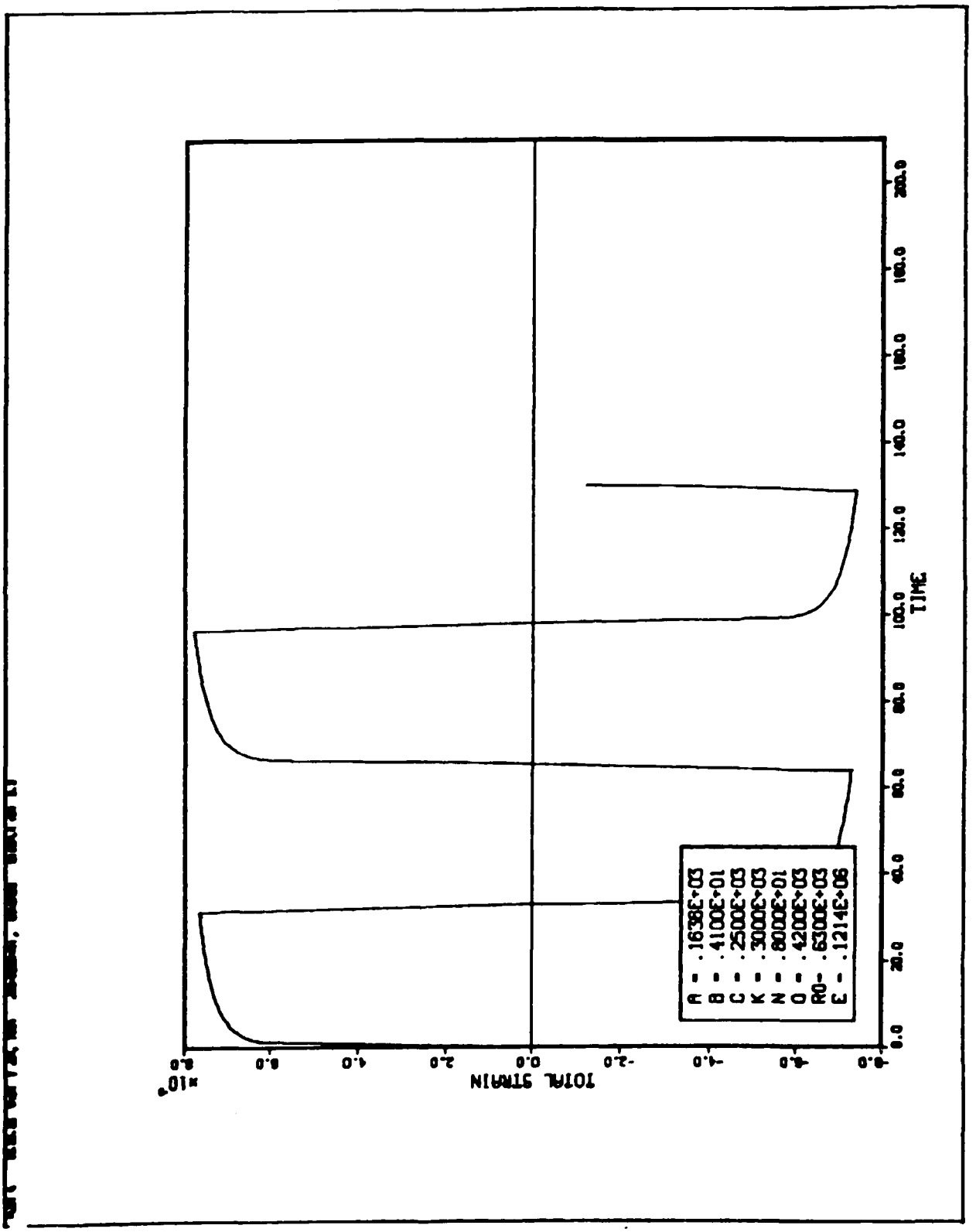

Fig. 2.32. Total strain versus time for stress-controlled cyclic loading with hold times.

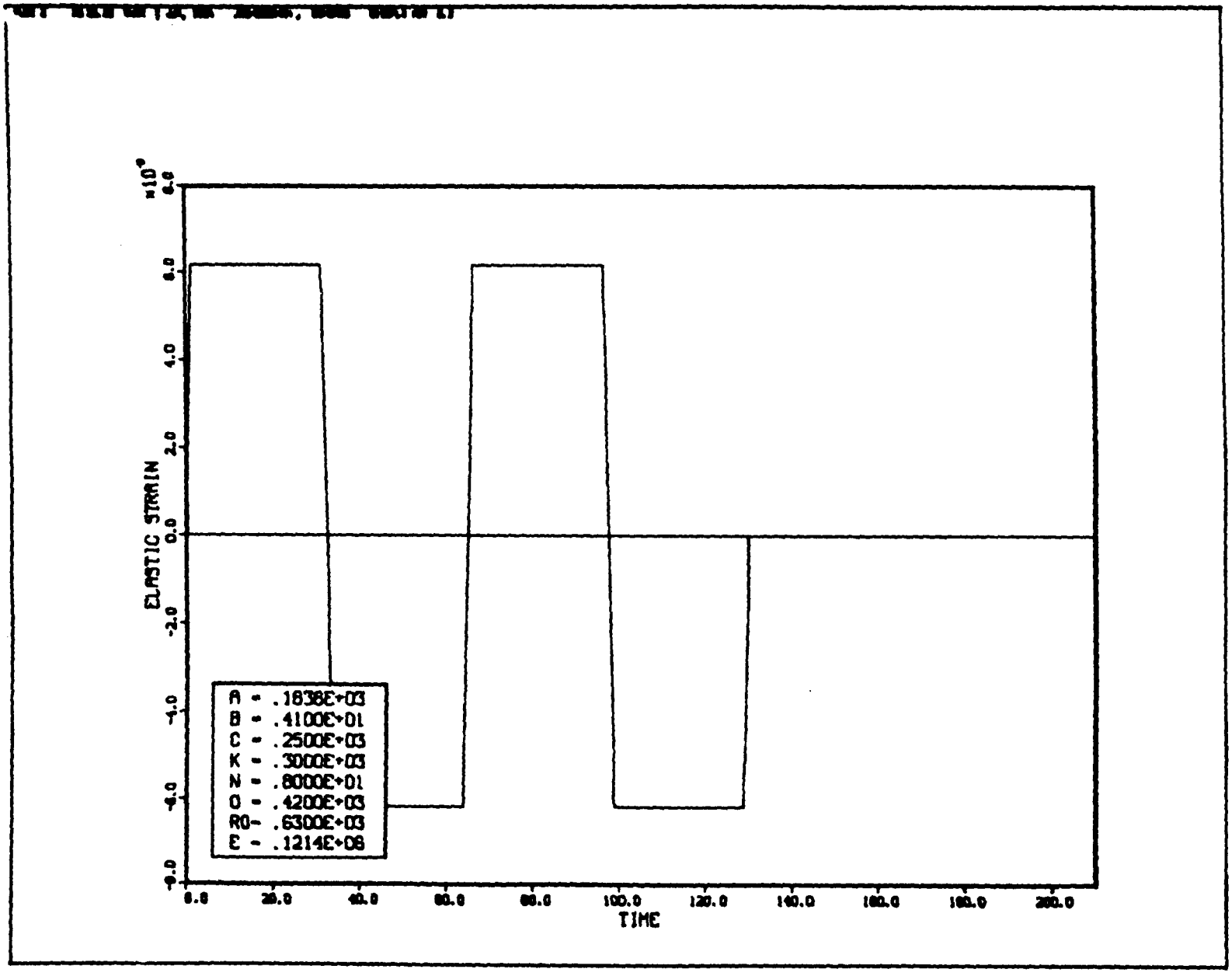

Fig. 2.33. Elastic strain versus time for stress-controlled cyclic loading with hold times.

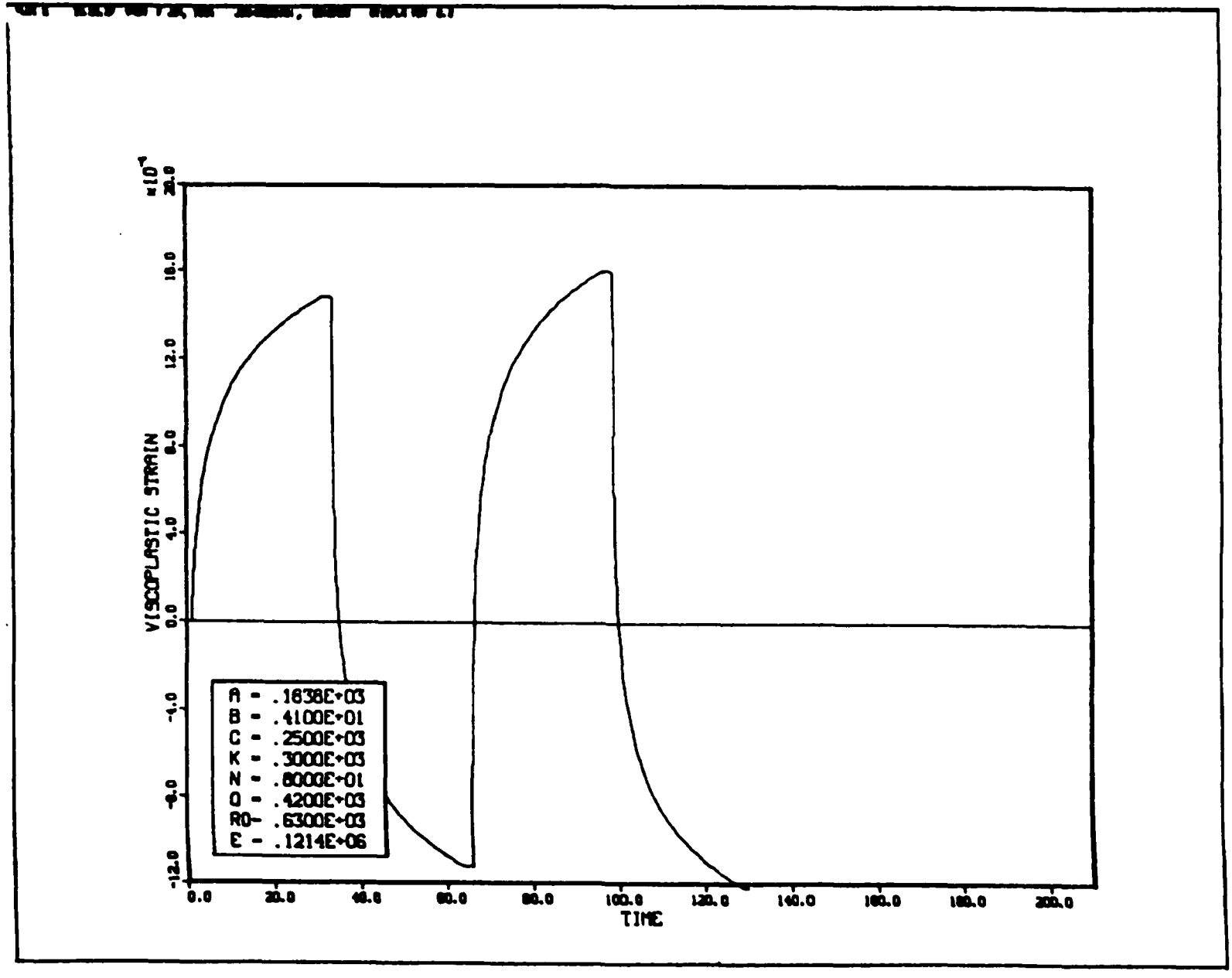

Fig. 2.34. Viscoplastic strain versus time for stress-controlled cyclic loading with hold times.

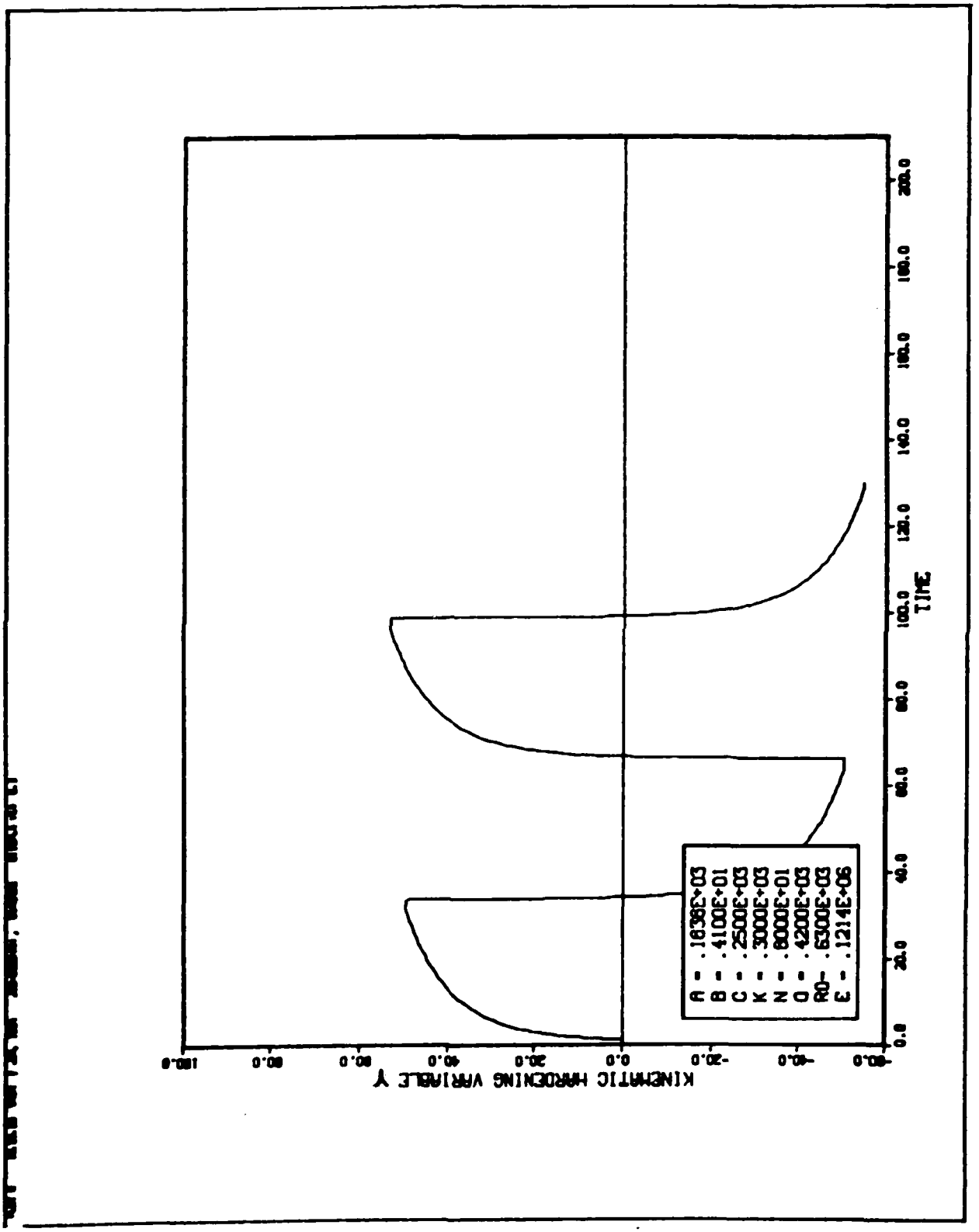

Fig. 2.35. Kinematic hardening variable versus hold time for stress-controlled cyclic loading with hold times.

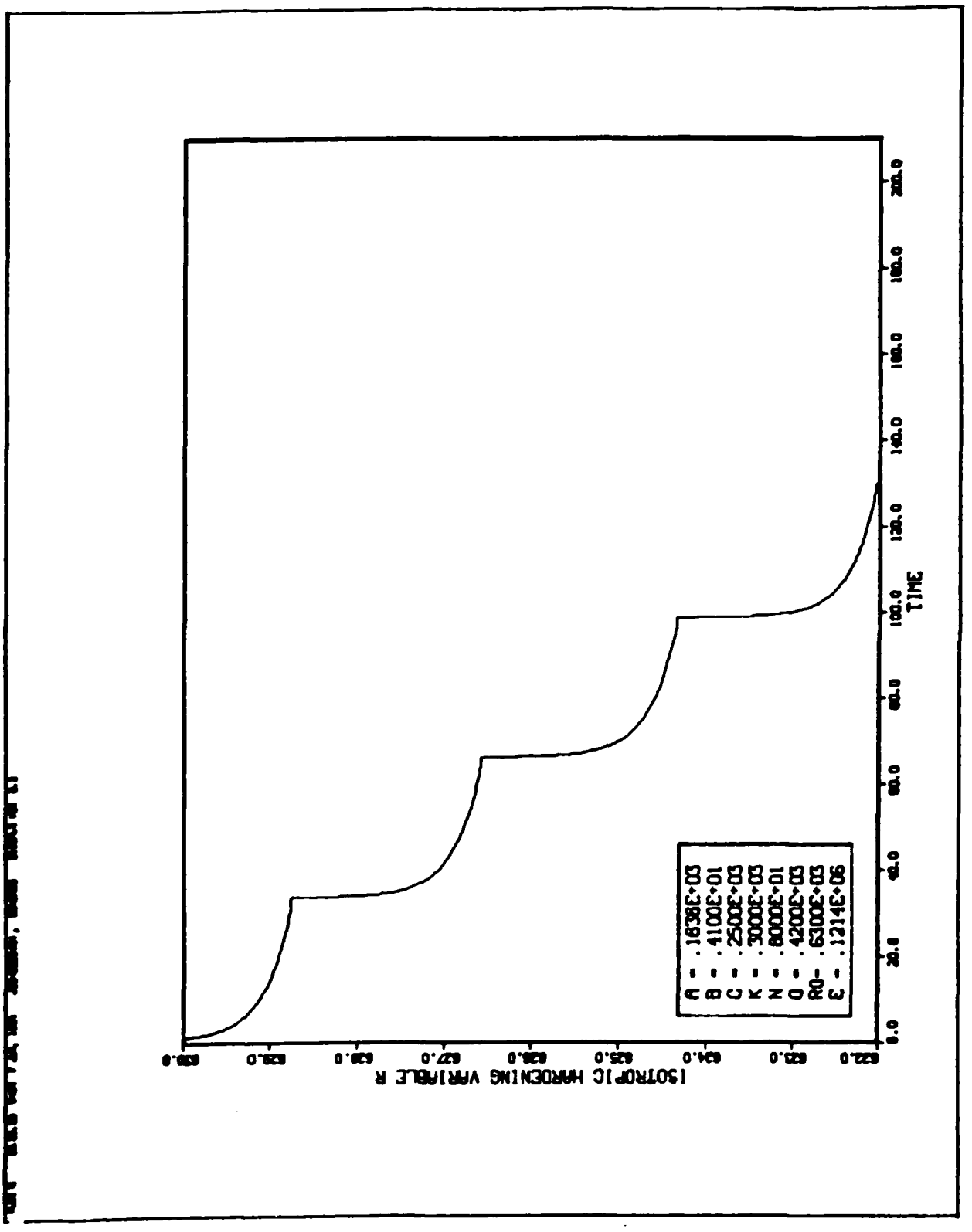

Fig. 2.36. Isotropic hardening variable versus time for stress-controlled cyclic loading with hold times.

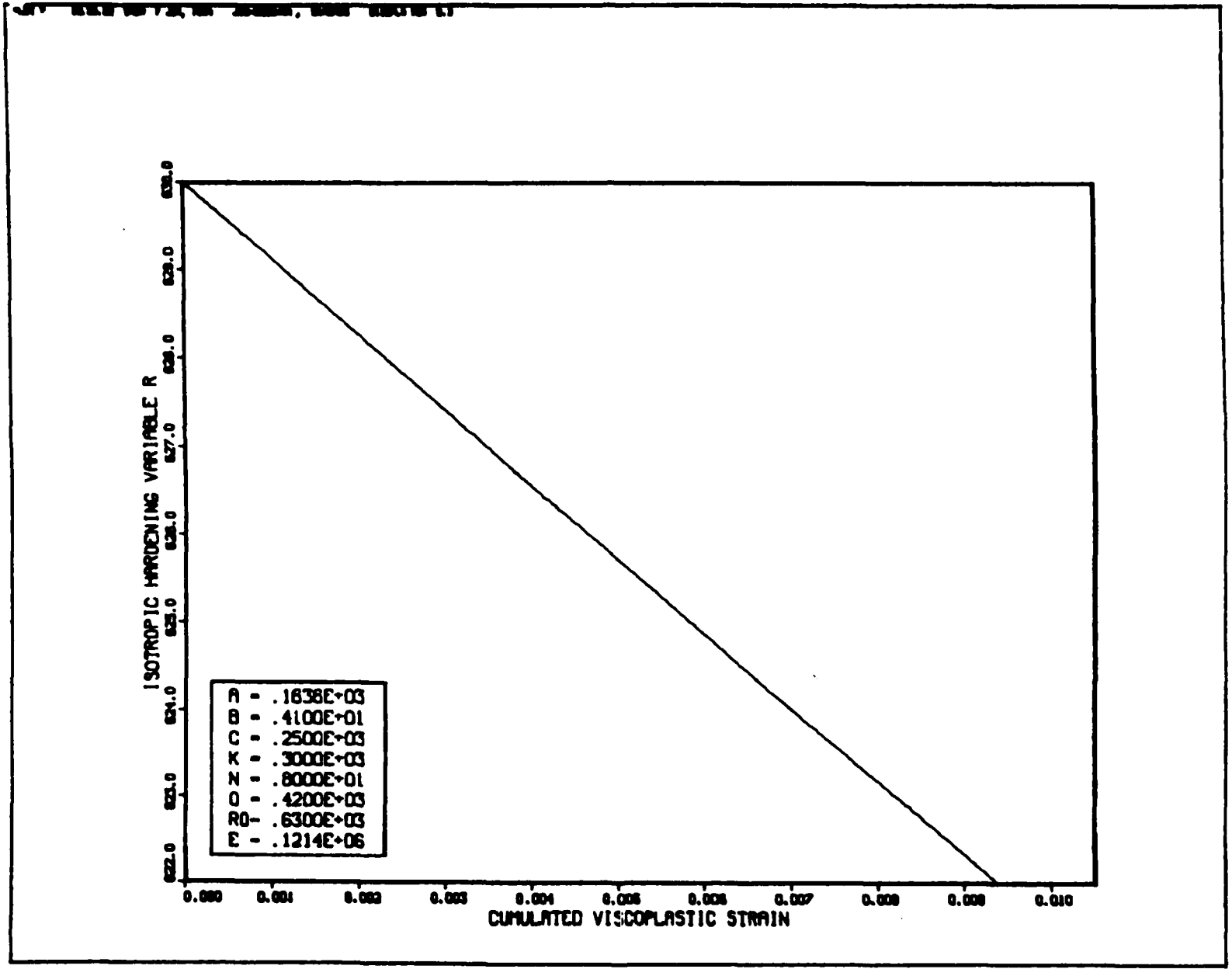

Fig. 2.37. Isotropic hardening variable versus accumulated viscoplastic strain for stress-controlled cyclic loading with hold times.

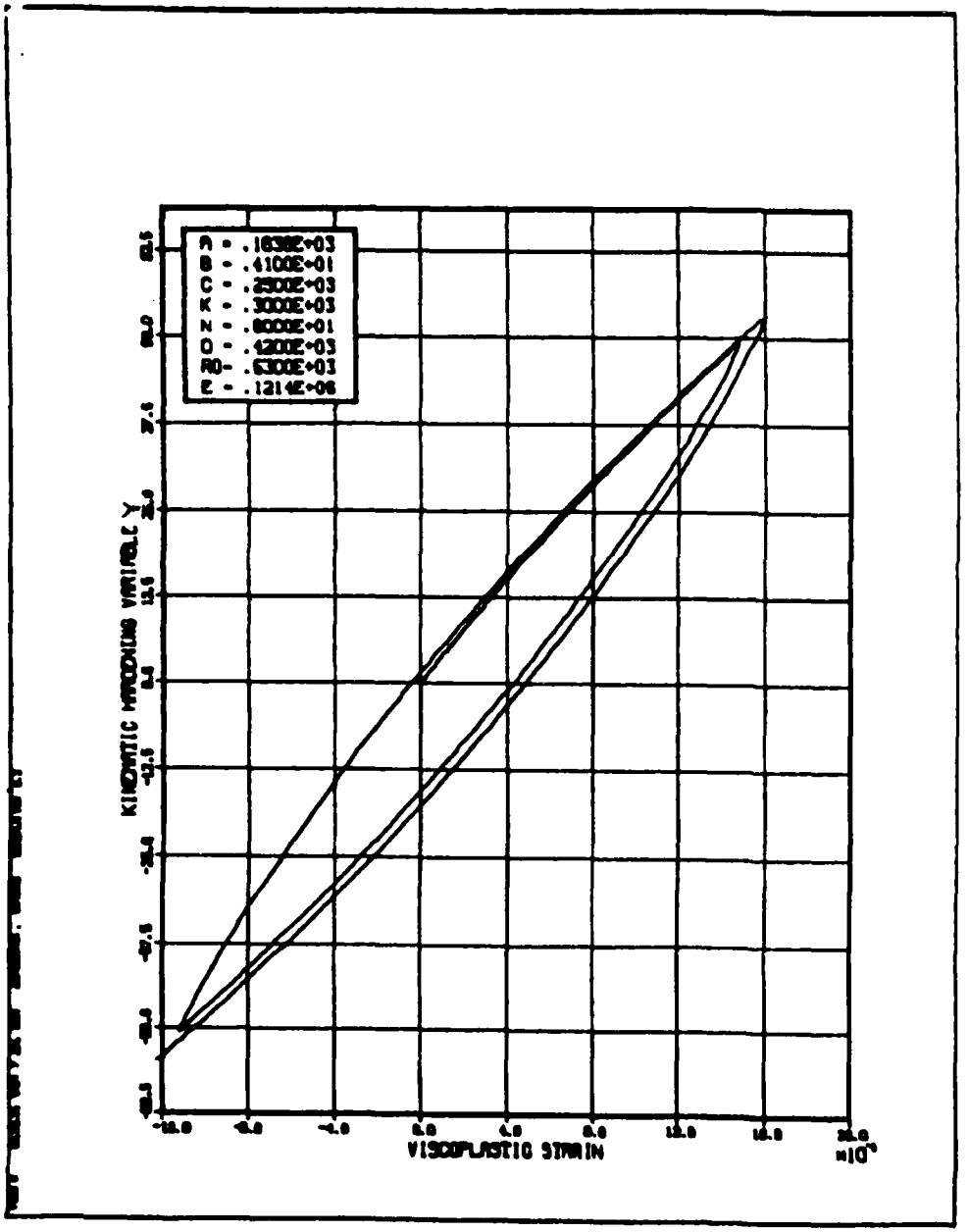

Fig. 2.38. Kinematic hardening variable versus viscoplastic strain for stress-controlled cyclic loading with hold times.

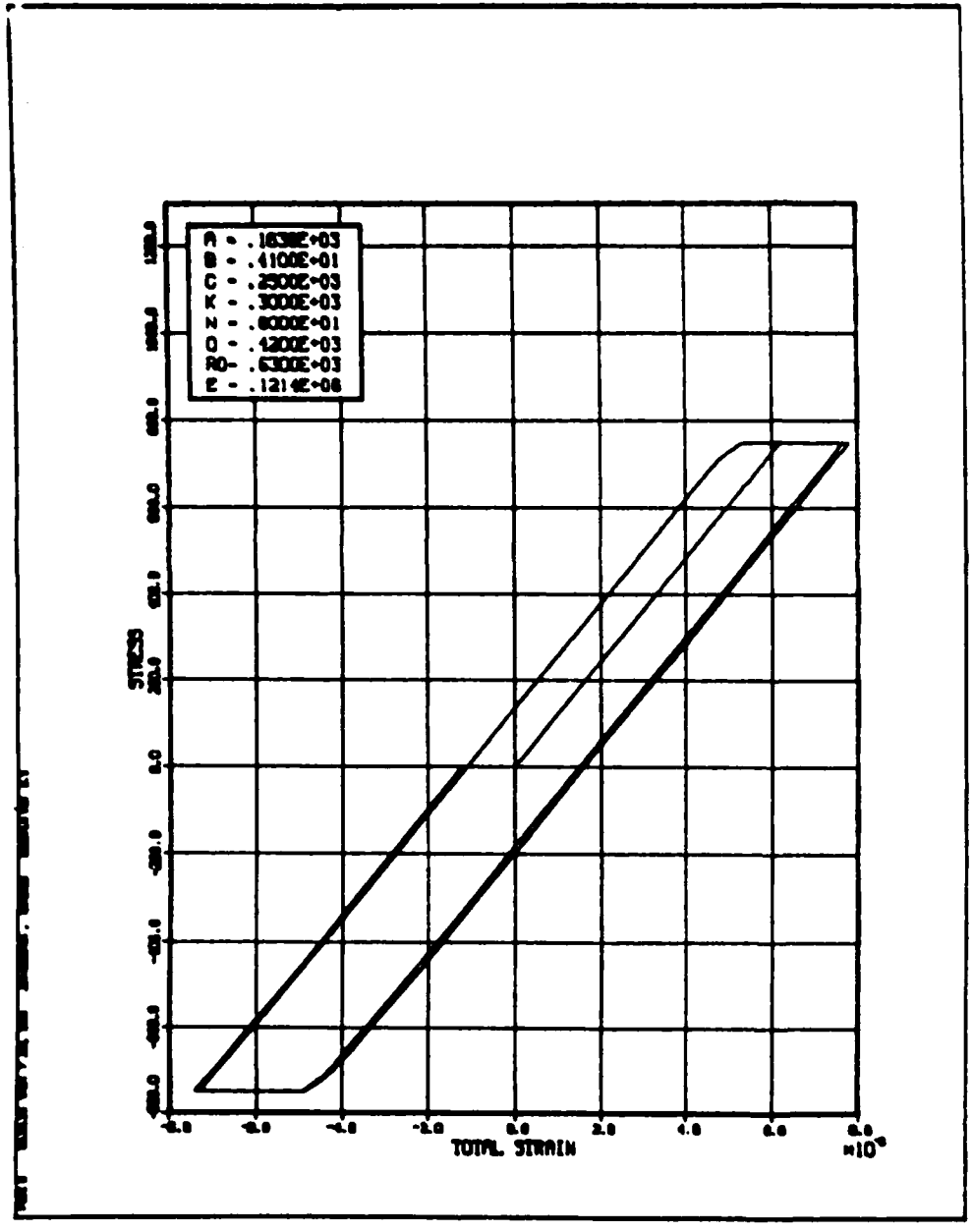

Fig. 2.39. Stress versus total strain for stress-controlled cyclic loading with hold times.

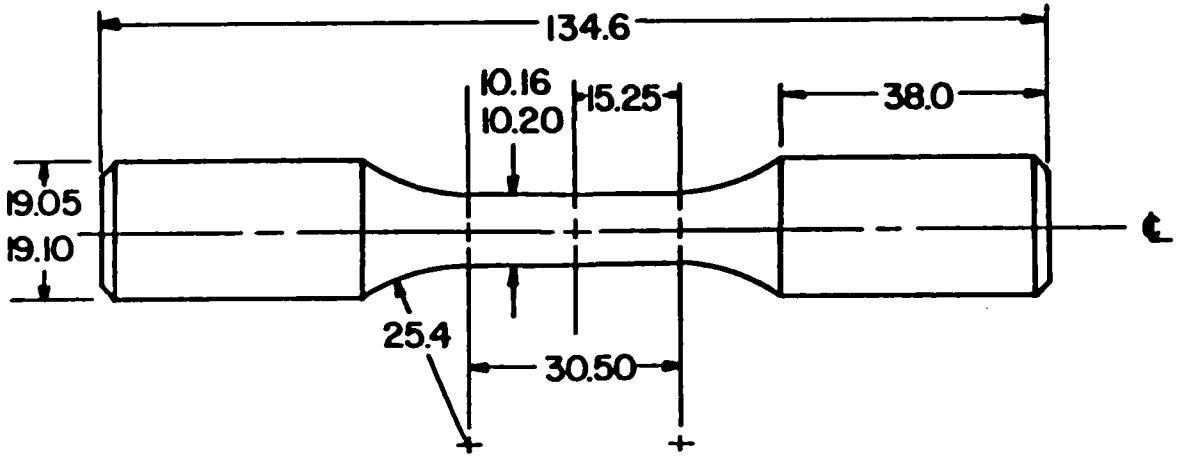

Note 1: All dimensions in mm.

Note 2: Gage section to be polished to a 5μ finish.

Fig. 3.1. Test specimen design.

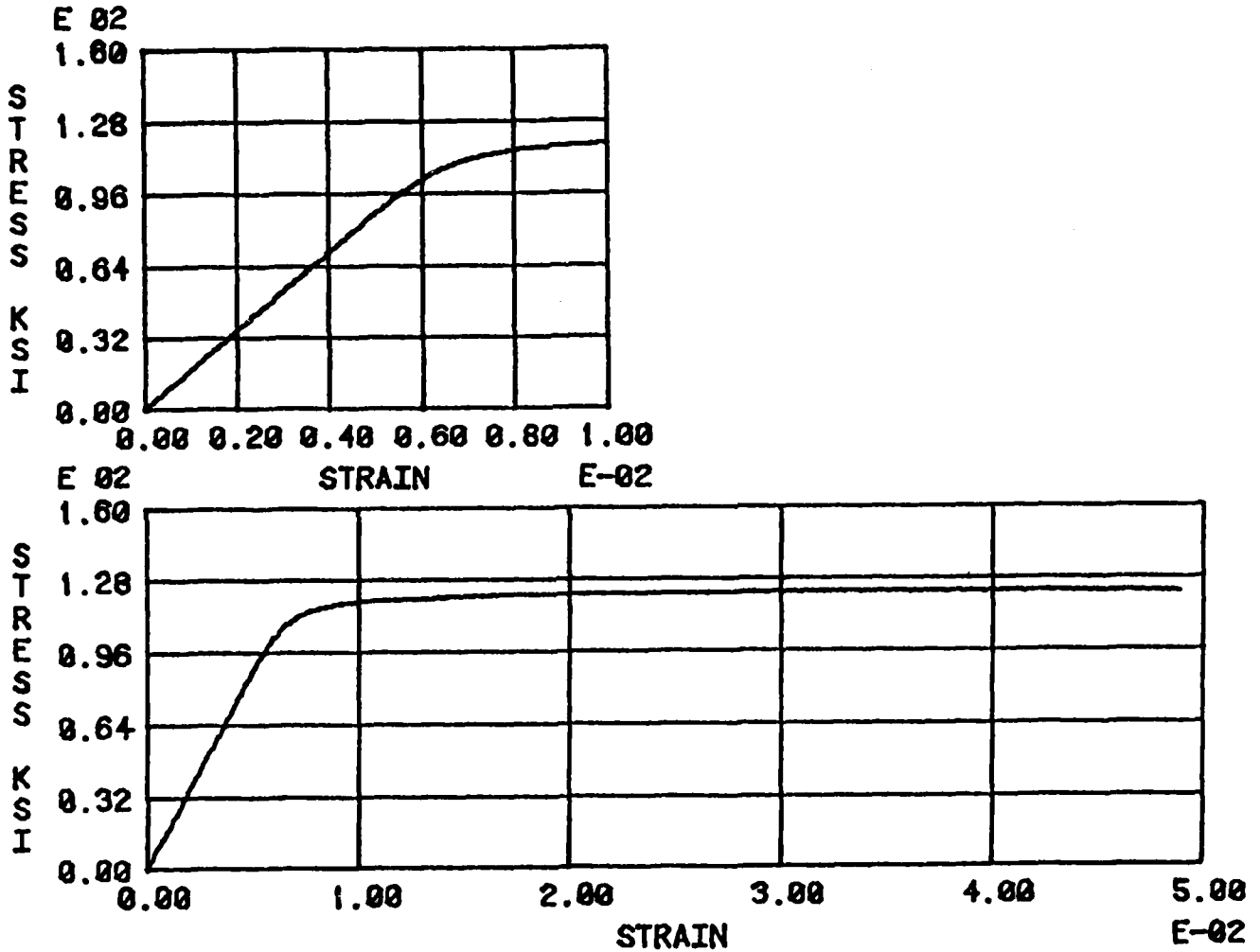

Fig. 3.2. Early portion of the monotonic stress-strain curve, Specimen Number 8.

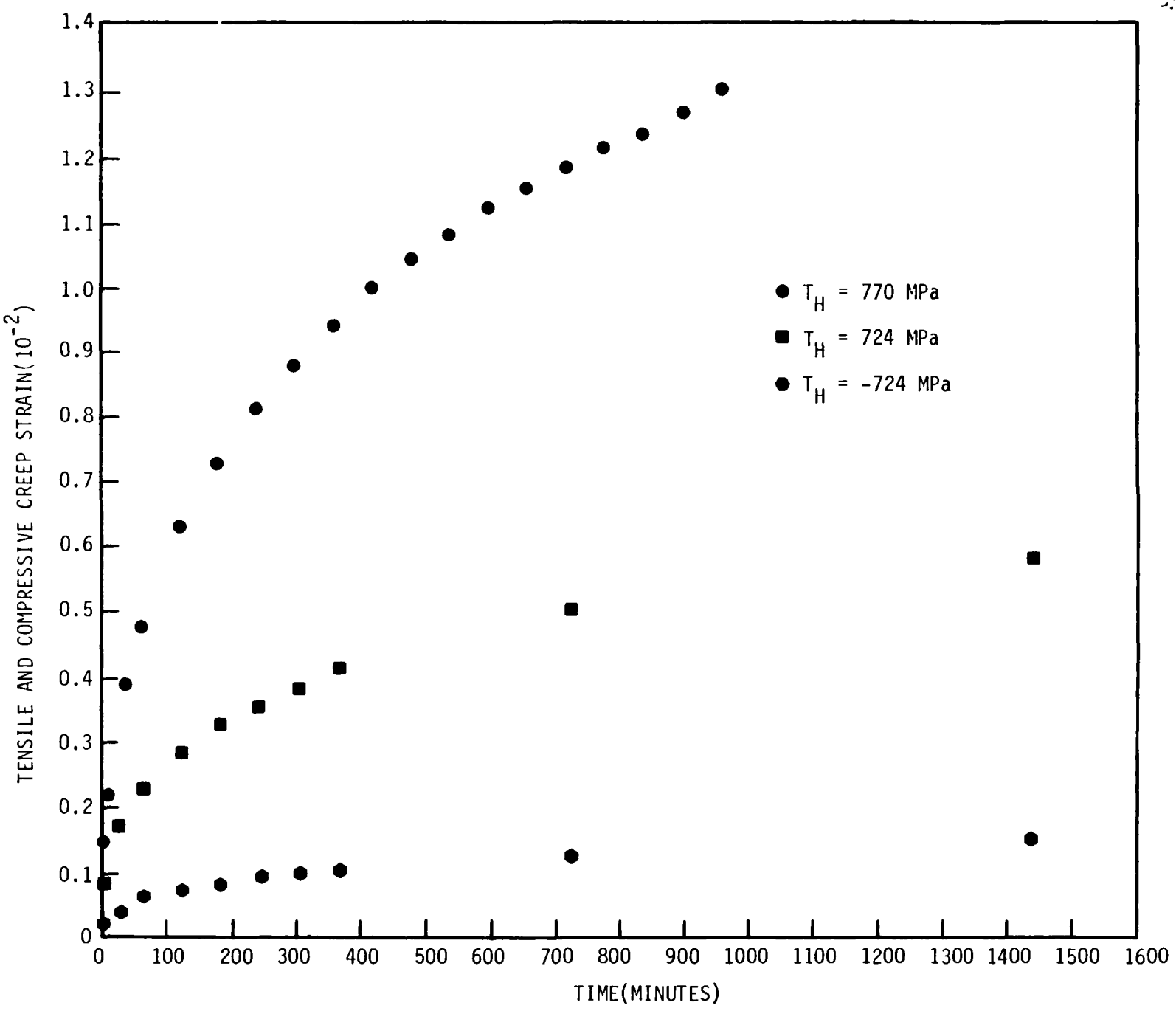

Fig. 3.3. Room temperature creep behavior of Ti-6Aℓ-4V SUPER ELI.

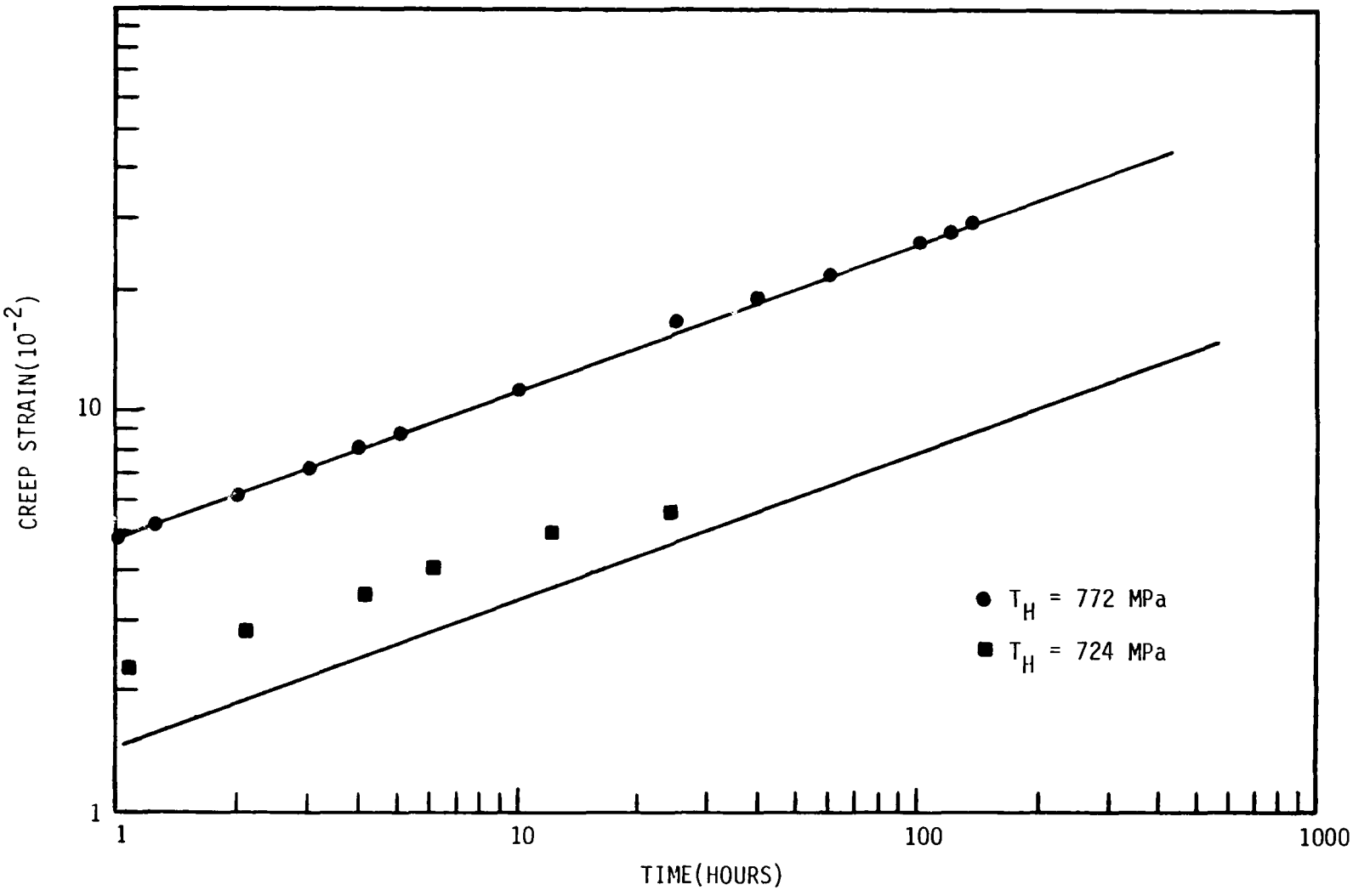

Fig. 3.4. Calculated versus measured creep strain for two stress levels.

AD-A164 082 LIFE PREDICTION FOR A STRUCTURAL MATERIAL UNDER CYCLIC 2/2
LOADS WITH HOLD TI.. (U) GEORGE WASHINGTON UNIV
WASHINGTON DC SCHOOL OF ENGINEERING AN..
UNCLASSIFIED J EFTIS ET AL. 31 DEC 84 AFOSR-TR-85-1237 F/G 20/11 NL

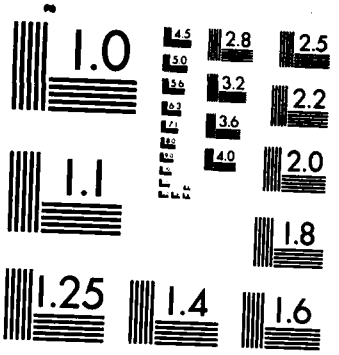

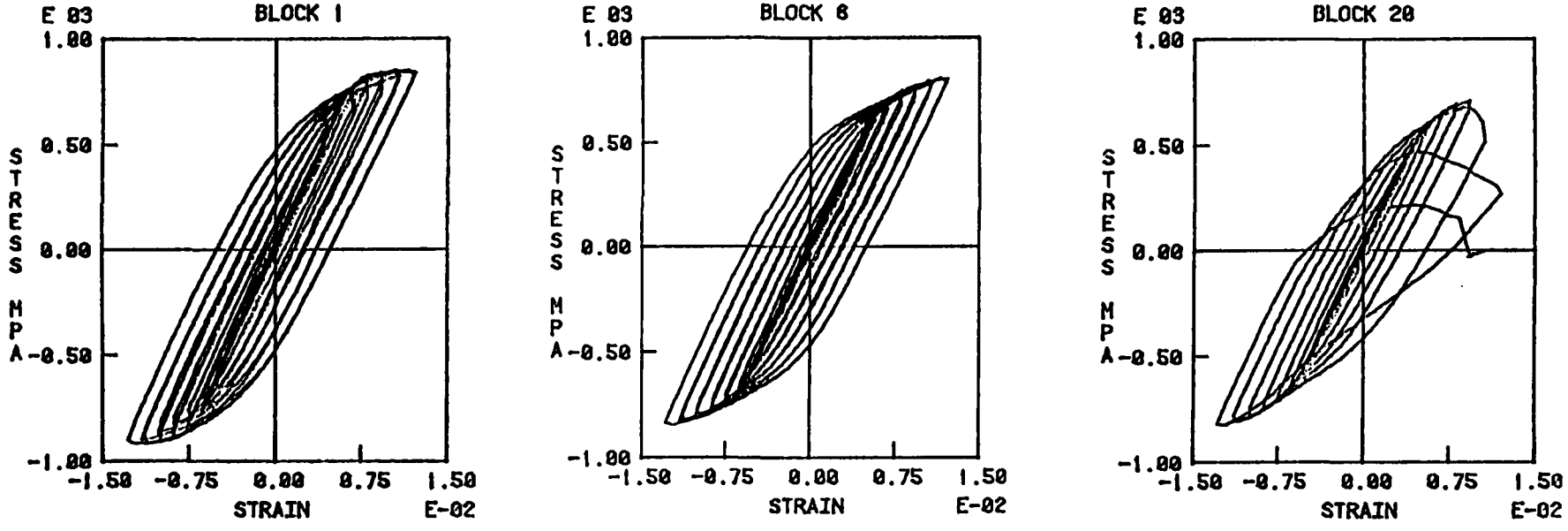

Fig. 3.5. Hysteresis loops for three blocks of incremental stress tests on Specimen No. 14.

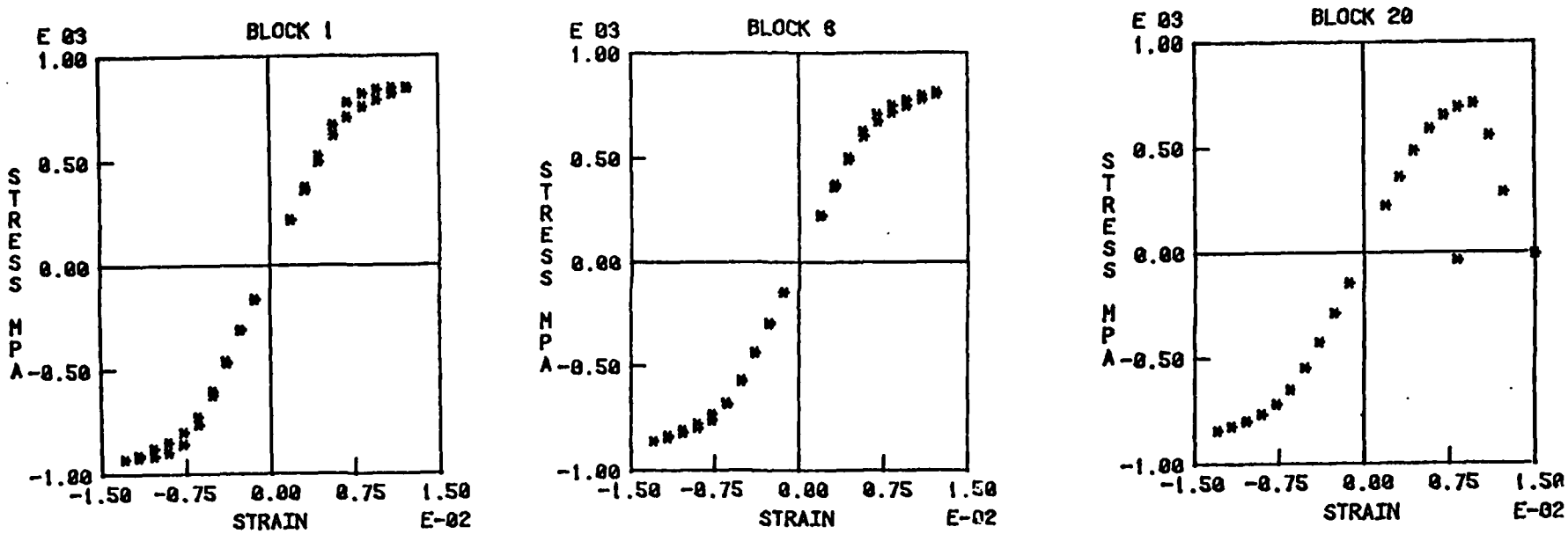

Fig. 3.6. Stabilized cyclic stress-strain curves for three blocks of incremental step tests on Specimen No. 14.

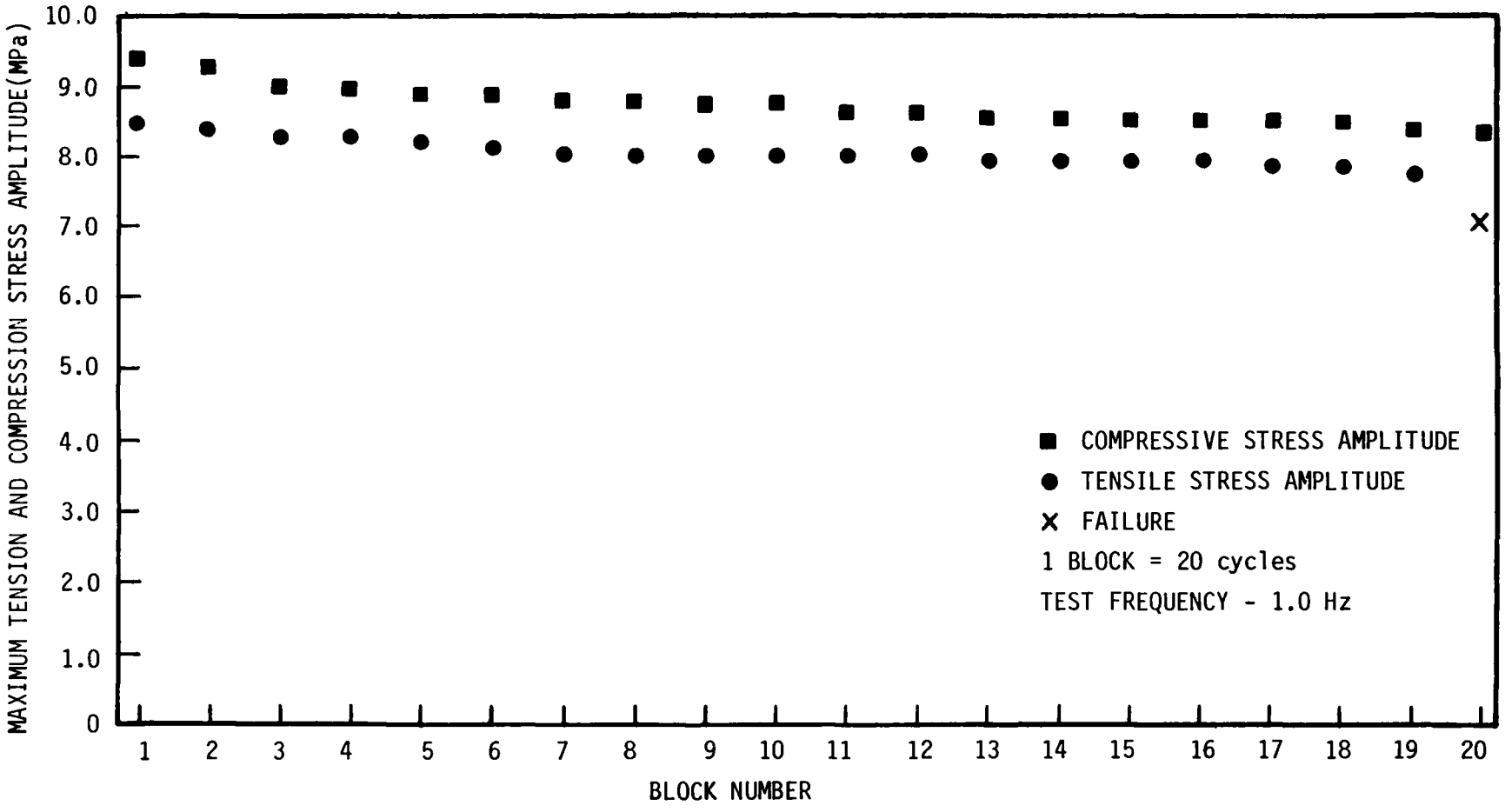

Fig. 3.7. Tension and compression stress amplitudes versus block number, Specimen Number 14.

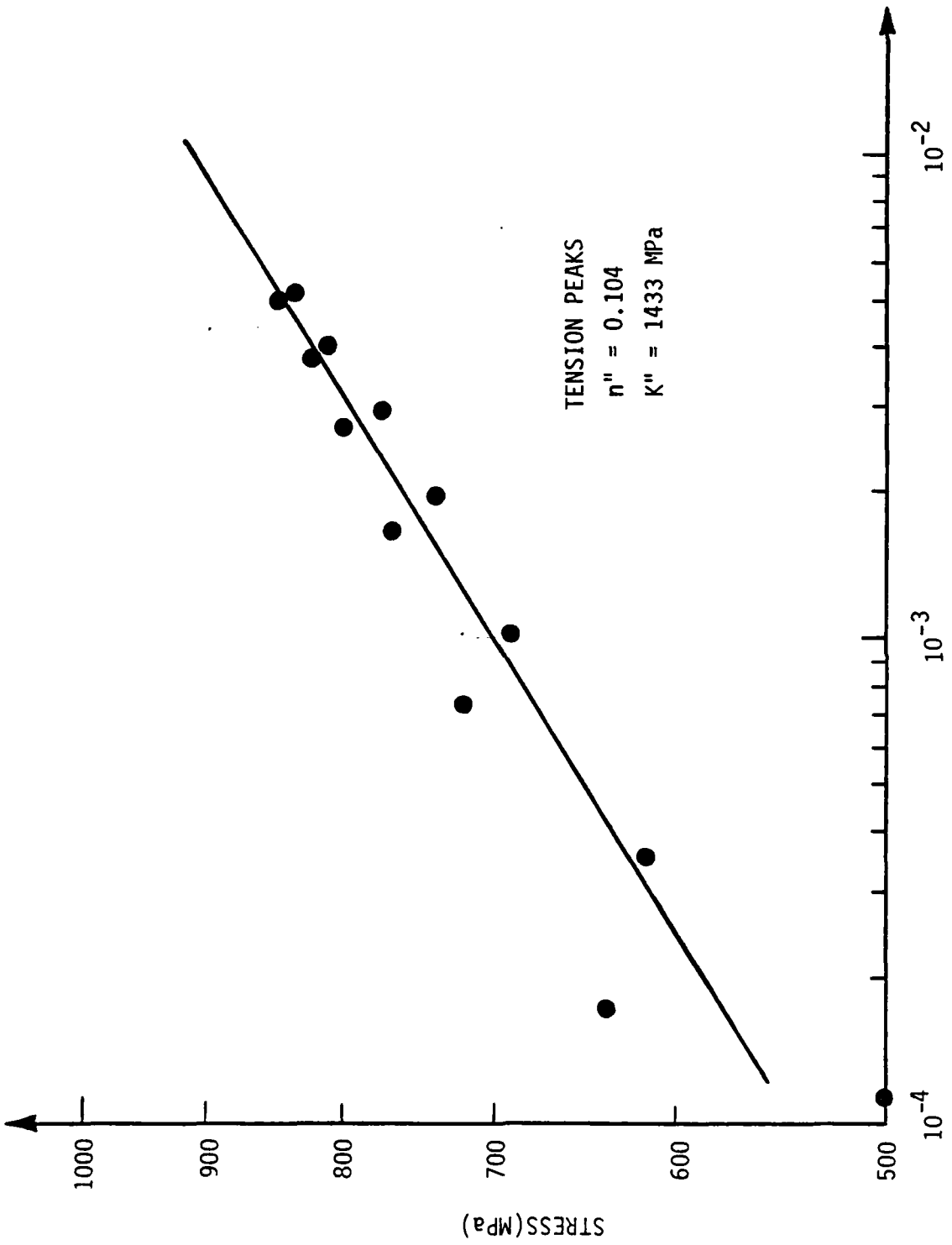

Fig. 3.8. Tensile and compressive peaks for Block 8, increasing and decreasing strain values shown.

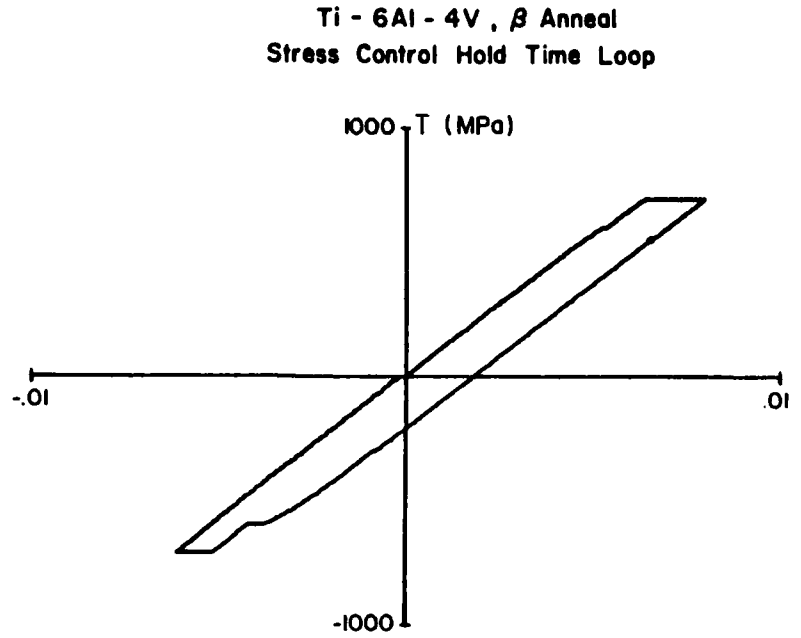

(a) Cycle 157

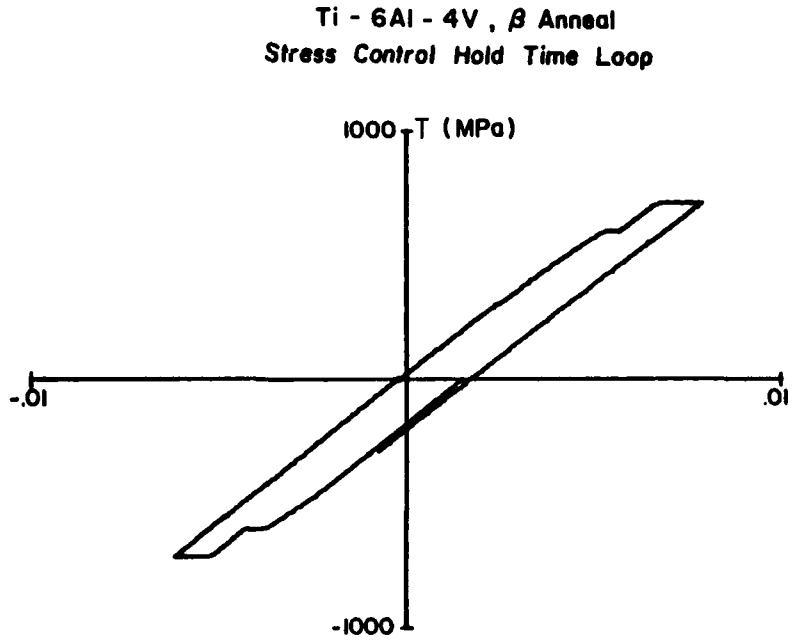

(b) Cycle 158

Fig. 3.9. Stress control hold-time hysteresis loops for Specimen No. 11.

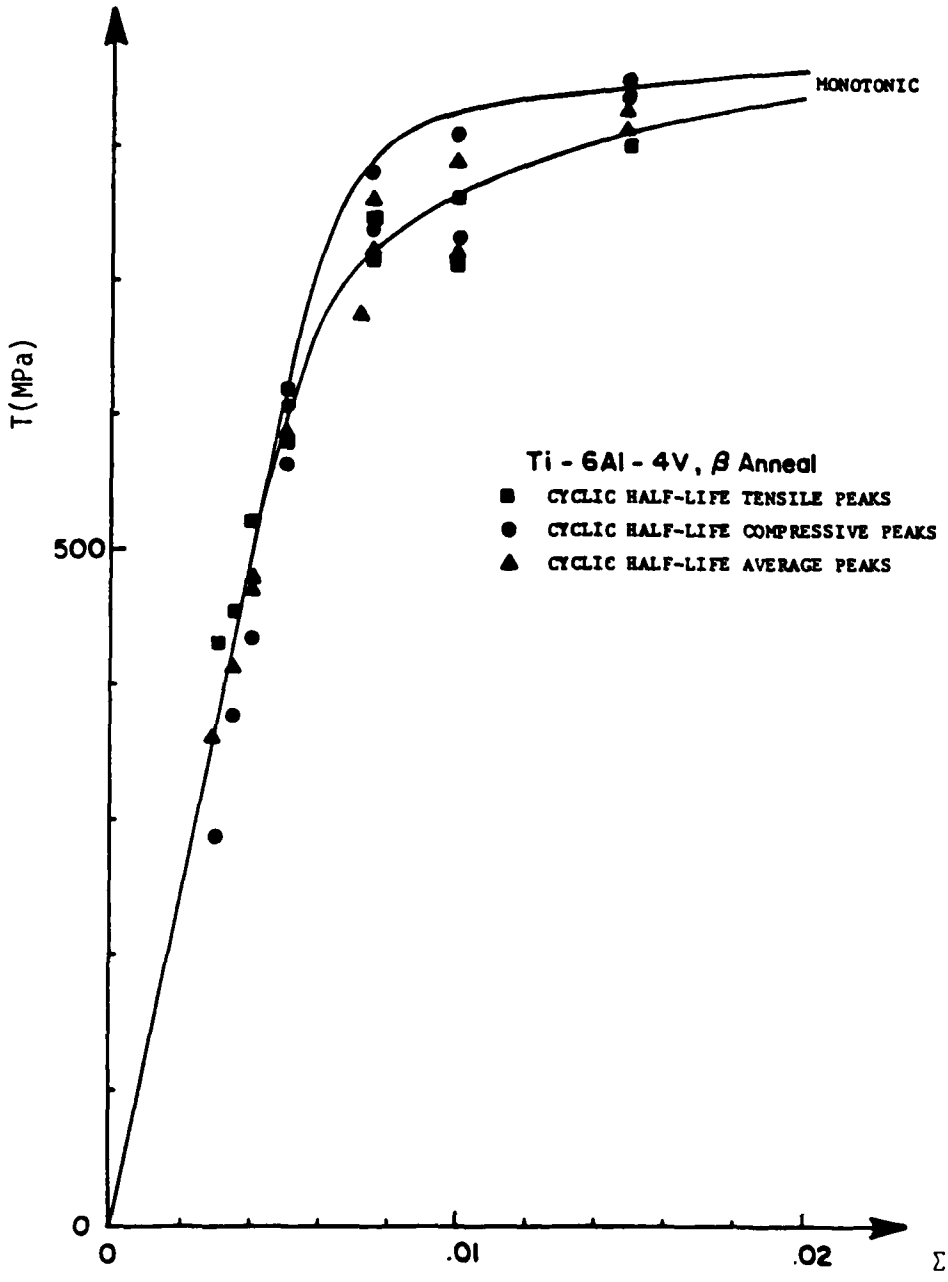

Fig. 3.10. Cyclic stress-strain response of Ti-6Aℓ-4V.

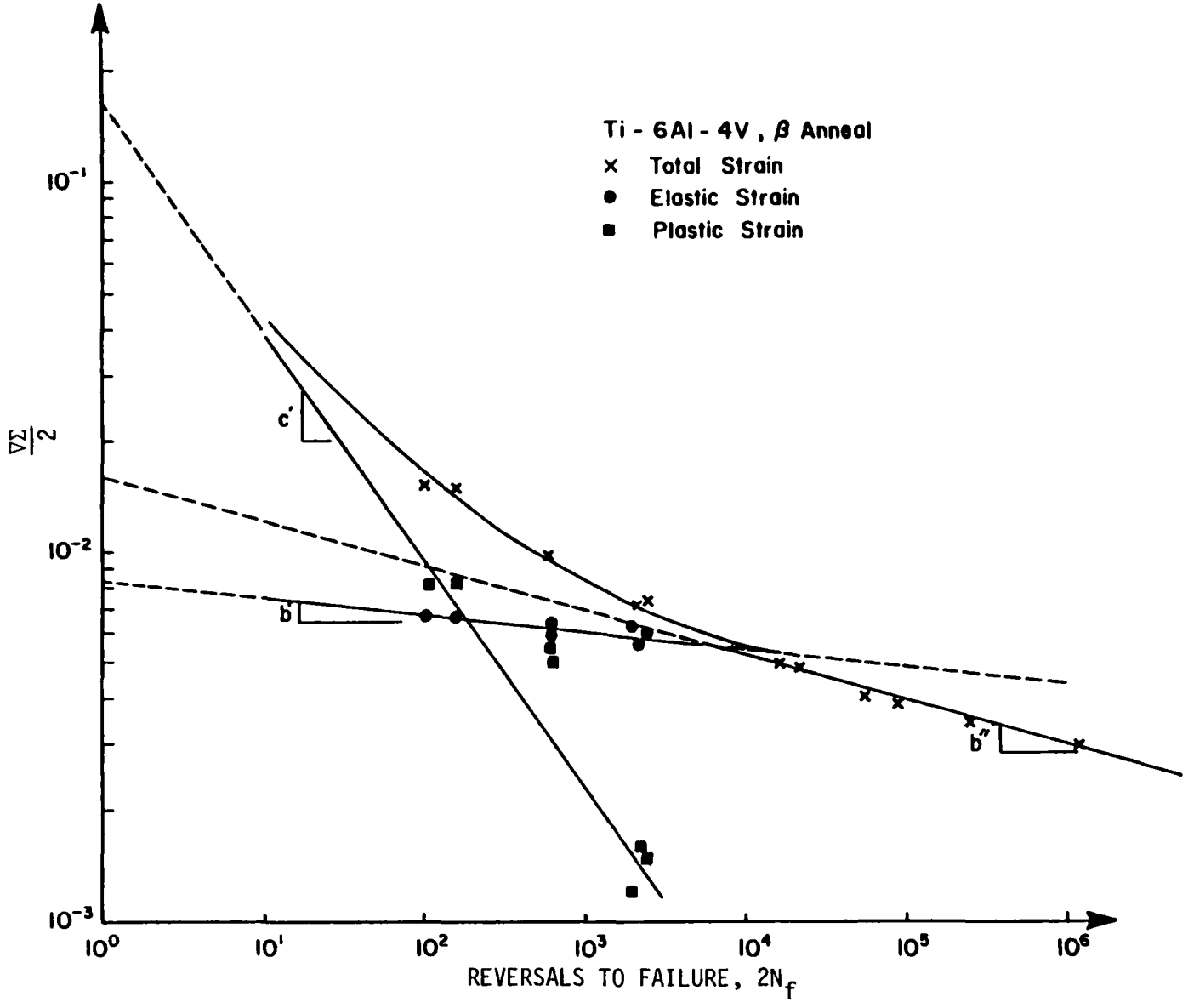

Fig. 3.11. Cyclic strain versus reversals to failure for Ti-6Aℓ-4V.

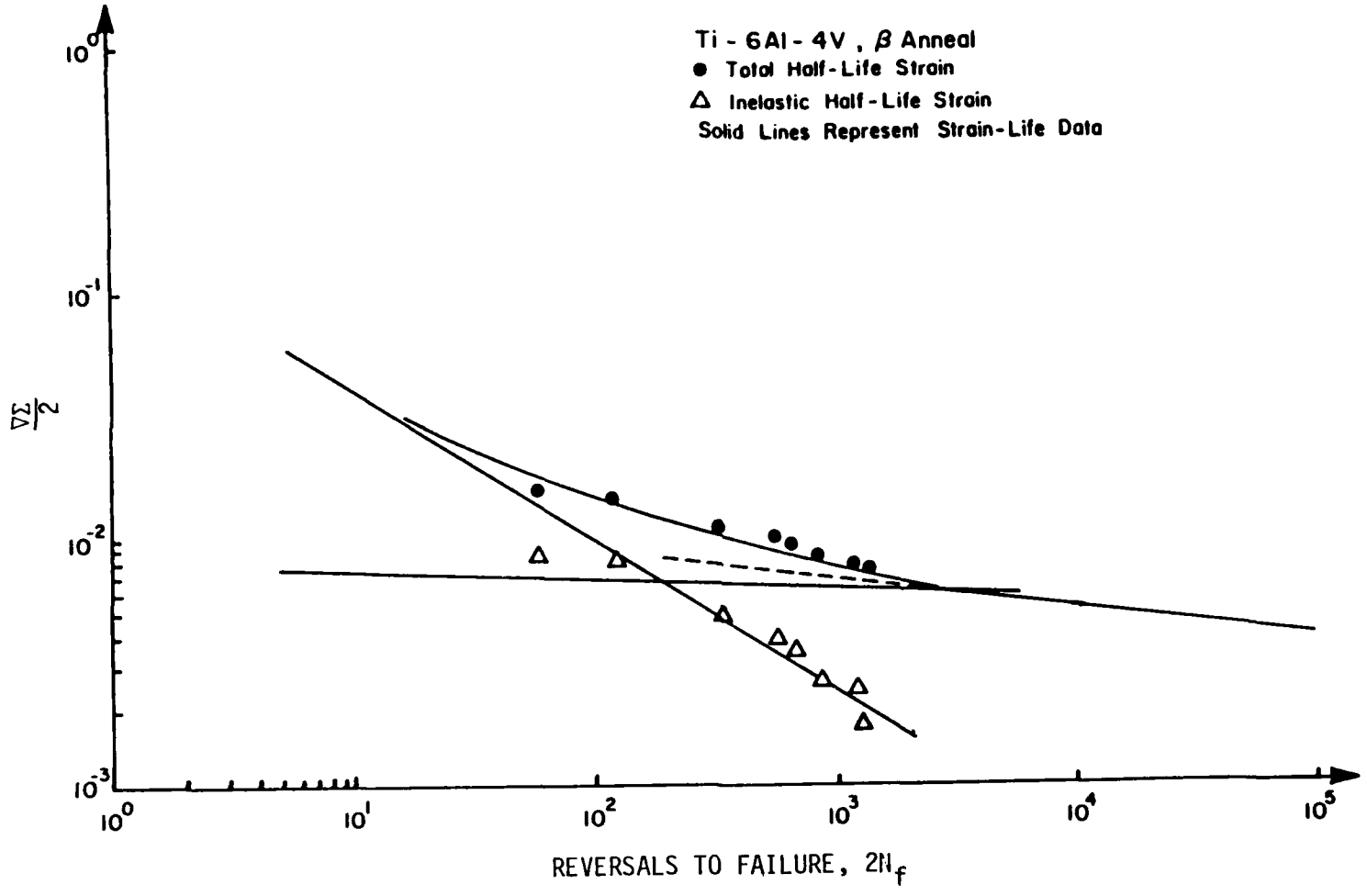

Fig. 3.12. Cyclic stress(with hold times) versus fatigue life for Ti-6Aℓ-4V.

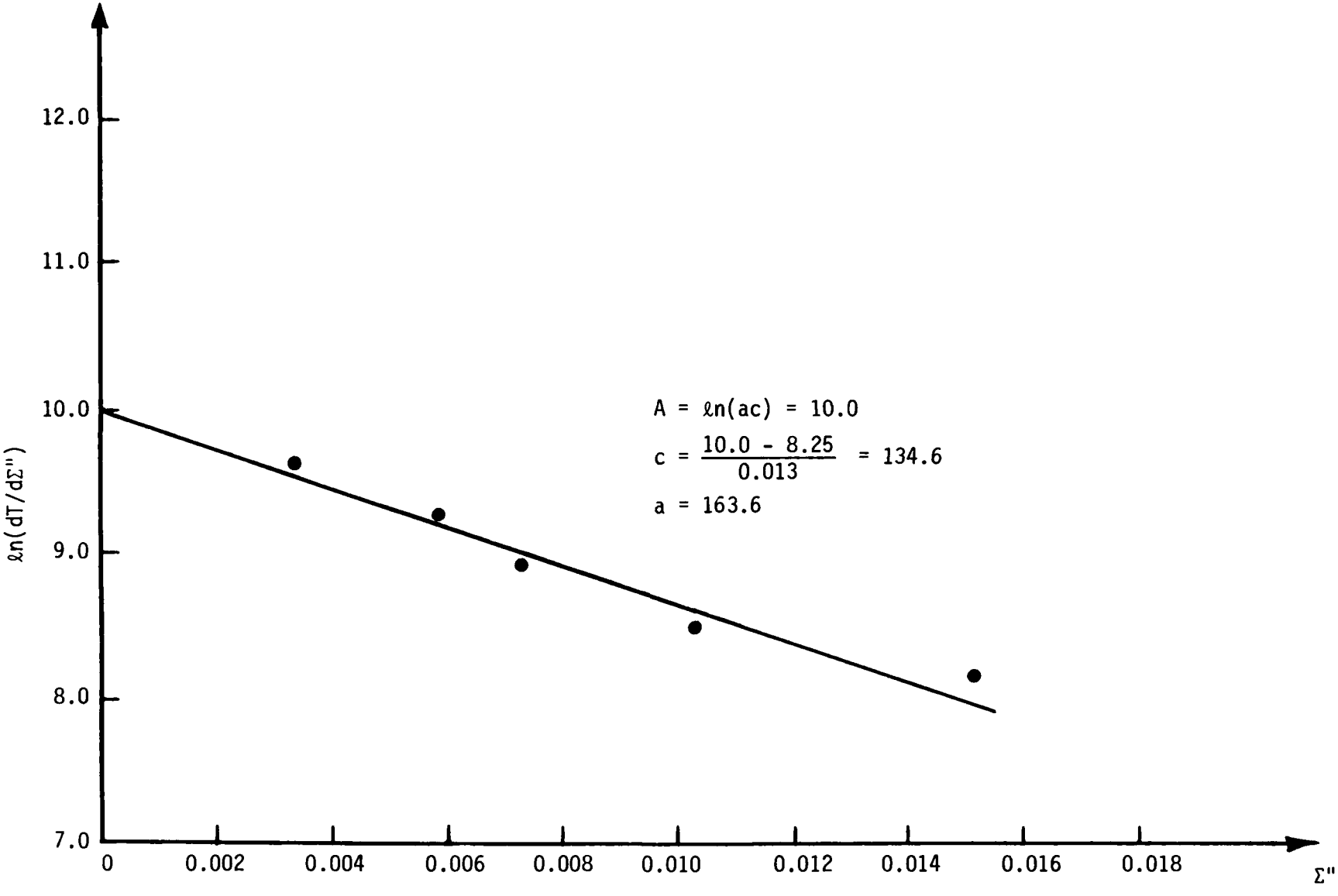

Fig. 4.1. Plot of equation (4.6), $\ell n(dT/d\Sigma")$ versus $\Sigma"$ for the cyclic stress-strain curve.

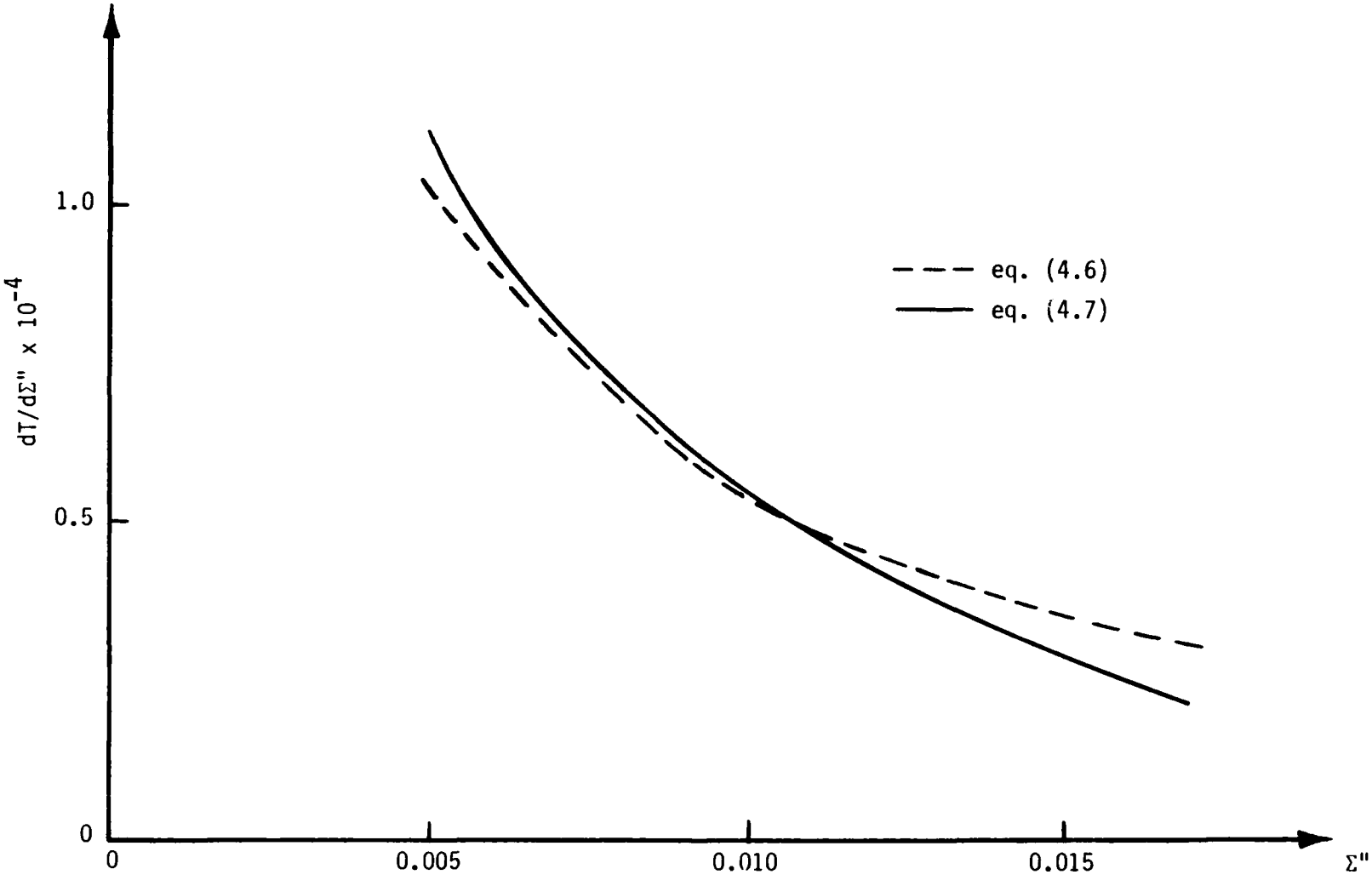

Fig. 4.2. Comparison of equations (4.6) and (4.7) for $dT/d\Sigma''$ versus Σ''.

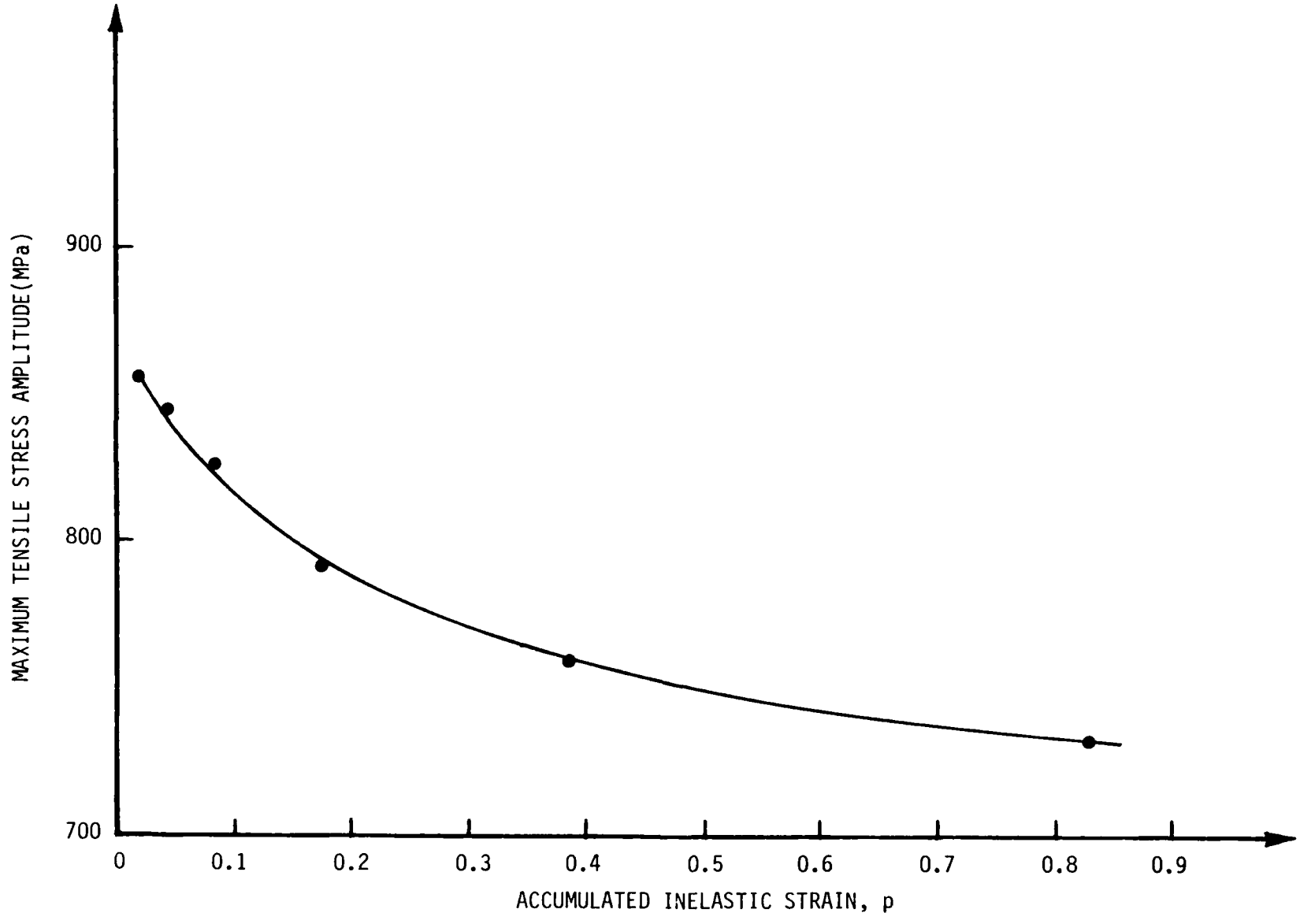

Fig. 4.3. Maximum tensile stress amplitude versus accumulated inelastic strain.

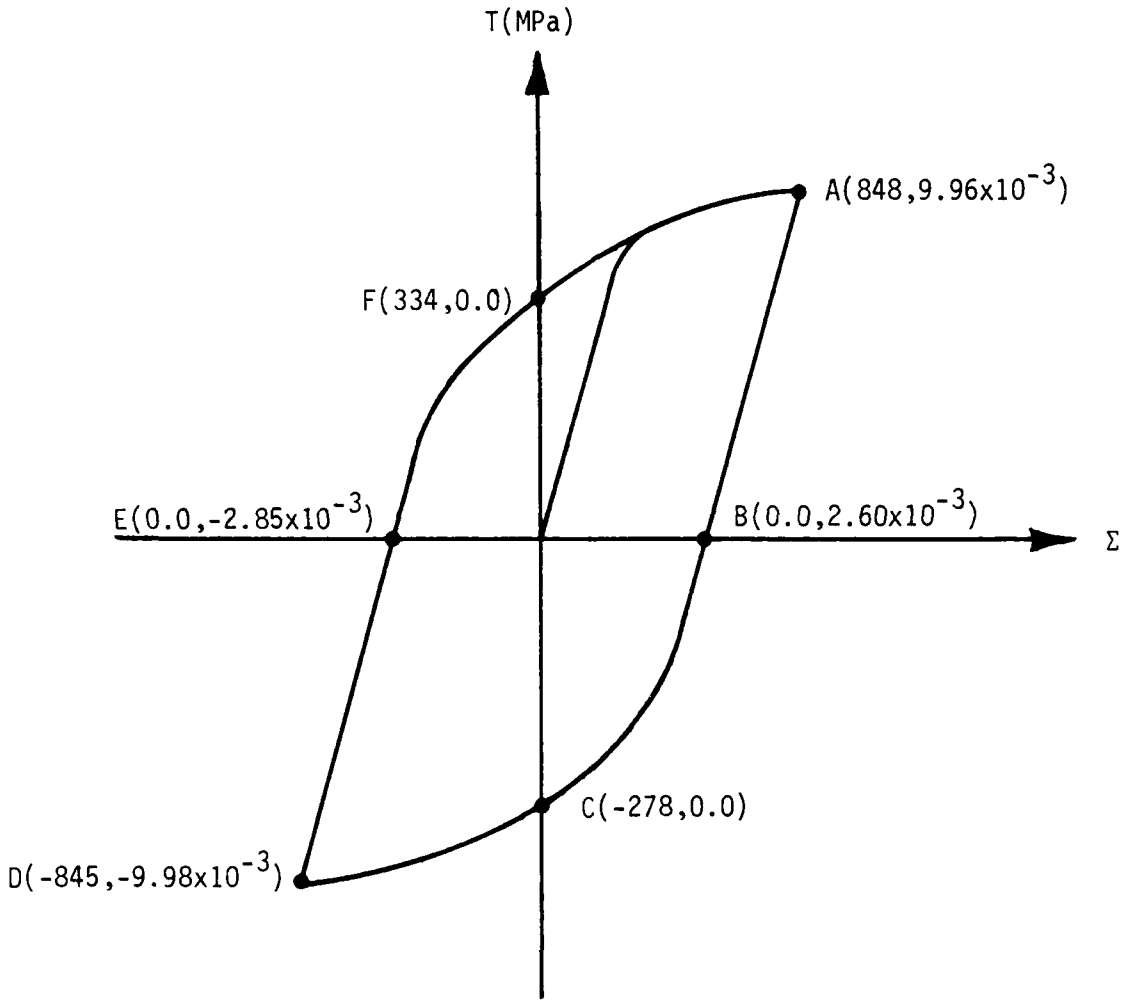

Fig. 4.4. Schematic representation of hysteresis loop for load cycle No. 4, Specimen No. 26.

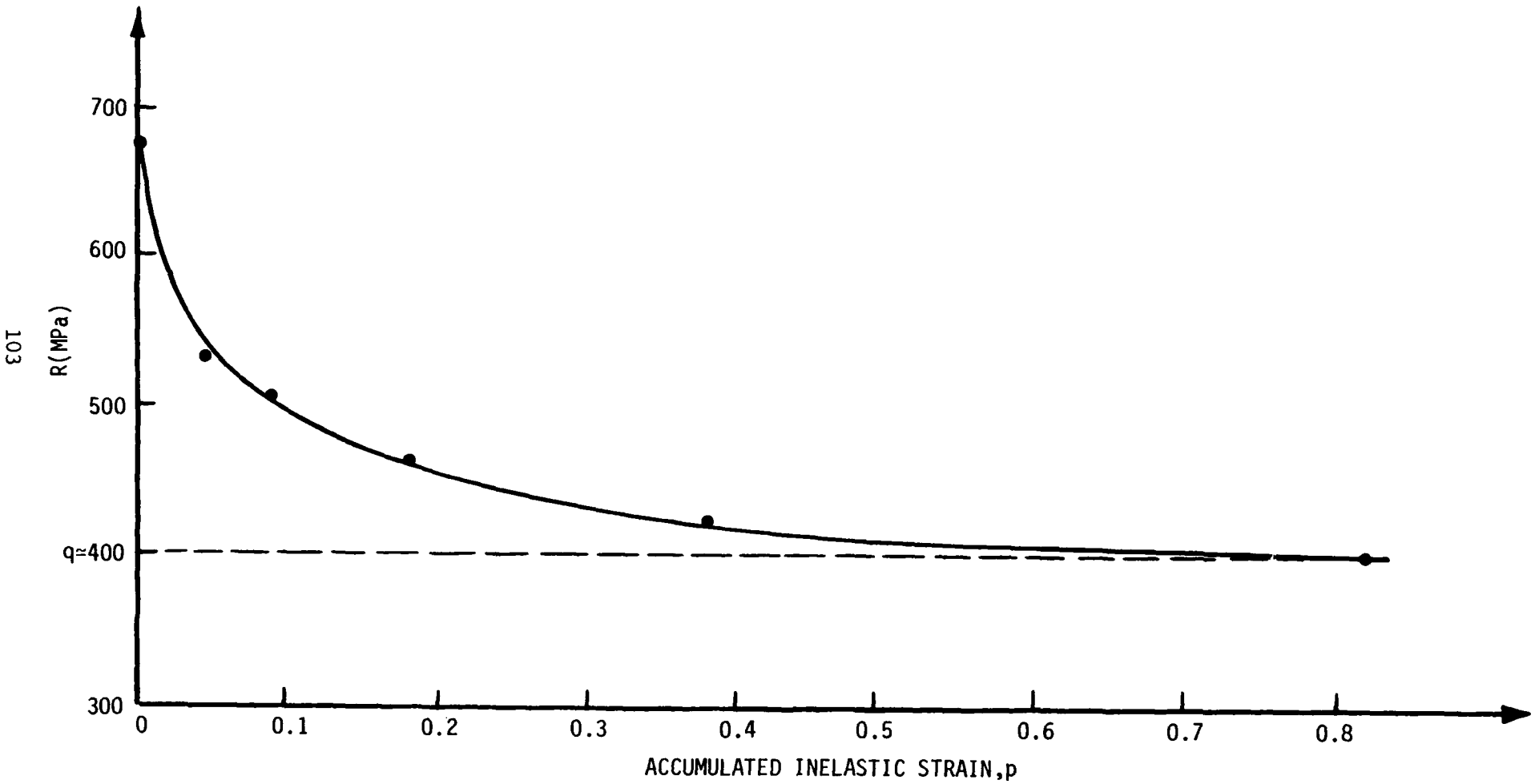

Fig. 4.5. Isotropic hardening variable versus accumulated inelastic strain.

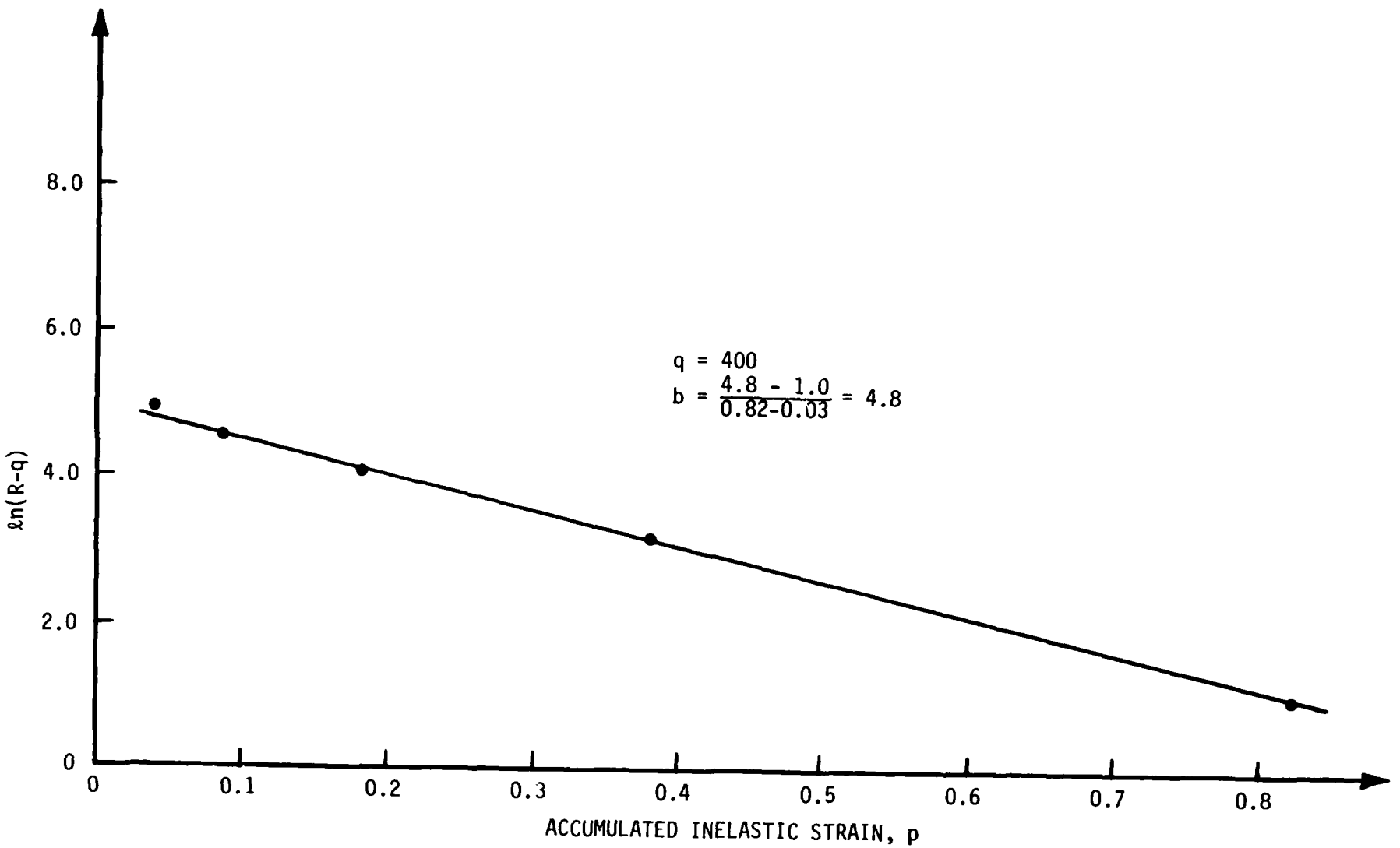

Fig. 4.6. Relationship between ℓn(R-q) and accumulated inelastic strain.

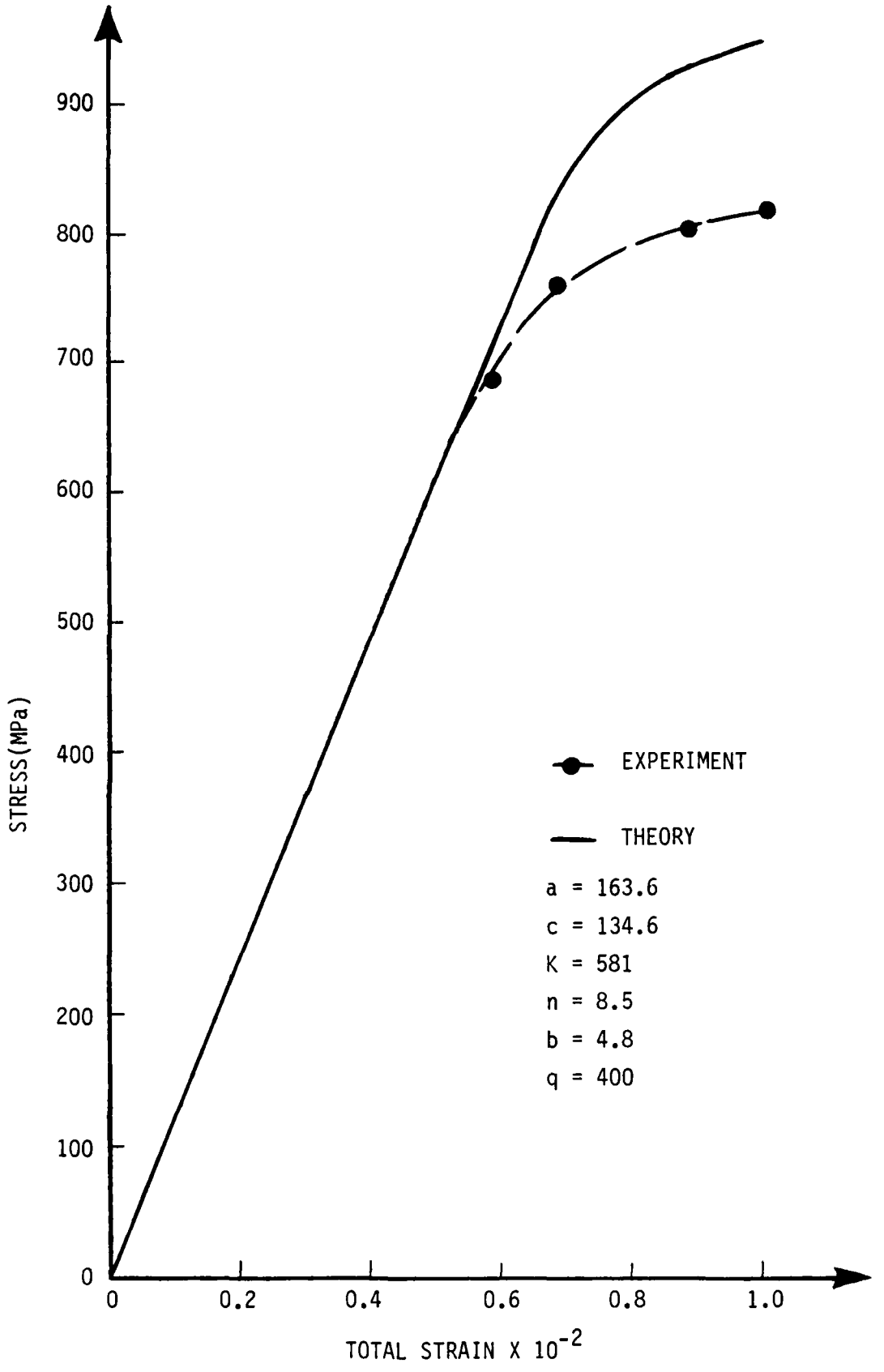

Fig. 4.7. Monotonic stress-strain curve of Ti-6Aℓ-4V at $\dot{\Sigma} = 5.0 \times 10^{-4}$ in/in/sec.

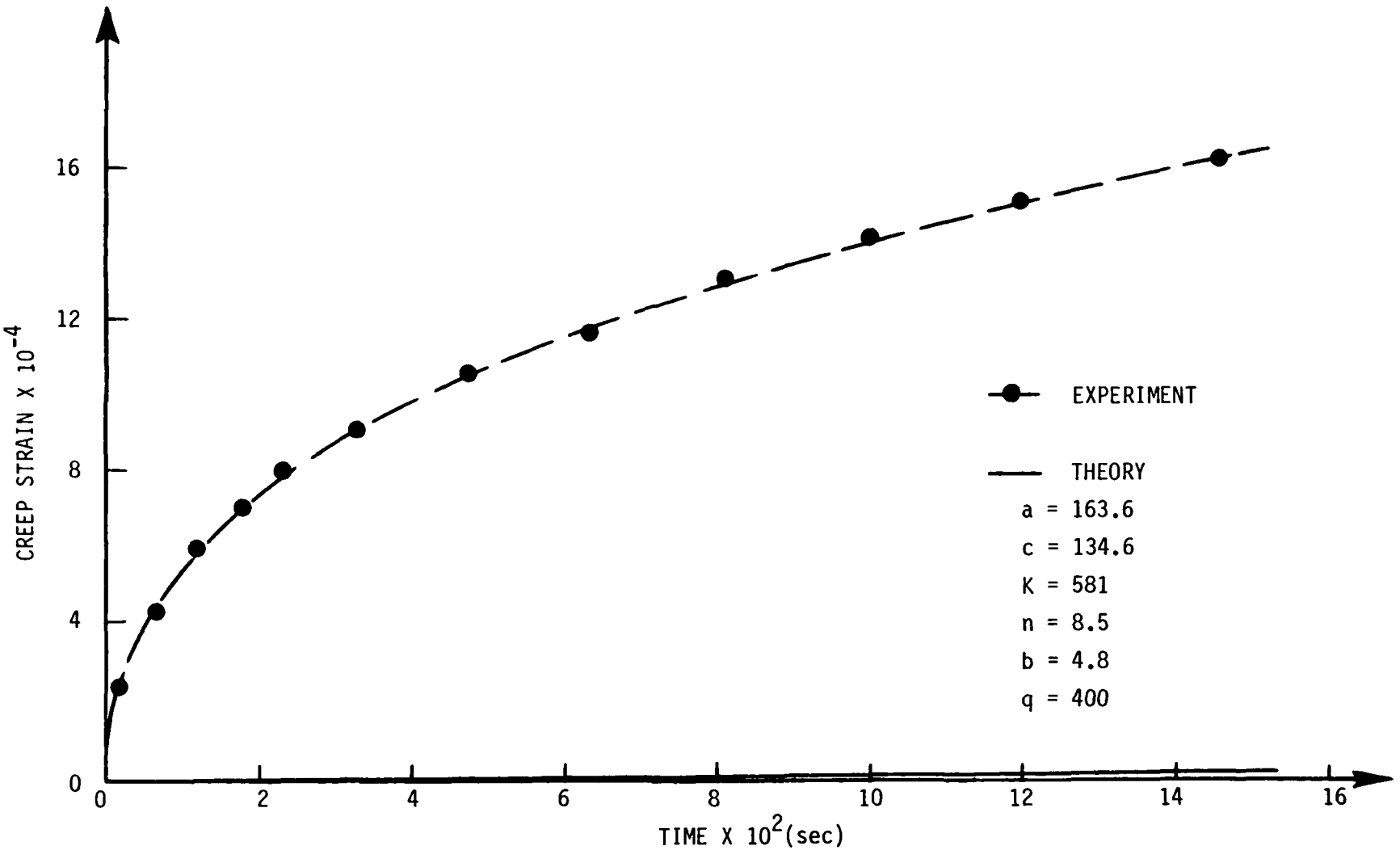

Fig. 4.8. Primary creep at T_H = 723 MPa (room temperature).

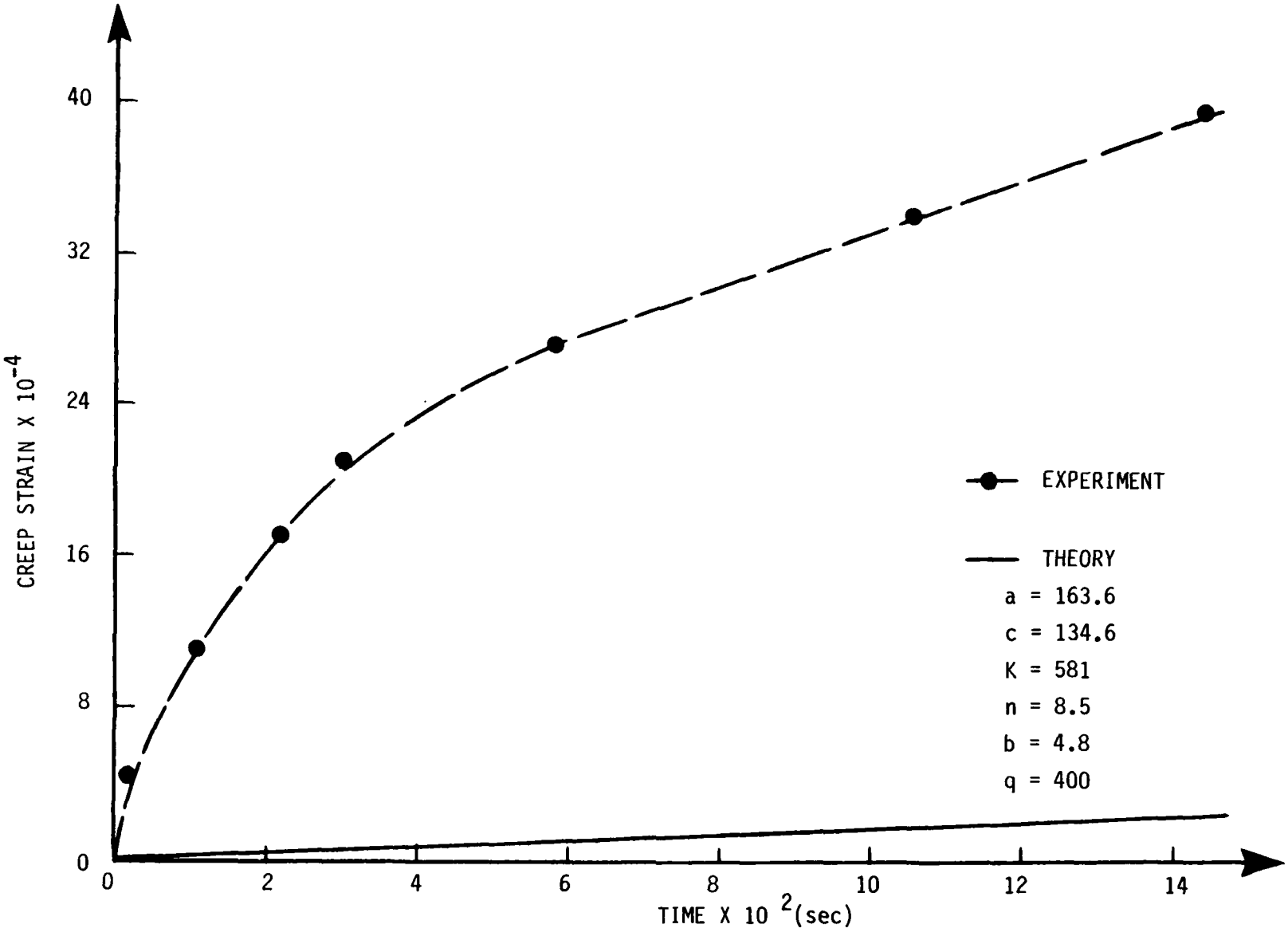

Fig. 4.9. Primary creep at T_H = 770 MPa (room temperature)

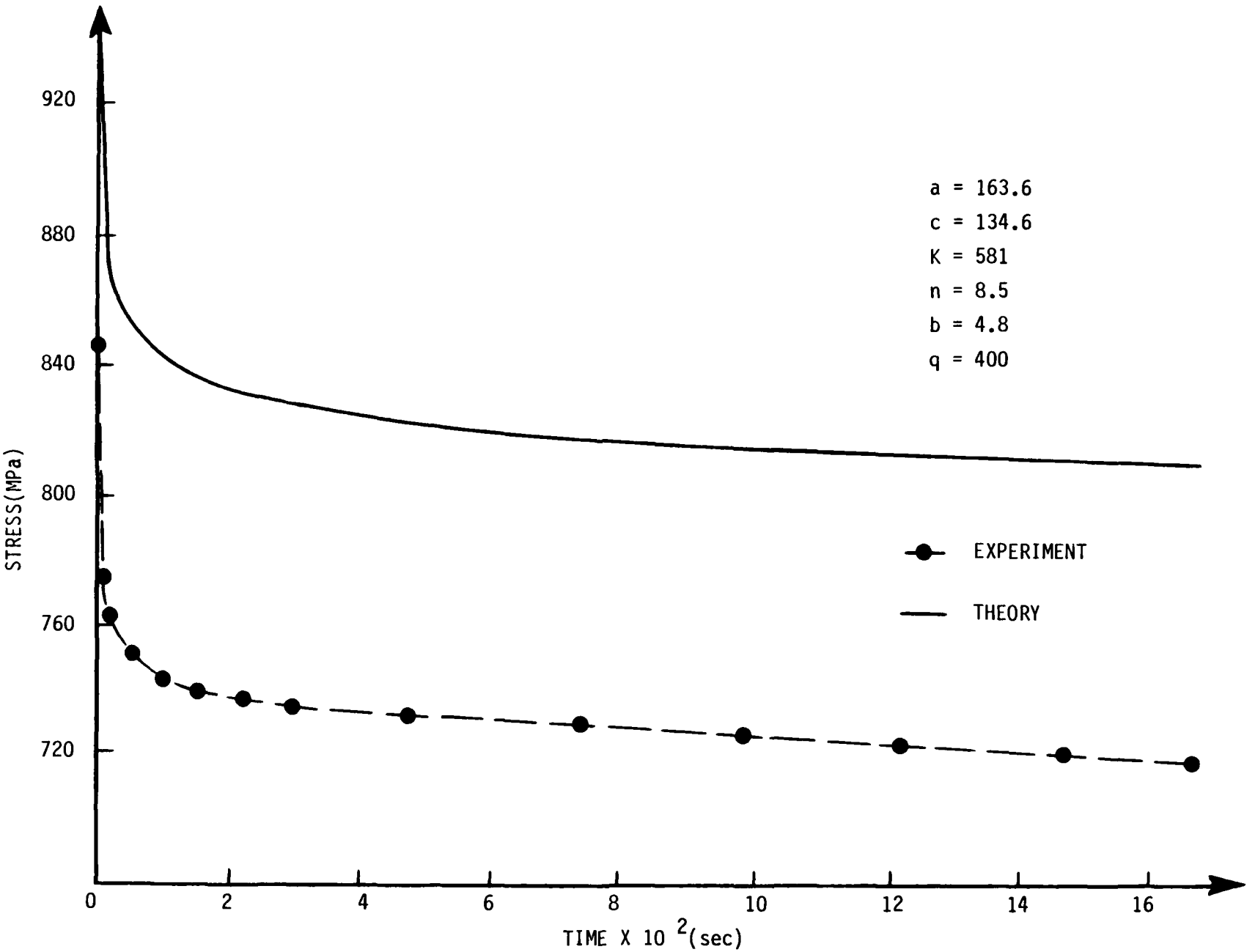

Fig. 4.10. Stress relaxation at Σ_H = 0.01 (room temperature).

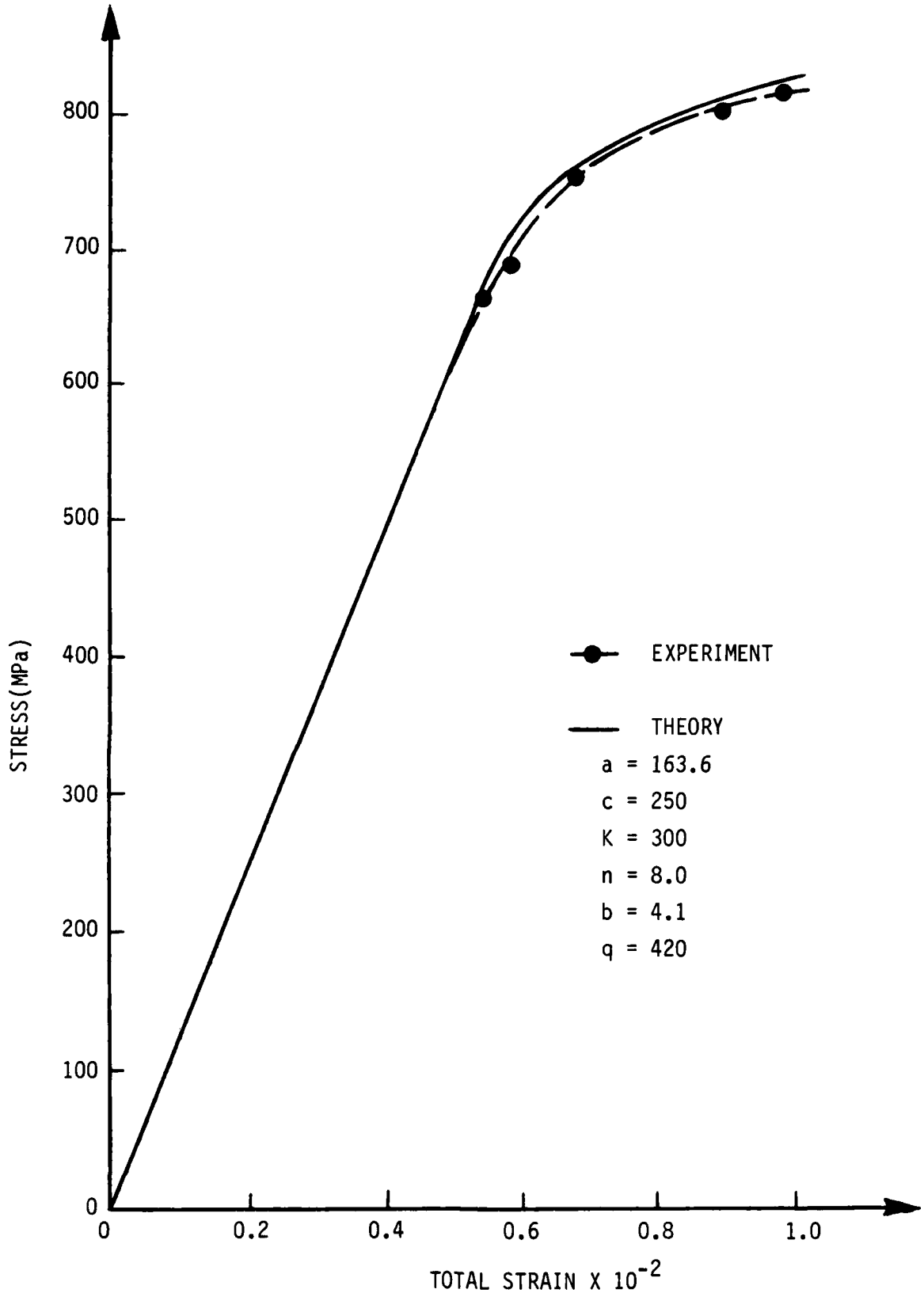

Fig. 4.11. Monotonic stress-strain curve for Ti-6Aℓ-4V at $\dot{\Sigma}$ = 5.0×10^{-4} in/in/sec.

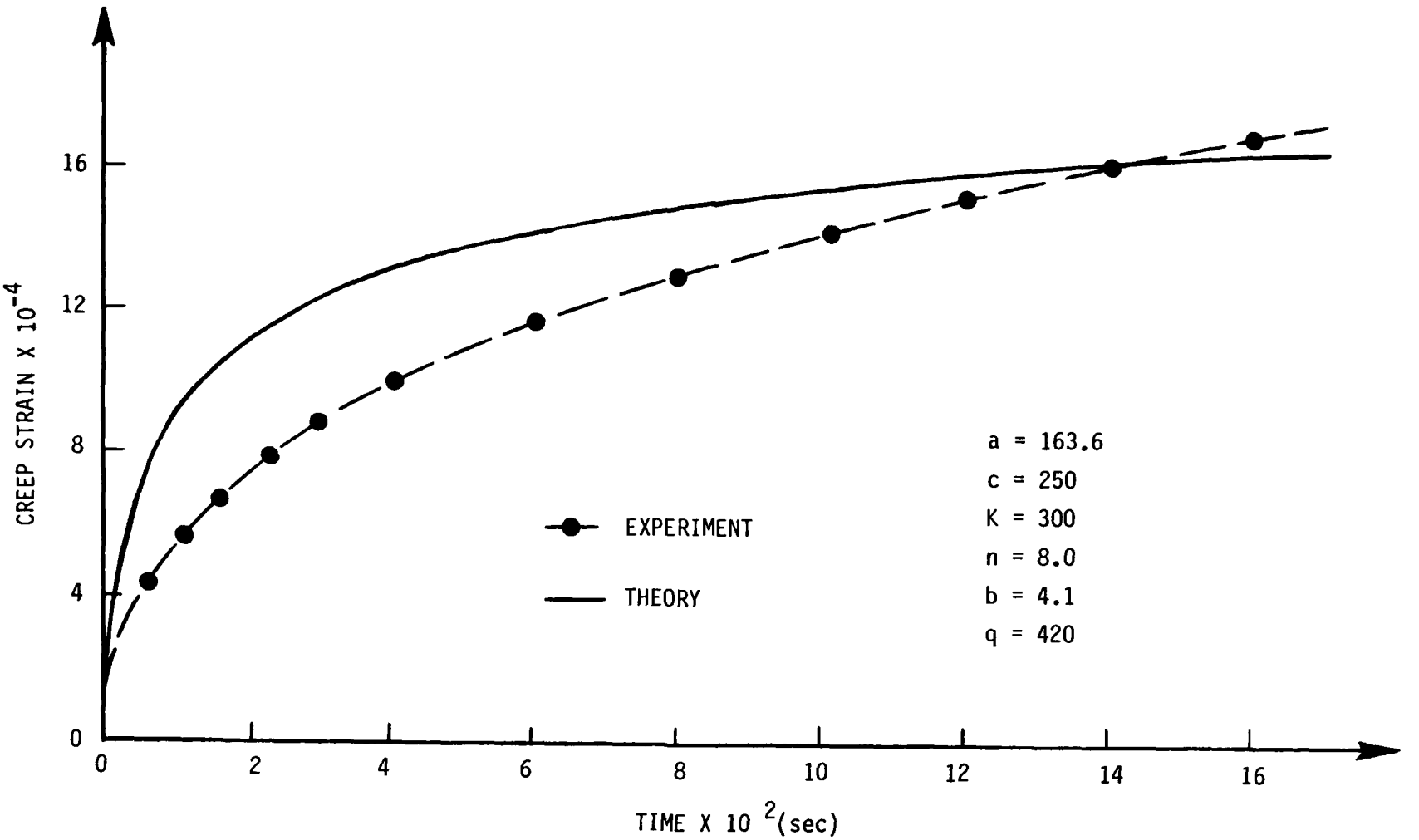

Fig. 4.12. Primary creep at T_H = 723 MPa (room temperature).

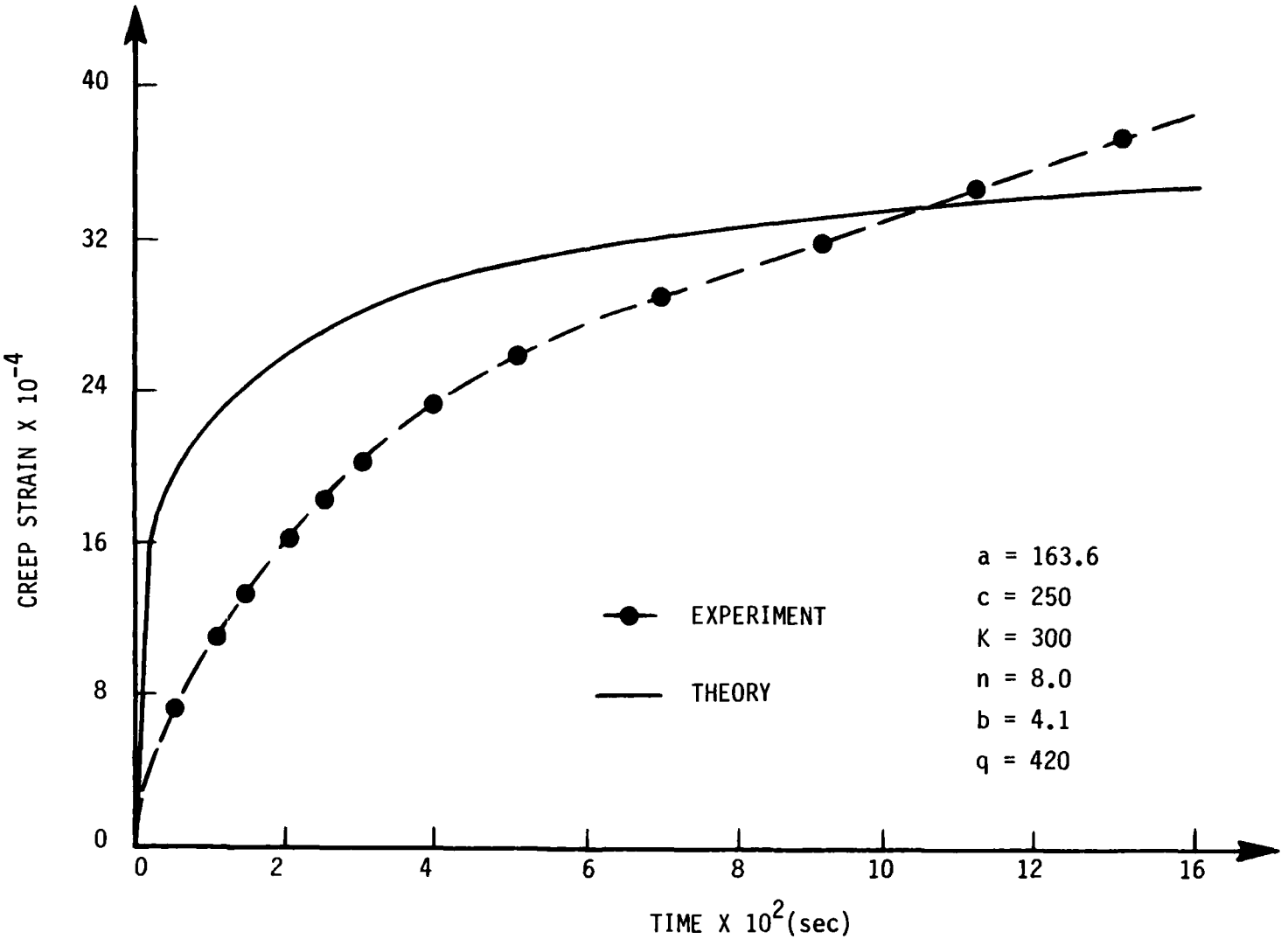

Fig. 4.13. Primary creep at T_H = 770 MPa (room temperature).

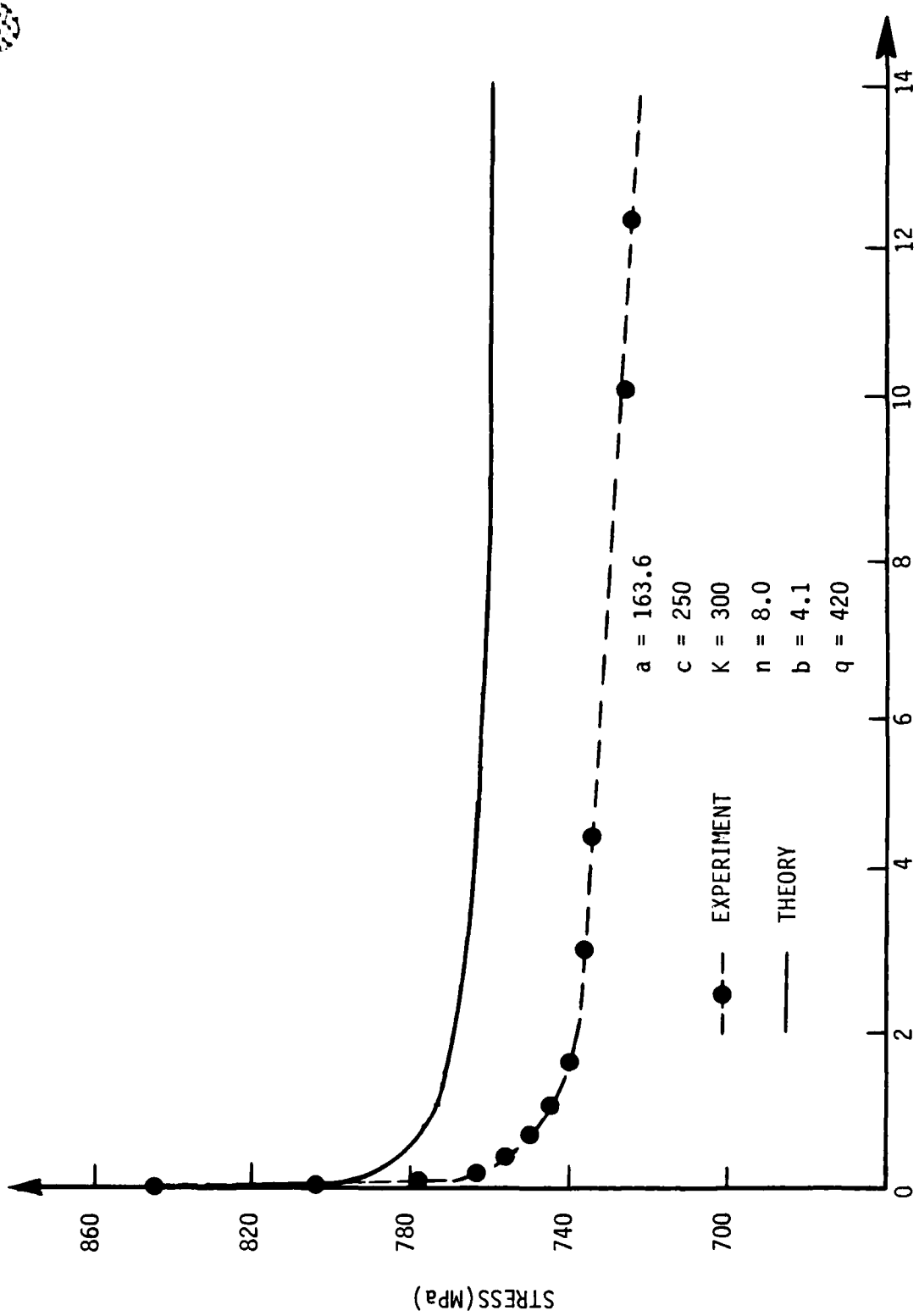

Fig. 4.14. Stress relaxation at Σ_H = 0.01 (room temperature).

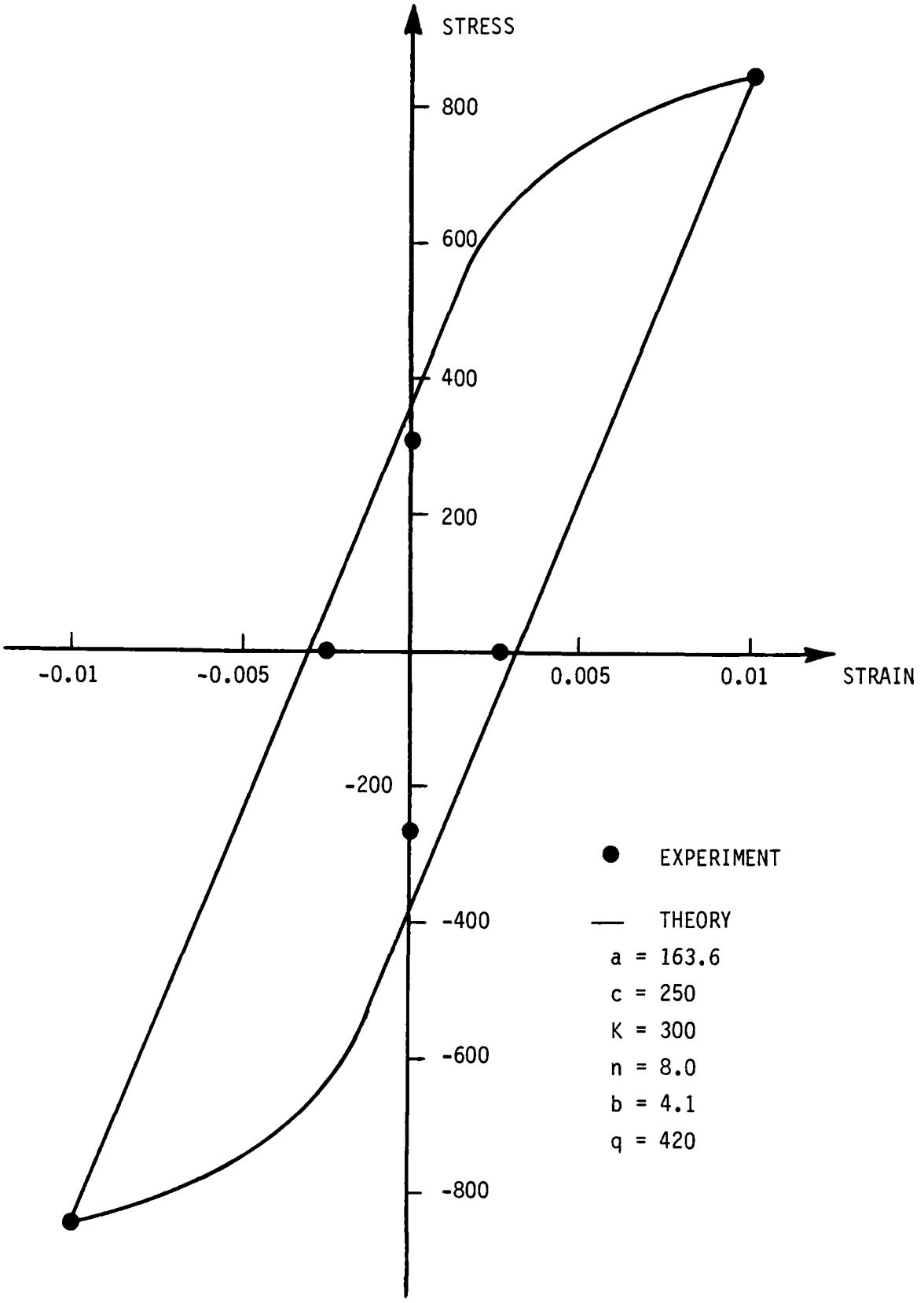

Fig. 4.15. Hysteresis behavior (cycle no. 4).

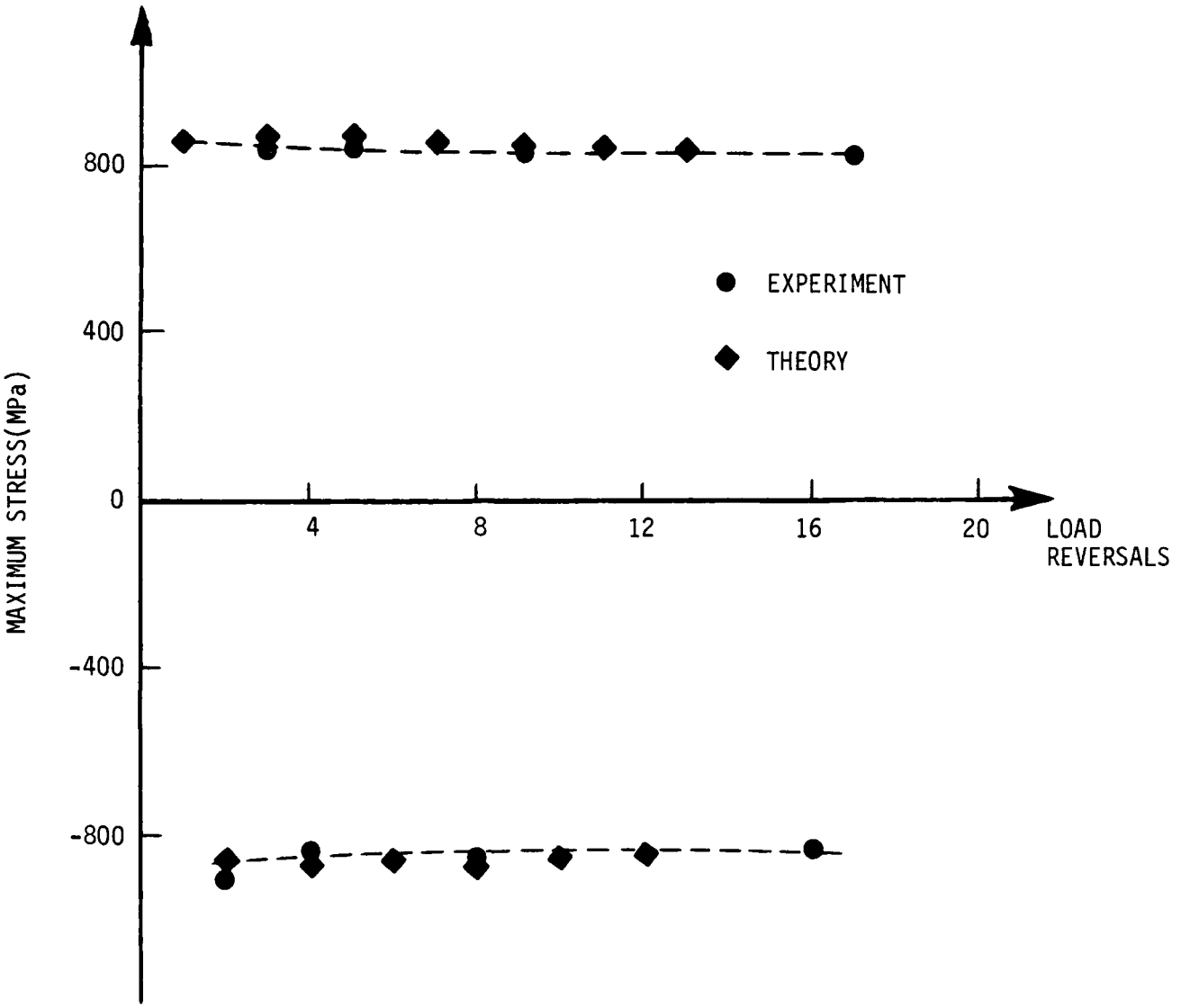

Fig. 4.16. Maximum hysteresis stress amplitude versus load reversals.

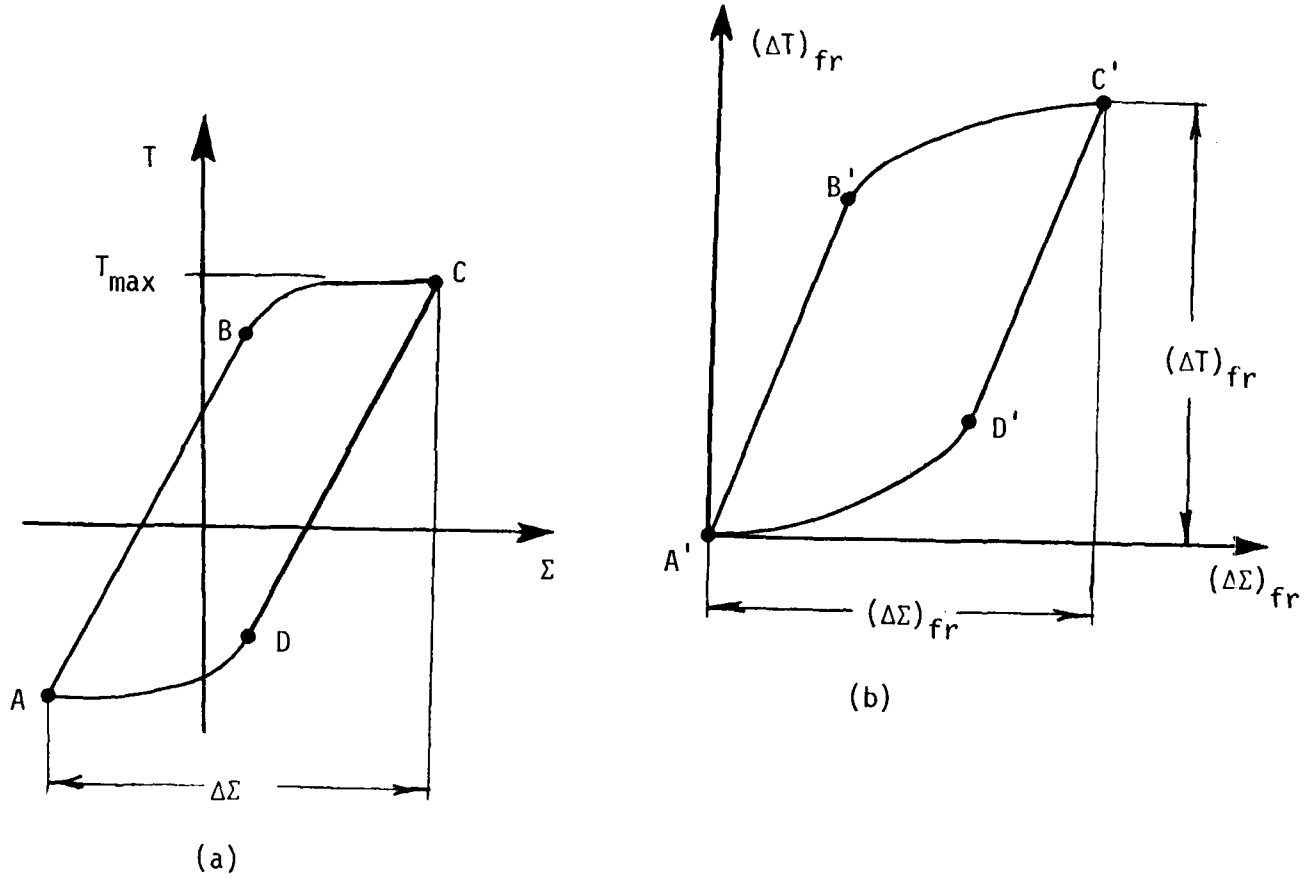

Fig. 5.1. Conversion of the i^{th} stress-strain cycle with mean stress and unequal creep strains into the i^{th} equivalent fully reversed symmetric cycle.

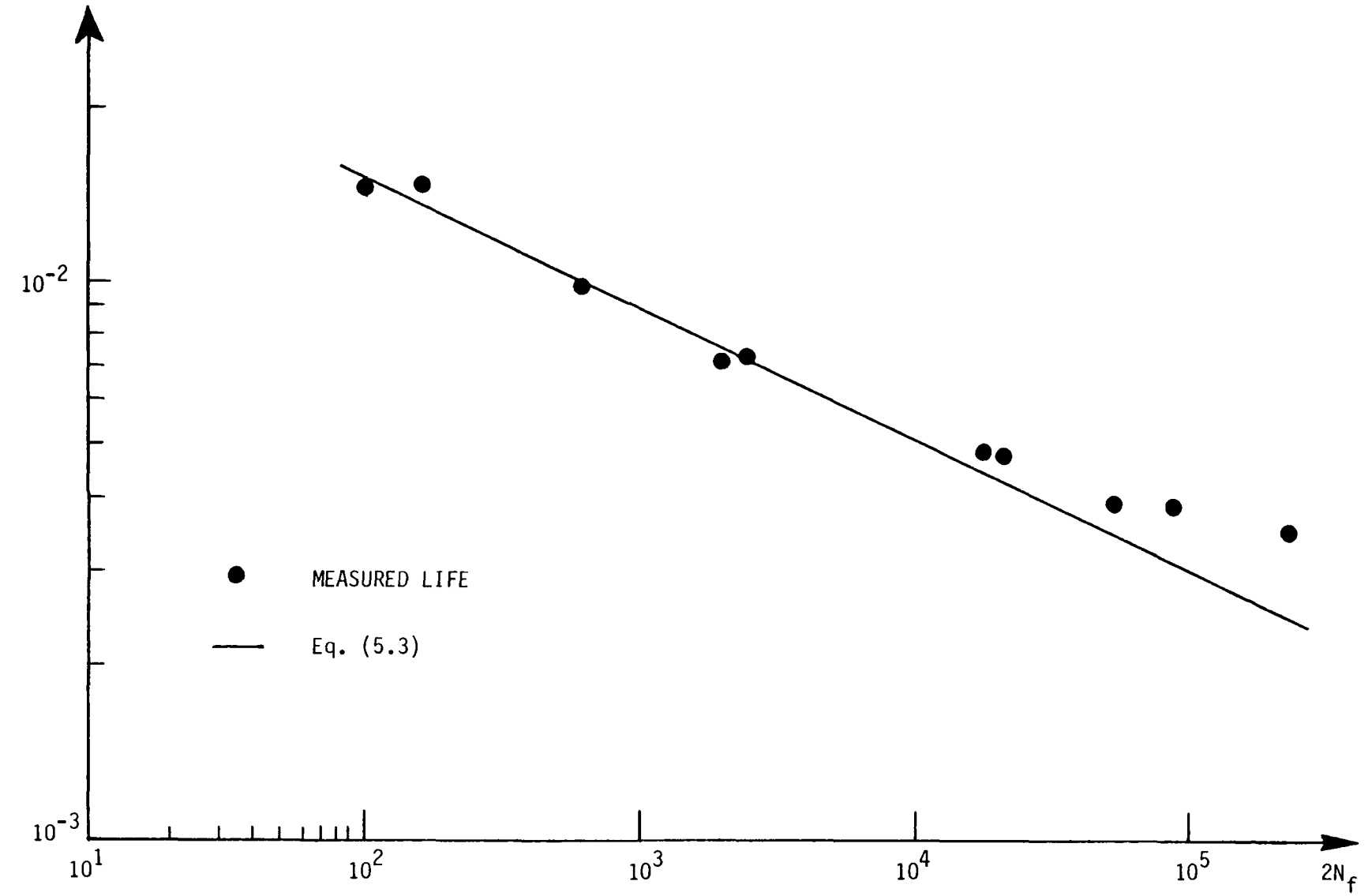

Fig. 5.2. Total strain amplitude versus number of load reversals to crack initiation.

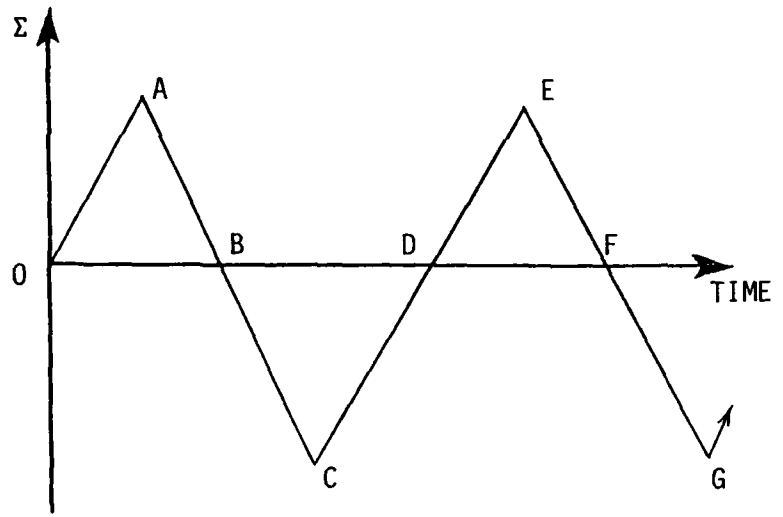

(a) Strain controlled loading.

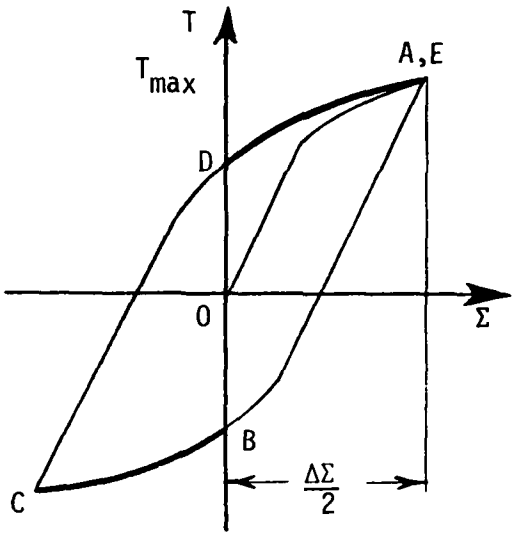

(b) Net-section stress-strain cycle.

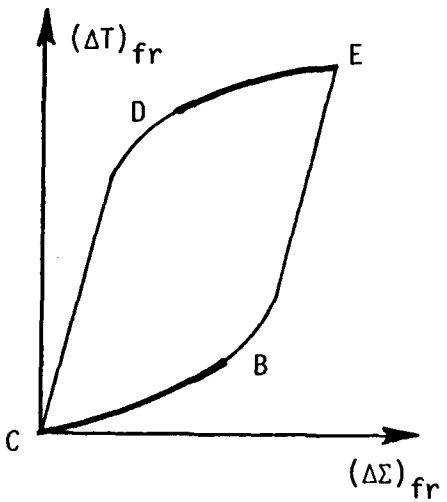

(c) Equivalent fully reversed cycle corresponding to the third load reversal CDE.

Fig. 5.3. Cumulative fatigue damage is calculated for portions of the stress-strain cycle where the stress rate, stress and the total strain have the same sign.

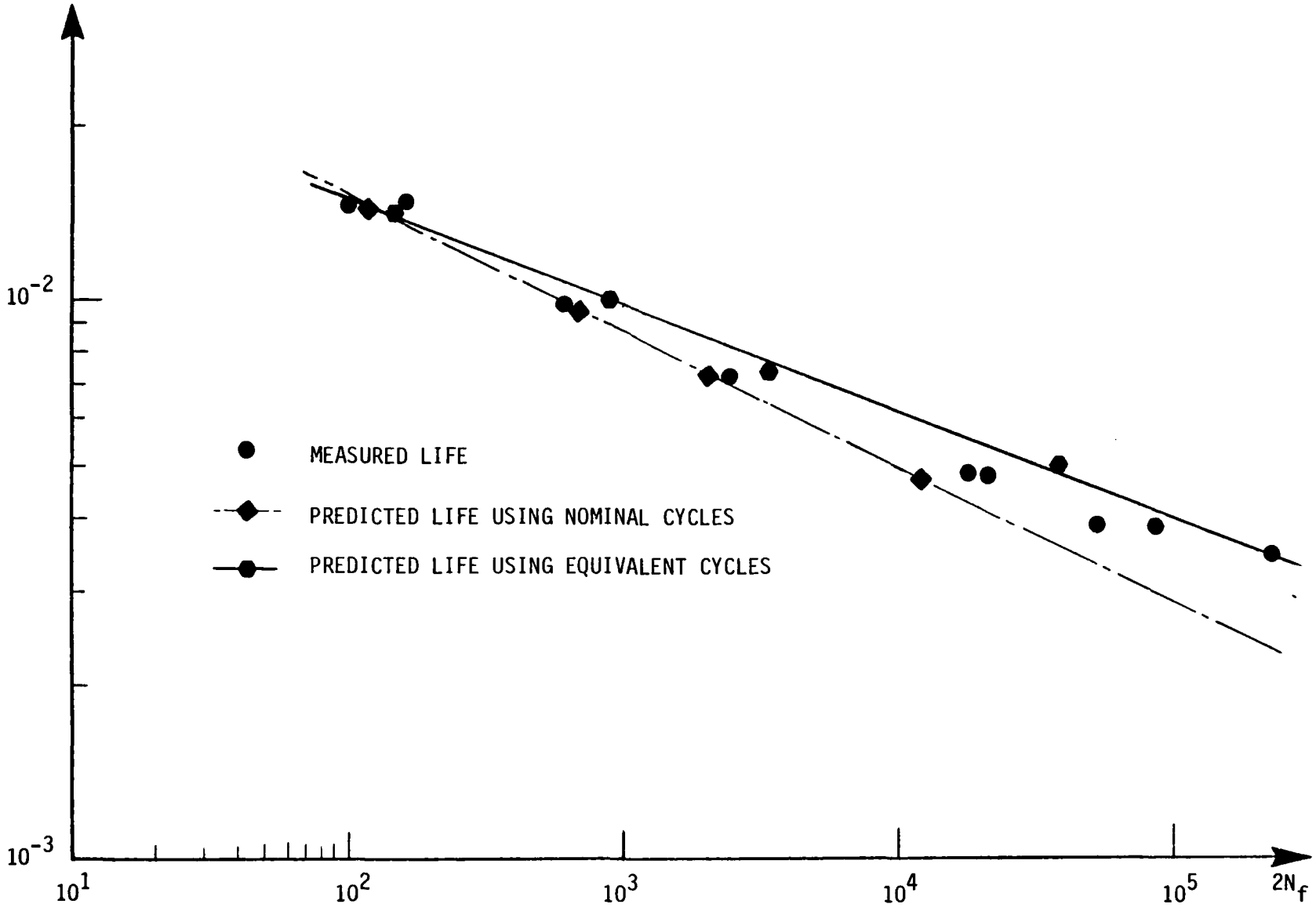

Fig. 5.4. Predicted versus measured fatigue life without stress hold times.

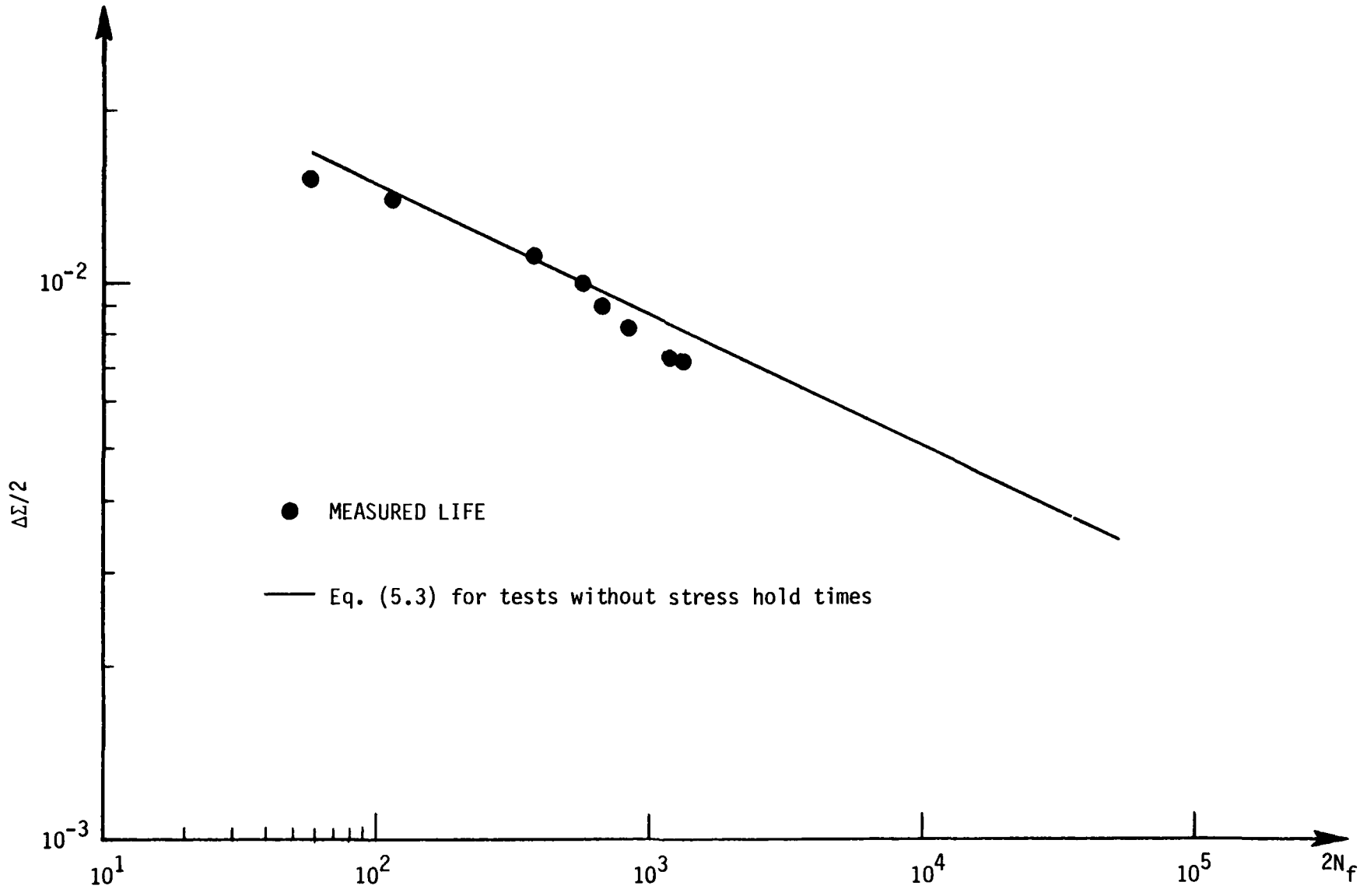

Fig. 5.5. Total strain amplitude versus number of load reversals to failure(stress-controlled tests with hold times).

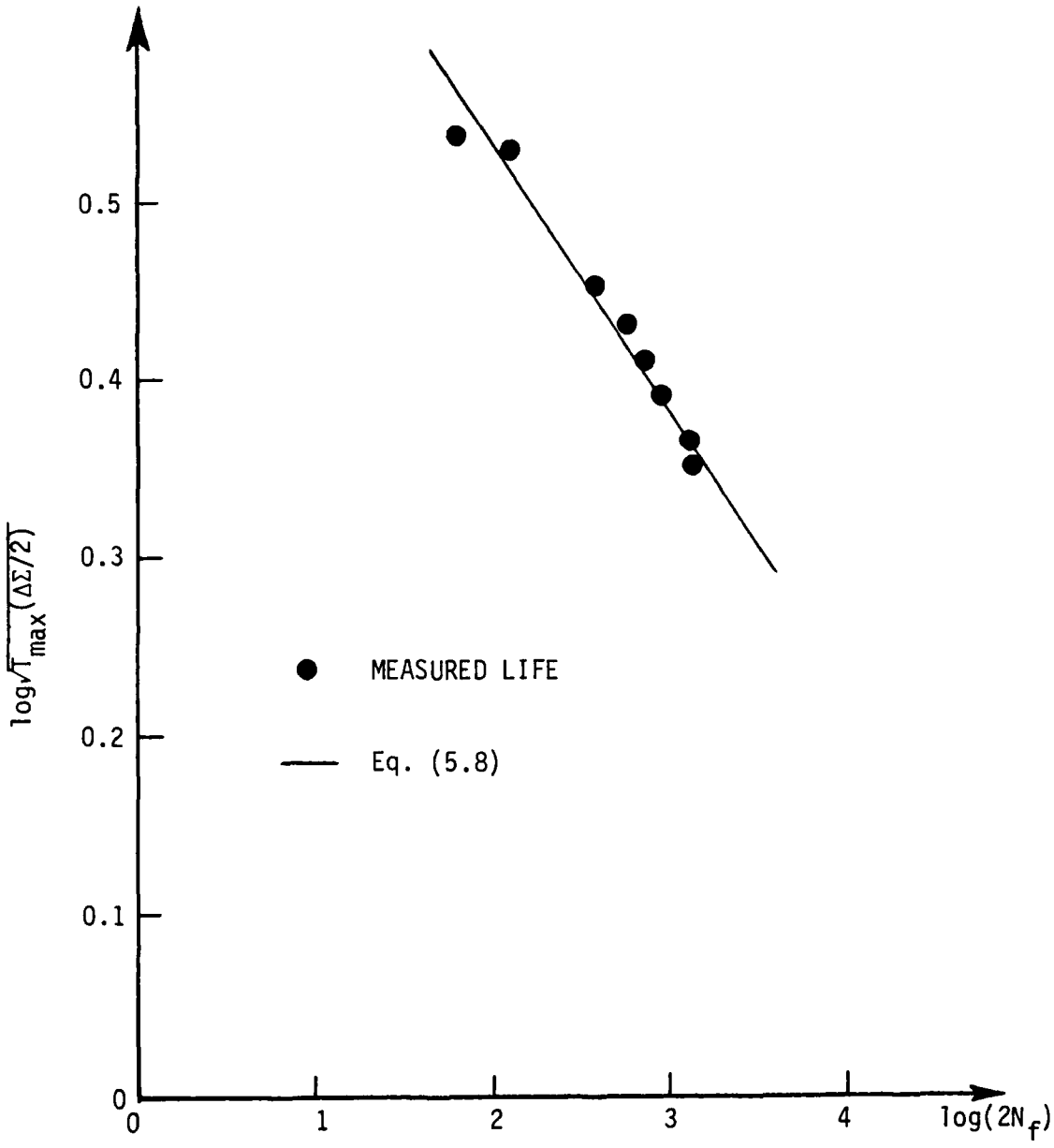

Fig. 5.6. Smith parameter versus fatigue life for tests with stress hold times.

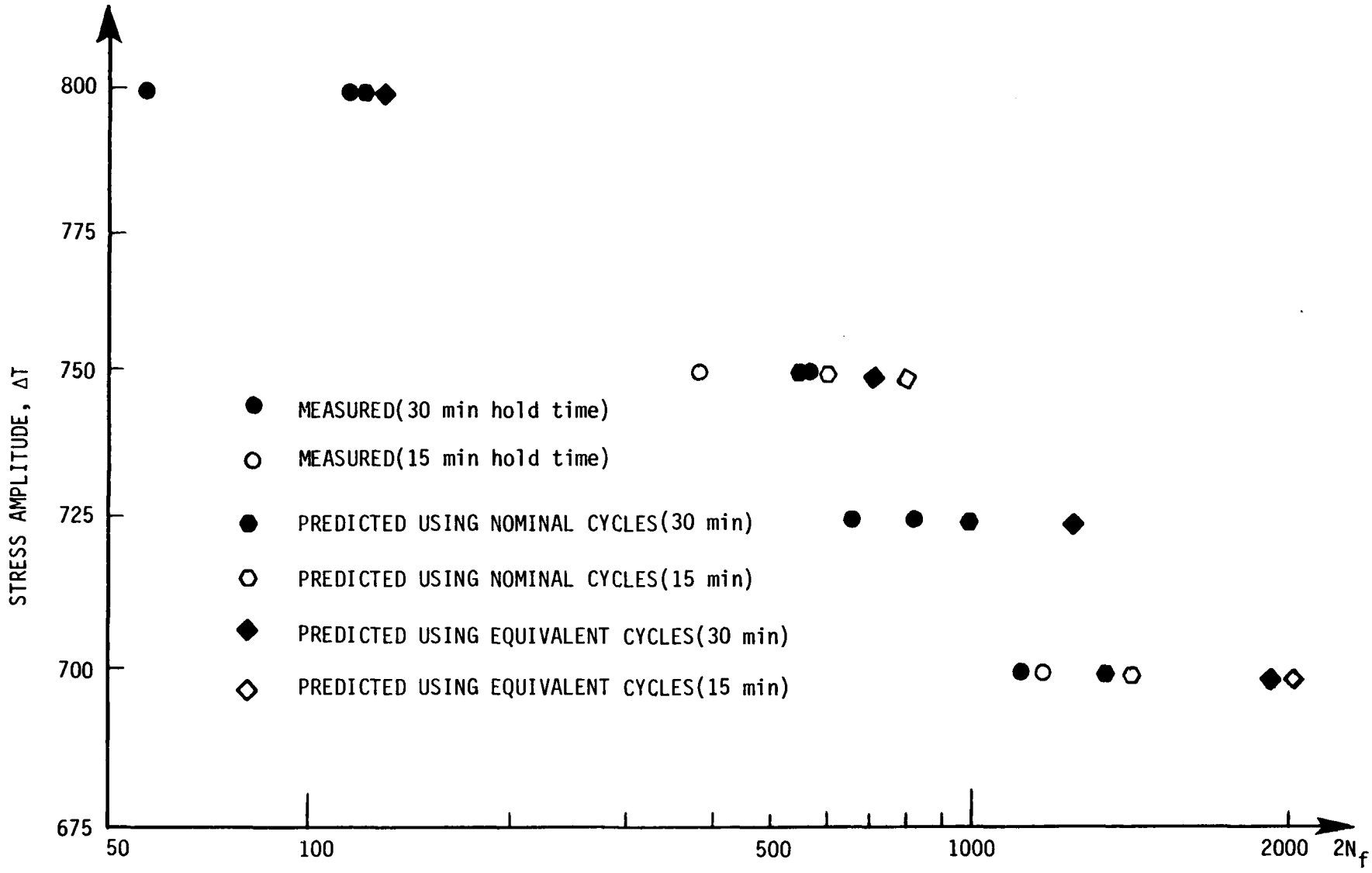

Fig. 5.7. Predicted versus measured fatigue life with stress hold times.

END

FILMED

3 -86

DTIC